



Proceedings of the 2nd **EVN/JIVE SYMPOSIUM**

Toruń, Poland
October 21st, 1994

Edited by
A.J. Kus,
R.T. Schilizzi,
K.M. Borkowski,
L.I. Gurvits

Toruń Radio Astronomy Observatory



Proceedings of the 2nd **EVN/JIVE Symposium**

Held at Toruń, Poland
October 21st, 1994

Edited by **A.J. Kus, R.T. Schilizzi,**
K.M. Borkowski and L.I. Gurvits

Toruń Radio Astronomy Observatory

PREFACE

The EVN/JIVE Symposium series was established a year ago to bring European astronomers together to hear the latest results in VLBI-related research. The first Symposium was held at Jodrell Bank just preceding the autumn meeting of the EVN Board of Directors. A key factor in the timing was to bring young researchers in Europe in contact with their more senior colleagues from other countries and vice versa. This successful formula was continued in the second in the series hosted by the Toruń Radio Astronomy Observatory of the Nicolaus Copernicus University at the time of the opening of the new 32 m radio telescope on 22 October 1994.

These Proceedings present the contributions made to the second EVN/JIVE Symposium in Toruń. Seventy four participants discussed 21 papers on subjects ranging over most areas impacted by current VLBI: astrometry, geodesy, astrophysical applications in millimetre-wavelength and spectral lines, surveys with milliarcsecond resolution, gravitational lenses, active galactic nuclei, and corresponding new telescopes, instrumentation and data processing. The authors were requested to bring their manuscripts in computer readable form to the Symposium or to send them ahead of time via electronic mail. Less than one month after the Symposium, these Proceedings are ready for issue, a tribute to the authors themselves and the hard work of the staff at the TRAO.

We thank the TRAO staff for their help in organising this very successful Symposium and the Polish Ministry of Education, the State Committee for Scientific Research, the Nicolaus Copernicus University and Mostostal Gdańsk S.A. for financial support. A number of participants wish to thank the Joint Institute for VLBI in Europe for travel funds to enable them to attend the Symposium.

A.J. KUS, R.T. SCHILIZZI, K.M. BORKOWSKI, L.I. GURVITS

Toruń – Dwingeloo, 16 November, 1994

Contents

Preface	iii
-------------------	-----

Bold names denote the presenter of the paper at the Symposium

VLBI APPLICATIONS FOR PHYSICS, ASTROMETRY,
GEODESY AND DATA PROCESSING

VLBI Astrometry of Radio-Emitting Stars	
J.-F. Lestrade , <i>R.B. Phillips, D.L. Jones and R.A. Preston</i>	1
Influence of Radio Source Structure on Geodetic VLBI Analysis	
A.-M. Gontier and <i>S. Britzen</i>	9
High Frequency Variations of EOP from Extensive VLBI Operations in January, 1994	
<i>S.L. Bolotin</i>	13
A New Approach to the Analysis of Interferometric Data	
D. Fraix-Burnet , <i>V. Despringre, E. Anterrieu and A. Lannes</i>	19
Status of the Space VLBI User Assistance Software Being Developed at the Satellite Geodetic Observatory, Hungary	
I. Noszticzius	25
GPS QSO 2022+171 — A Possible Target for VLBI Detection of Gravitational Waves	
S. Pogrebenko , <i>M. Mingaliev, S. Montebugnoli, S. Neizvestny,</i> <i>N. Borisov and V. Stolyarov</i>	33

MM-VLBI

Fringe Finding for 3mm-VLBI: Application to 3C111	
S. Doeleman , <i>A.E.E. Rogers and J.M. Moran</i>	39
Jets of Blazars at Sub-mas Scales: a Status Report on mm-VLBI	
T.P. Krichbaum , <i>K.J. Standke, A. Witzel, C.J. Schalinski, M. Grewing,</i> <i>A. Grave, R.S. Booth, L.B. Bååth, A.E.E. Rogers and J.A. Zensus</i>	47

SPECTRAL LINE VLBI

VLBI Study of Circumstellar Masers: Status Report	
Francisco Colomer	55
Towards Stellar Proper Motions in the Galactic Center	
Loránt Sjouwerman	57

VLBI SURVEYS

22 GHz VLBI Survey: Status Report and Preliminary Results	
<i>G. Moellenbrock, K. Fujisawa, R. Preston, L. Gurvits, R. Dewey,</i> <i>H. Hirabayashi, M. Inoue, D. Jauncey, V. Migenes, D. Roberts,</i> <i>R. Schilizzi, S. Tingay and A. Zensus</i>	61

Global VLBI Observations of Bright AGN	
<i>Kaj Wiik, Esko Valtaoja and Kari Leppänen</i>	65
Investigation of a Unique Sample of Faint Peaked Spectrum Sources	
<i>Ignas Snellen, Richard Schilizzi, George Miley, Ger de Bruyn and Malcolm Bremer</i>	71
GRAVITATIONAL LENSES	
Wide-field VLBI Observations of Gravitational Lenses	
<i>M.A. Garrett, A.R. Patnaik and R.W. Porcas</i>	73
A Global VLBI Search for Milli-lenses	
<i>D.R. Henstock, P.N. Wilkinson, I.W.A. Browne, G.B. Taylor, A.C.S. Readhead, T.J. Pearson, R.C. Vermeulen and W. Xu</i>	79
AGN	
Sub-arcsecond Structure of the ‘Optically Quiet Quasar’, 0646+600	
<i>C.E. Akujor, R.W. Porcas and J.V. Smoker</i>	87
Multifrequency VLBI Monitoring and Jet Physics	
<i>A.P. Lobanov and J.A. Zensus</i>	93
Aberration of Light and Time Delay Effects in Parsec-scale Relativistic Jets	
<i>A. Alberdi, J.L. Gómez, J.C. Guirado, L. Lara and J.M. Marcaide</i>	99
Current Observational Status of the Object 1308+328	
<i>Jerzy Machalski</i>	105
NEW TELESCOPES AND INSTRUMENTATION FOR VLBI	
The Recent Status of the TIGO Project	
<i>Hayo Hase</i>	107
A New S/X–band Receiver for the Simeiz VLBI Station	
<i>A. Ipatov, I. Ipatova, D. Ivanov, A. Kutuzov, V. Mardyshkin and A. Mikhailov</i>	113
VLBI Station “Simeiz”	
<i>A.V. Stepanov, L.I. Matveenko and A.V. Ipatov</i>	117
Pulsar Processing Facility of the EVN MK-IV Correlator	
<i>S. Pogrebenko and G. Tuccari</i>	119
Author Index	123
List of Participants	125

VLBI Astrometry of Radio-Emitting Stars

J.-F. LESTRADE¹, R.B. PHILLIPS², D.L. JONES³ and R.A. PRESTON³

¹Observatoire de Paris-Meudon, F92195 Meudon, Principal Cedex, France

²Haystack Observatory, Massachusetts Institute of Technology, Westford, MA 01886, USA

³Jet Propulsion Laboratory, California Institute of Technology, 4800 Oak Grove Dr., Pasadena, CA 91109, USA

Abstract

High-accuracy astrometric VLBI observations of 7 radio stars are presented with applications to the connection between the Hipparcos and VLBI extragalactic reference frames, to the identification of the radio emitting region in the ternary system Algol and the detectability of Jupiter-size planet orbiting the radio star σ^2 CrB.

Introduction

Very Long Baseline Interferometry (VLBI) observations of radio-emitting stars conducted over the last decade have yielded their positions, annual proper motions, trigonometric parallaxes with a precision of 1 milliarcsecond or better. The applications of such a high-accurate astrometric parameters include the improvement of the astronomical distance scale through trigonometric parallax measurements, the connection of the radio and optical celestial reference frames, the attempt to detect Jupiter-size companions orbiting radio-emitting stars, the determination of the orientation (node) and angular separation of binary system orbits for dynamical studies of these systems, the crucial proper motion of the reference star in the Gravity Probe B mission to test the Lense-Thirring effect of General Relativity amongst others.

There are about 30 stars detectable with the state of the art VLBI data acquisition system and there might be 100 detectable by the end of the decade with the new VLBI capabilities being developed in the US and in Europe.

Our VLBI astrometric program of 11 radio-emitting stars (Figure 1) started in 1982 and its initial motivation was to connect the Hipparcos optical reference frame to the VLBI (radio) extragalactic reference frame at the milliarcsecond level. The flux densities of these 11 stars are variable between a few millijansky and a few tens millijansky, i.e. substantially weaker than the extragalactic radio sources usually observed by VLBI. We had to resort to the phase-referencing VLBI technique both to enhance sensitivity with multi-hour integrations and to achieve high astrometric accuracy through use of the differential interferometric phase between the target star and an angularly nearby VLBI extragalactic source. The details of this technique is described in Lestrade *et al.* (1990).

We shall summarise the state of the Hipparcos/VLBI connection based on our program and present 2 additional results as spin-offs of these VLBI observations.

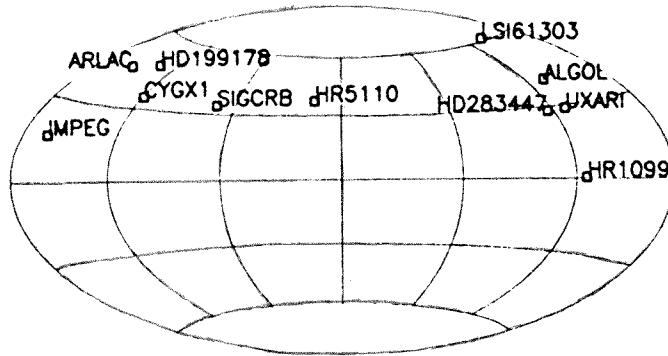


Figure 1: Sky distribution of the VLBI link stars for Hipparcos.

Preliminary link of the Hipparcos and VLBI reference frames

We have carried out a comparison between the VLBI and Hipparcos astrometric parameters of 7 radio-emitting stars of our program. Both techniques (VLBI and Hipparcos) have provided positions, annual proper motions and trigonometric parallaxes of these stars with comparable formal uncertainties at the 1 milliarc-second level or better. We have found that the systematic discrepancies between these 2 sets of astrometric parameters can be removed by performing a single global rotation between the extragalactic and Hipparcos reference frames. The three angles and annual rates of this rotation are determined at better than the milli-arcsec level as shown in Table 1. The Hipparcos parameters used for this determination are from the Hipparcos reduction consortium FAST but similar result has been found with the other consortium NDAC.

Table 1: VLBI/Hipparcos-FAST connection: the 3 angles ($A_1 = A1$, $A_2 = A2$, $A_3 = A3$) and the 3 rates of rotation ($PA1 = \dot{A}_1$, $PA2 = \dot{A}_2$, $PA3 = \dot{A}_3$) between the Hipparcos and VLBI reference frames have been determined with 7 link stars.

Weighted least-square-fit solution :

Rotation angles at epoch 1991 4 1 :

$$A1 = -26.87 \text{ +/- } 0.46 \text{ mas}$$

$$A2 = -12.64 \text{ +/- } 0.55 \text{ mas}$$

$$A3 = 22.99 \text{ +/- } 0.46 \text{ mas}$$

Rotation rates :

$$PA1 = 0.60 \text{ +/- } 0.48 \text{ mas/yr}$$

$$PA2 = 0.06 \text{ +/- } 0.46 \text{ mas/yr}$$

$$PA3 = 1.35 \text{ +/- } 0.43 \text{ mas/yr}$$

The robustness of the solution has been tested by splitting the 7 FAST link stars into two independant subsets, one with 3 stars (HR1099, HR5110, AR Lac) and one with 4

stars (UX Ari, σ^2 CrB, CygX1, IM Peg). Rotation angles and rates have been solved independently for with these 2 subsets and compared. The differences are no more than the quadratically combined uncertainties of the 2 solutions (Table 2).

Table 2: Differences between the angles and rates of rotation determined after splitting the 7 VLBI link stars into 2 independent subsets of 3 and 4 stars. The symbol σ is the quadratically combined uncertainties of the 2 solutions.

	Differences between solutions FAST(3 stars) – FAST(4 stars) (mas or mas/yr, correspondingly)
A_1	+0.53 \sim 0.5 σ
A_2	–0.48 \sim 0.5 σ
A_3	+0.08 \sim 0.1 σ
\dot{A}_1	+1.17 \sim 1.0 σ
\dot{A}_2	+0.91 \sim 1.0 σ
\dot{A}_3	+0.54 \sim 0.5 σ

The 3 angles of rotation are consistent with the expected values since the FAST Hipparcos coordinate system is aligned upon a *quasi-FK5* reference frame and the FK5 is aligned with the VLBI reference frame to within 70 mas. The measured rotation rates are consistent with the uncertainty of about 0.5 mas/yr, although the \dot{A}_3 rate reaches 3 σ . This means that the procedure used in the Hipparcos data reduction to stop the rotation of the Hipparcos sphere is efficient.

The angles of rotation found are relative to a VLBI extragalactic reference frame that is defined by the International Earth Rotation Service (IERS) VLBI coordinates of the extragalactic reference sources (Arias, Feissel, Lestrade 1991) used for the differential VLBI measurement of the link stars. The post-fit residuals of the star coordinates and proper motion components after the adjustment of the global rotation indicate that the consistency between the Hipparcos and VLBI astrometric techniques is at the milliarcsecond level. This is the first cross-check between these two astrometric techniques of comparable precision. The level of agreement found is consistent with the expected accuracy of the technique, even though the astrometric parameters used are from preliminary reductions of the data for both techniques. A complete account of this preliminary link is in Lestrade *et al.* (1994a).

VLBI astrometric identification of the radio-emitting region in Algol

Spectroscopy, photometry and speckle interferometry have already provided accurate values for almost all the geometric and orbital parameters of the ternary system Algol (e.g. Soderhjelm 1980). Consequently, it is known that the mass ratio M_A/M_B between the primary (main-sequence) and secondary (subgiant) stars of the close binary of this system is ~ 4.5 and thus significantly different from unity. This makes the motion of the radio source quite different depending on whether it is associated with the subgiant or the main sequence star of the close-binary (astrometric measurements exclude that the third

component of the system could be responsible for the radio emission). The maximum displacement of the radio source projected on the sky occurs between the quadrature points of the close binary orbit. This means between orbital phase $\phi = 0.25$ and $\phi = 0.75$, if $\phi = 0$ is the primary eclipse time when the cool subgiant is in front of the bright B8V star. The magnitude of this displacement would be $0.0036''$ (from $2 \times \frac{M_A}{M_A+M_B} \times a$) if the emitting region is centered on the subgiant but it would be $0.0008''$ (from $2 \times \frac{M_B}{M_A+M_B} \times a$) if centered on the more massive main sequence star B8. a is the semi-major axis and is known. The displacement would be intermediate if the emitting region is associated with the transient flow of gas between the two stars.

In April 1989, we made four VLBI astrometric observations of the Algol radio emission. The observations took place on April 12th, 15th, 16th and 19th, allowing 2.5 orbital revolutions of the close binary to be sampled over these 7.5 days. These four epochs were chosen so that the observations took place when the two stars of the close binary were as close as possible to the orbital phases $\phi = 0.25$ and $\phi = 0.75$. A single observation at each of these two orbital phases would have sufficed but two additional observations were scheduled because of possible technical failures during the observations and for redundancy of the measurement. All four observations were successful.

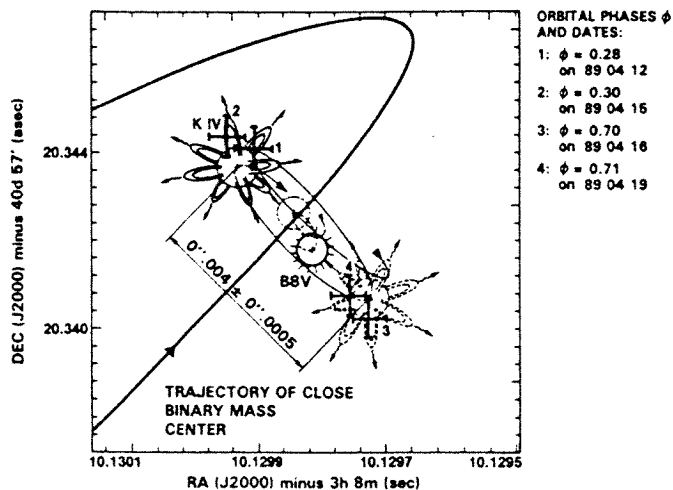


Figure 2: The four positions of the radio emission of Algol (crosses) measured by VLBI are superposed on the configuration of the close binary during the observations at orbital phases 0.25 and 0.75. A portion of the trajectory of the close binary mass center orbiting the third star in 1.86 yr is displayed.

We measured the displacement of the radio source in Algol of 4 ± 0.5 milliarcsecond between two orbital phases 0.25 and 0.75 over two consecutive orbital revolutions of the close binary (see Figure 2). The *magnitude* of the displacement unambiguously indicates that the less massive star of the close binary, the K subgiant, is the star responsible for the non-thermal radio emission of the system. This is consistent with the idea that the radio emission in Algol is related to the strong magnetic activity of the subgiant.

The *orientation and sense* of the displacement on the sky that are directly deduced from our astrometric VLBI observations imply 1) that the orbital plane of the close binary is at p.a. = $+52 \pm 5^\circ$ (p.a. = 0° is North and p.a. = 90° is East) and 2) that the sense of circulation of the close binary is clockwise, as seen on the sky. Thus, the long-period and close binary orbital motions are almost orthogonal and counter-revolving (Figure 3). The orientation and sense of circulation of the close binary determined by our VLBI observations are identical to the findings of Rudy (1979) and Kemp *et al.*

(1981, 1983) obtained less directly with optical polarisation observations. This intriguing configuration is difficult to reconcile with our present idea on the formation, evolution and dynamical stability of multiple stellar systems since it is difficult to conceive that the angular momentum of the primordial cloud of this ternary system was split along two orthogonal axis. The full account of these observations is in Lestrade *et al.* (1993).

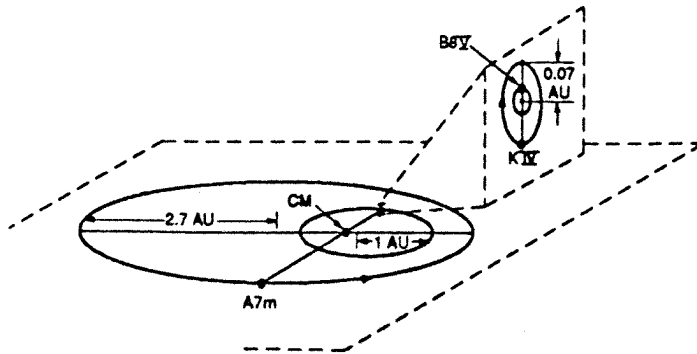


Figure 3: Configuration of the two orbital planes in the Algol ternary system.

Astrometric detectability of a Jupiter-size planet orbiting the radio-emitting star σ^2 CrB

The motion of a single planet in a circular orbit around a star causes the star to undergo a reflexive circular motion around the star-planet barycenter. When projected on the sky, the orbit of the star appears as an ellipse with angular semimajor axis θ given by

$$\theta = \frac{m_p a}{M_* d} \quad (1)$$

where θ is in arcsec when the semimajor axis a is in AU, the mass of the planet (m_p) and the mass of the star (M_*) are in solar masses and the distance d is in pc. For example, observing the solar system from a distance of 10 pc, the presence of Jupiter would be revealed as a periodic circular displacement in the Sun's position, with a diameter 2θ of 1.0 milliarcsecond and a period of 11.9 years.

Ground-based optical astrometry has generally been limited to a precision of a few tens of milliarcseconds although the best measurements are at the 1 milliarcsecond level now (Gatewood *et al.* 1992). VLBI astrometric observations of σ^2 CrB conducted by us at 13 epochs between 1987 and 1994 have yielded its position, proper motion and trigonometric parallax and the resulting post-fit coordinate residuals are characterised by an rms as small as 0.2 mas (see Figure 4). The formal uncertainties for the 5 fitted astrometric parameters are 0.08 mas for the relative position between σ^2 CrB and the reference source 1611+343, 0.04 mas/year for the proper motion and 0.08 mas for the trigonometric parallax (Lestrade *et al.* 1992, 1994b).

The lack of a clear sinusoidal signature in the post-fit coordinates residuals of Figure 4 sets a limit on the presence of a planet around σ^2 CrB for the 7 years observation span. The rms of the post-fit residuals (0.2 mas in Figure 4) is an upper limit on any systematic departure from linear motion of the star. Eq (1) can be used to exclude a range of planetary perturbations by taking $2\theta = 0.2$ mas, $M_* = 2.26 M_\odot$ and $d = 22.7$ pc for σ^2 CrB. The log-log representation of eq (1) with these parameters is in Figure 5 and in

Lestrade *et al.* (1994b). The diagonal line of constant astrometric signature in Figure 5 follows eq (1) for $2\theta = 0.2$ mas. We assume that a full orbital period of the planet must be sampled during the observations to separate the sinusoidal planetary signature from the fitted linear proper motion. In these conditions, the maximum semimajor axis a of the orbit of a planet corresponds to the total observation span through the third Kepler law. This lower limit on a is 4.8 AU for the 7 years of observations and is indicated by the vertical dashed line in Figure 5. Finally, the shaded area indicates the planet parameter space (a, m_p) that are excluded by the present observations, i.e. any planetary perturbations in the shaded area is too large to be consistent with the post-fit coordinate residual rms of 0.2 mas measured over 7 years by VLBI. Note that for $a = 4.8$ AU, the upper limit on the planet mass m_p is $0.0012 M_\odot$, (~ 1 Jupiter mass) as derived by eq. (1) for σ^2 CrB and $2\theta = 0.2$ mas.

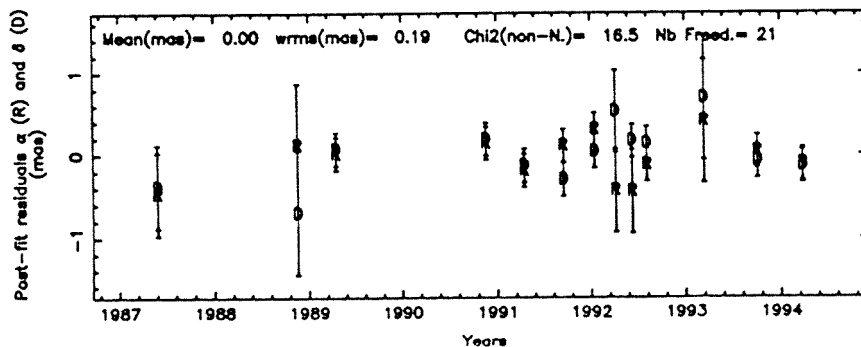


Figure 4: Post-fit coordinate residuals for σ^2 CrB. The 5 astrometric parameters of σ^2 CrB (coordinates, proper motion components and trigonometric parallax) are adjusted to the coordinates measured by VLBI at 13 epochs.

This limit will become more stringent if the period of observation is extended. The ultimate goal of our program is now to extend these 7 years of astrometric VLBI observations of σ^2 CrB to complete a full 12 year cycle typical of a Jupiter-size planet that might orbit this star. The goal is also to improve the level of precision of our astrometric measurement since this level is not presently SNR-limited. It might reach 20 **microarcseconds** if all systematic errors could be removed by an improved strategy of observations and data analysis.

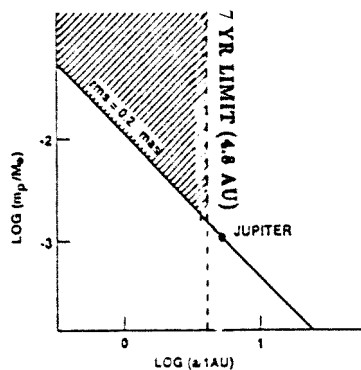


Figure 5: Log-log representation of eq (1) for the rms of the post-fit coordinate residuals (0.2 mas) of σ^2 CrB. The shaded area is the parameter space (semi-major axis a , mass m_p) that are excluded by our 7 years of VLBI observations for a planet around this star.

References

- [1] Arias, F., Feissel, M., Lestrade, J-F., 1991, The IERS extragalactic Reference Frame and its Tie to Hipparcos, IERS Technical Note 7, December 1991, Observatoire de Paris, France.
- [2] Gatewood, G., Stein, J., Joost Kiewiet de Jonge, T., Persinger T., Reiland, T., 1992, *Astron. J.*, **104**, 1237.
- [3] Lestrade J.-F., Rogers A.E.E., Whitney A.R., Niell A.E., Phillips R.B., Preston R.A., 1990, *Astron. J.*, **99**, 1663–1673.
- [4] Lestrade J.-F., Phillips R.B., Preston, R.A., D. C. Gabuzda, 1992, *Astron. Astroph.*, **258**, 112–115.
- [5] Lestrade J.-F., Phillips R.B., Hodges, M.W., Preston, R.A., 1993, *Astroph. J.*, **410**, 808–814.
- [6] Lestrade J.-F., Jones, D.L., Preston, R.A., Phillips R.B., Titus M.A., Kovalevsky J., Lindgren L., Hering R., Froeschle M., Falin, J-L, Mignard, F., Jacobs, C.S., Sovers, O.J., Eubanks, M., Gabuzda, D., 1994a, *Astron. Astroph.* (submitted).
- [7] Lestrade J.-F., Jones, D.L., Preston, R.A., Phillips R.B., 1994b, *Astroph. and Space Science*, vol. **212**, Kluwer Academic Publishers, p. 251–260.
- [8] Rudy, R.J., 1979, *MNRAS*, **186**, 473.
- [9] Kemp, J.C., Barbour, M.S., McBinney, R.E., Rudy, R.J., 1981, *Astroph. J.*, **243**, 557.
- [10] Soderhjelm, S., 1980, *Astron. Astroph.*, **89**, 100.

DISCUSSION

S. Doeleman (Q): Based on emission mechanisms, are you looking at the stars as they flare or in a quiescent state? How would this confuse an attempt to find a planet?

J.-F. Lestrade (A): The positional stability of the radio-emitting region within the star is a crucial question. Presently, we can say that if there is a jitter, it is no more than 0.2 milliarcsecond for the star σ^2 CrB. Now, it is possible to discriminate between the sinusoidal signature of a Jupiter-size planet with a period of ~ 12 years or more and the erratic signature of the possible positional variations of the radio-emitting region in various states of activity.

Influence of Radio Source Structure on Geodetic VLBI Analysis

A.-M. GONTIER^{1,2} and S. BRITZEN^{1,3}

¹Max-Planck-Institut für Radioastronomie, Bonn, Germany.

²IERS/cb, Observatoire de Paris, Paris, France.

³Geodätisches Institut der Universität, Bonn, Germany.

Abstract

VLBI is at present the most powerful technique to construct the best approximation to an inertial reference frame. After more than a decade of VLBI observations several hundreds of extragalactic objects have positions known within $\pm 0.0003''$. The accuracy of source position determination has reached a limit where second-order contributions, like source structure effects, become significant. As there is essentially no point like source at the milliarsecond level, we need to correct for source structure to reach and maintain 0.1 mas accuracy on sources positions and millimeter accuracy on geodetic parameters. Status report on the software to correct source structure will be presented together with recent comparisons between observed and computed closure quantities.

Introduction

VLBI (Very Large Baseline Interferometry) is at present the most powerful technique to construct the best approximation to an inertial reference frame. The IERS (International Earth Rotation Service) celestial reference frame is based on the positions of compact extragalactic objects measured by VLBI and it's maintained on the basis of the analysis of several observation programmes for the study of Earth rotation, crustal deformations, astrometry and for deep space navigation. The latest realizations of the IERS celestial reference frame is compiled from five individual extragalactic reference frames obtained in global solutions at the Goddard Space Flight Center, the Jet Propulsion Laboratory, the National Astronomical Observatory of Mizusawa, the National Oceanic and Atmospheric Administration and the United States Naval Observatory (Charlot (ed.) 1994). It contains 531 objects uniformly distributed on the sky ($-86^\circ < \delta < +85^\circ$), over 239 objects have positions known within $\pm 0.00025''$ (IERS 1994).

A limiting factor of the precision and the maintenance of the extragalactic VLBI reference frame is the structure of the radio sources. As there is essentially no point like source at the milliarsecond level, source structure effects must be accounted for in high-precision geodetic VLBI analysis.

Source structure correction

The effect of source structure on the bandwidth synthesis delay is defined as the fringe phase derivative with respect to the angular frequency:

$$\tau_s = \frac{\partial \phi_s}{\partial \omega} \quad (1)$$

where ϕ_s is the part of fringe phase due to structure effect and ω the observing frequency.

As we are not only interested in phase computation but also in phase variation with respect to frequency, we have expanded equation (1) into two parts and we obtain:

$$\tau_s = \frac{\partial \phi_s}{\partial u} \frac{\partial u}{\partial \omega} + \frac{\partial \phi_s}{\partial v} \frac{\partial v}{\partial \omega} = \nabla \phi_s \frac{B}{\lambda \omega}$$

where $\nabla \phi_s$ is the gradient of phase with respect to u, v -coordinates and λ the wavelength, B represents the baseline projection onto the plane of sky.

The fringe phase and the derivative of the phase are only functions of the complex visibility of the observed source calculated from a given brightness distribution using a two dimensional Fourier Transformation. Then to obtain the delay due to source structure-effects we only need the map of delta functions representing the brightness distribution of the source in the plane of sky (Thomas 1980).

Closure quantities

For source imaging we use the closure phases which are computed by summing the phases around a triangle (*i.e.* a closed loop of baselines). As all effects known today, except source structure effects, are associated with individual antennas, we expect that the non-zero closure quantities are only due to source structure effects (Pearson and Readhead 1984).

Provided that all computations are based on the same experiment and same frequency, the closure quantities (phase, delay and delay rate) derived from the map should agree with observed data to within the noise level due to uncertainties in observations and mapping algorithms. We have performed comparisons between the predicted and the observed closures in order to test our computation of delay corrections due to source structure.

Geodetic observations, performed the 25 february 1992 on the source 1803+784 at X and S band using 4 stations: Mojave, Westford (USA), Wettzell (Germany) and Hartebeesthoek (South Africa), are used for the test. Figure 1 show the good agreement between computed and measured closure phases and closure delays.

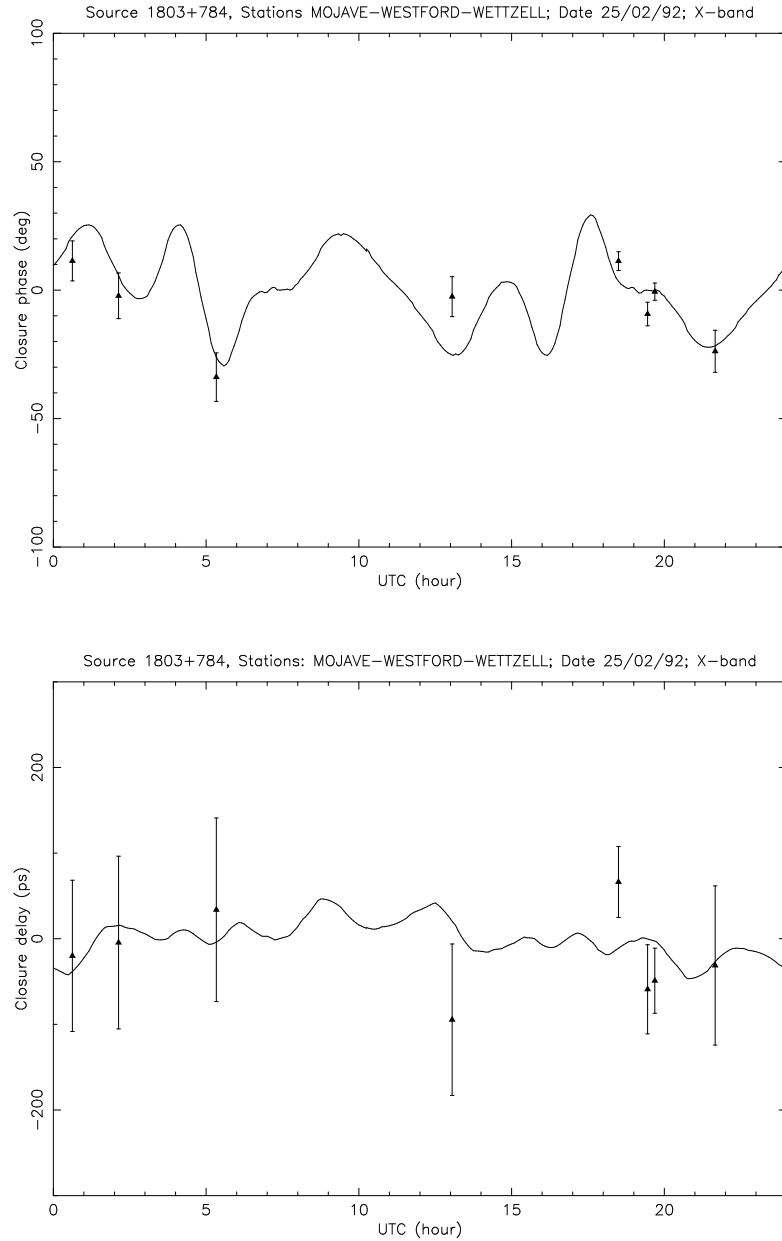


Figure 1: Closure phases and closure delays with respect to time for the triangle Mojave – Westford – Wettzell. Dots are observed closure quantities with their uncertainties, and computed closure quantities are the continuous curves.

Conclusion

The comparisons between computed and measured closure quantities have shown a good agreement. The computation of the additional delay due to source structure is now available and can be used with the geodetic/astrometric VLBI software CALC and SOLVE. We have now to map all sources observed during this experiment and compute source structure delay corrections for each observation in order to analyse the influence of source structure on the accuracy of geodetic parameters and source positions.

Acknowledgements

The first author gratefully acknowledges the receipt of a Research Fellowship in the VLBI project of the EC Human Capital and Mobility Programme to carry out this research.

References

- IERS: 1994, *Technical note 17*, P. Charlot, ed., Observatoire de Paris.
 IERS: 1994, *The 1993 Annual report*, Observatoire de Paris.
 Pearson, T.J. and Readhead, A.C.S.: 1984, *Ann. Rev. Astron. Astroph.*, p. 97f.
 Thomas, J.B.: 1980, *JPL Publ. 80-84*, Pasadena, California, USA.

DISCUSSION

L. Gurvits (Q): Do you take into account frequency dependent effects in “positioning” of a bright feature in source structure?

A.-M. Gontier (A): Not at the moment.

R.T. Schilizzi (Q): At a resolution of 0.25 mas, most compact sources will be variable. How do you take account of variability?

A.-M. Gontier (A): Geodetic campaigns, which are made regularly (every month), can be used to monitor source structure and detect time variations.

L. Bååth (Q): Is anyone working on looking into going back into the 25 years of geodetic data and connect for source structure?

A.-M. Gontier (A): This study is actually made on recent geodetic data but possibly will be extended to previous data.

High Frequency Variations of EOP from Extensive VLBI Operations in January, 1994[†]

S.L. BOLOTIN

Main Astronomical Observatory, Kiev, Ukraine

Abstract

Results of processing the VLBI observations of extensive VLBI/GPS campaign in January 12–24, 1994, are presented. The IERS Standards (1992) have been used for modelling group delays and SRIF-technique (Square Root Information Filter) has been used for estimating, predicting and smoothing of solved for parameters. Clock parameters, wet zenith delays, corrections to Earth orientation parameters ($UT1$ and pole coordinates X , Y) have been considered as stochastic parameters in conformity with random walk stochastic model. The power spectral densities of $d(UT1 - UTC)$, dX and dY values have been calculated.

Introduction

The geodetic Very Long Baseline Interferometry (VLBI) is a unique technique permitting determination of all five Earth orientation parameters ($UT1$, pole coordinate X , Y and celestial pole offset $\Delta\psi$, $\Delta\epsilon$) simultaneously. During the last few years there was a significant progress both in the accuracy of VLBI-observations and reducing of these observations. It allows to obtain polar motion variations with precision higher than 0.1 mas for dX and dY and Earth rotation variation with precision higher than 0.05 ms for $d(UT1 - UTC)$. Majority of geodetic VLBI studies determine the estimations of EOP averaged over a one day period. However high accuracy of VLBI-observations allows to investigate the behaviour of EOP variations at subdaily time scales.

Recent theoretical studies of the Earth rotation have predicted the existence of diurnal and semidiurnal signals in $d(UT1 - UTC)$, dX and dY due to ocean tides (Gross [1993]). There are at least three different methods for determining the subdaily variations in the EOP from VLBI-observations:

- 1) parametric estimation;
- 2) LS-estimation of EOP values averaged over finite time interval;
- 3) stochastic estimation.

In case of parametric estimation the amplitudes and phases of signals at selected harmonics are estimated. The second method generates least square (LS) estimates averaged over finite time (usually, 1 – 2 hours). By introducing the mapping equation to tie the system state equations for adjacent sampling intervals, we turn to stochastic estimation. This allows also to decrease the lengths of sampling intervals. One could realize the third method by using the Kalman filter technique (for example, Herring *et al.* [1990]). For this purpose we have used Square Root Information Filter (SRIF) described in Bierman [1977] because of its numerical stability and ability to save results of calculations for following smoothing of parameters.

[†]Paper not presented orally

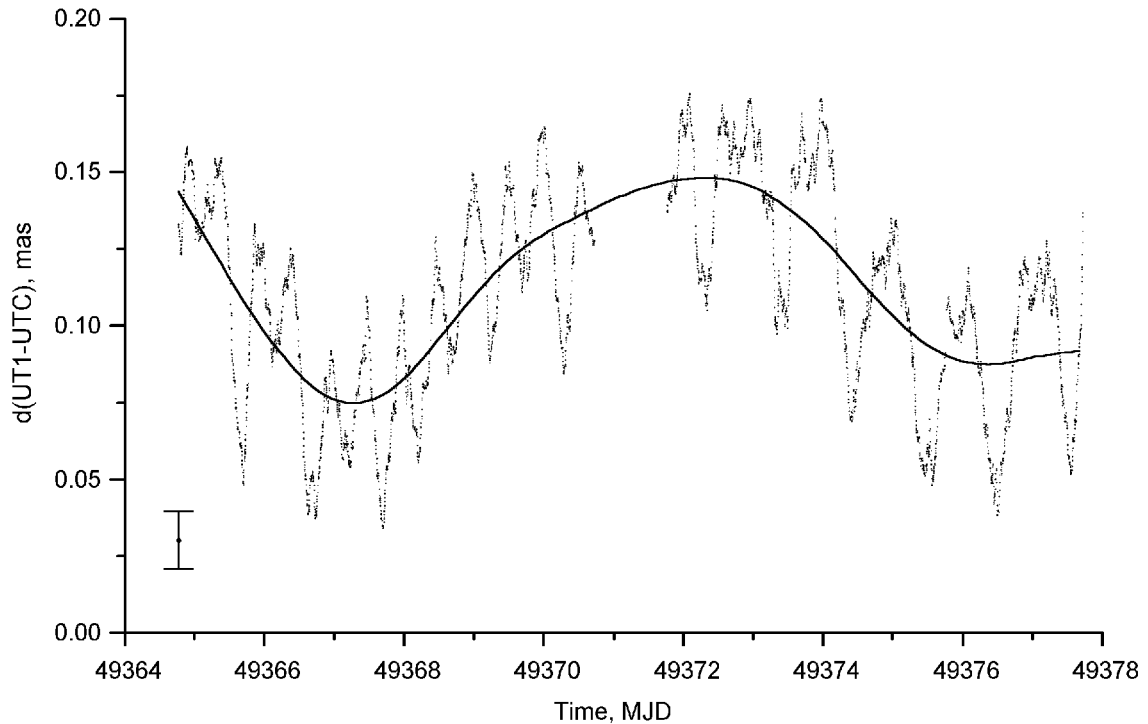


Figure 1. The estimates of $d(UT1 - UTC)$ at 13-days interval. The estimates of $d(UT1 - UTC)$ are shown by dots and 1 standard deviation error bar is placed in left bottom corner of the panel. Slowly varying part of $d(UT1 - UTC)$ is shown by solid line.

The SRIF-technique consist of the following steps:

- 1) initializing of equation of system state (*a priori* data);
- 2) “Data update”: involving the information of measurement equation into the equation of system state for given epoch;
- 3) “Time propagation”: prediction of system state at next observation epoch (an equation of mapping);
- 4) calculating of smoothed estimates and covariances.

Procedures 2) and 3) are repeated sequentially up to the moment when all data are processed. After performing “Data update” one can obtain filtered estimates from system state equation. These estimates contain information of *a priori* data and information of observations up to epoch of current observation. After “Time propagation” one can obtain estimates predicted at next observation epoch. Smoothed estimates contain information of *a priori* data and information of full set of processed data. In general, this property of smoothed estimates is the main difference between stochastic and LS estimation.

Data used

The extensive VLBI/GPS campaign in January 1994 was conducted by NASA GSFC VLBI group in order to compare Earth orientation results (hourly and daily values) derived by the VLBI networks and the IGS network, and the recovered stochastic atmosphere calibrations at collocated VLBI/GPS sites. This campaign was carried out during the period of January 11–26, 1994. It was supposed that VLBI stations would produce nearly continuous series of observation.

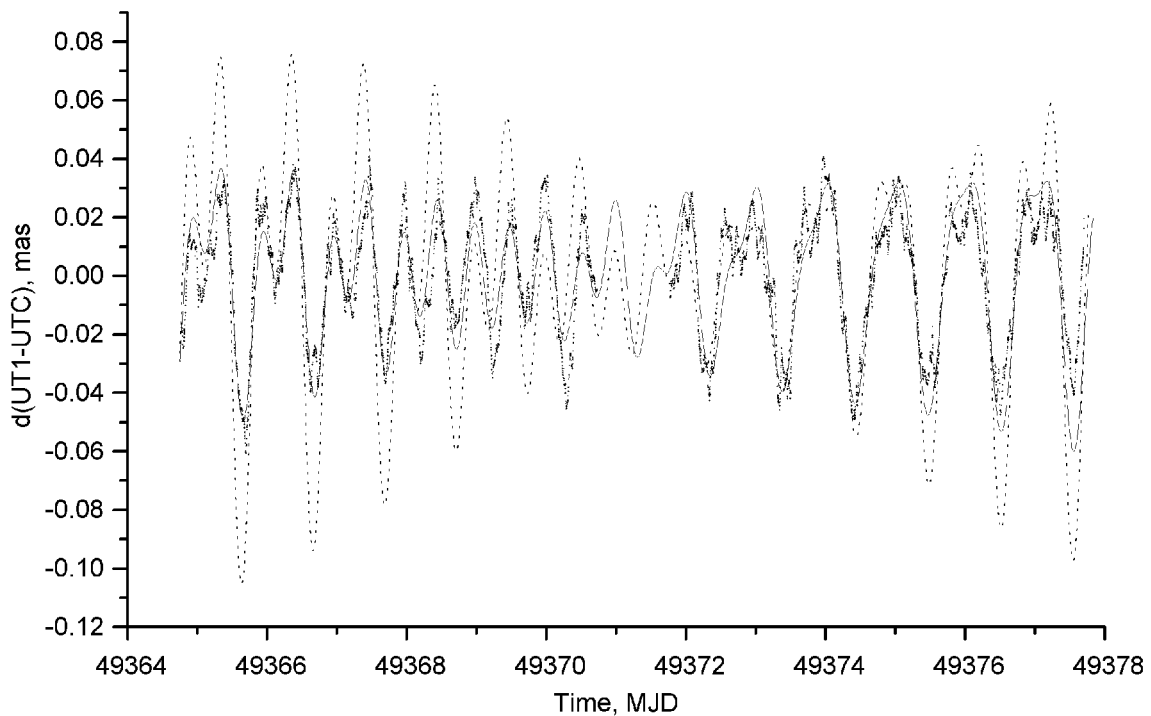


Figure 2. The subdaily variations in $d(UT1 - UTC)$. The dots are the subdaily variations of $d(UT1 - UTC)$ after eliminating long periodical variations. The solid and dotted lines are the variations of $d(UT1 - UTC)$ according to Herring and Dong [1993] and Gross [1993] respectively.

There were up to 24 VLBI stations that made observations simultaneously in three separate network (NASA-R&D, VLBA and NAVEX-G). We have processed observations of one of these networks (NASA-R&D). There were 7 stations: Fairbanks (Alaska), Kokee Park (Hawaii), Westford (Massachusetts), Los Alamos VLBA (New Mexico), Wettzell (Germany), Onsala (Sweden), and Fort Davis VLBA (Texas) and 41 radio sources. It turned out that the NASA-R&D observations were conducted from 12 January to 25 January and there was a one-day gap in observations on 18/19 January (when the stations took the day off).

Reduction of data

We have developed our own software **SteelBreeze 1.0** for reducing the VLBI observations. This software is based on the SRIF technique mentioned above and the IERS Standards [1992].

The ITRF92 (solution SSC(IERS)93C01) with its velocity field and ICRF92 (solution RSC(IERS)93C01) were used as a realizations of the Terrestrial Reference Frame (TRF) and the Celestial Reference Frame (CRF) respectively. The IAU 1980 Nutation model and initial values of EOP(IERS)90C04 were applied.

Tropospheric refraction in the local zenith direction caused by hydrostatic and water vapour components of the neutral atmosphere was modelled according to Saastamoinen [1972]. The zenith delays were mapped to line of sight elevations with the MTT mapping function of Herring [1992] for both hydrostatic and wet components.

The ionosphere effect was eliminated by using of simultaneous dual frequency observations.

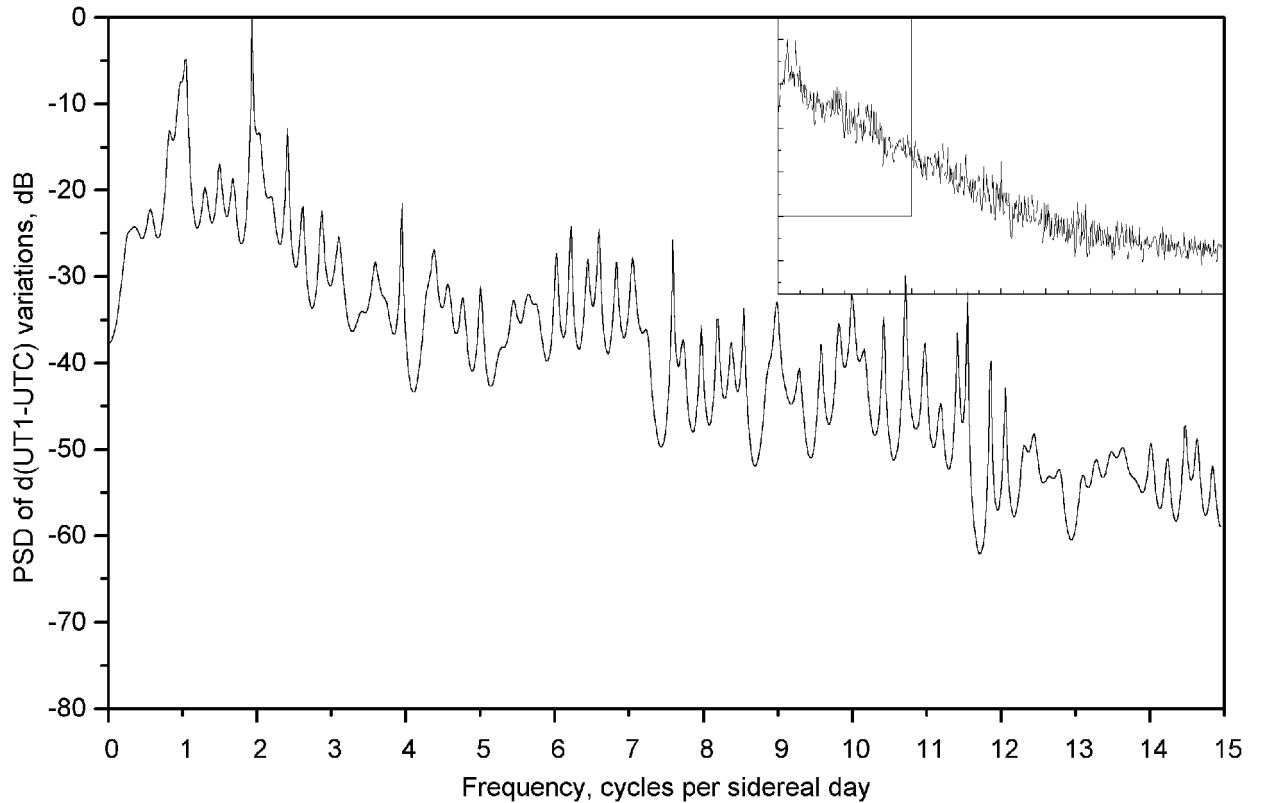


Figure 3. The power spectral densities of variations in $d(UT1 - UTC)$. Main plot is the PSD of variations in $d(UT1 - UTC)$ for selected frequency range 0 – 15 cycles per sidereal day. The PSD for full frequency range (0 – 50 cpsd) is plotted at the right top corner of the panel.

Calibration data collected at each observing site were applied to correct for variations in the electrical length of the cables between the radio receivers and the data acquisition systems.

All adjusted parameters have been treated as stochastic processes except for Celestial Pole offset. We have modelled the stochastic process as random walk with magnitudes of power spectral density of ruled white noise:

- for time offset in clock model: $18^2 \text{ ps}^2/\text{hour}$;
- for wet component of tropospheric delay: $1.0 \text{ cm}^2/\text{hour}$;
- for $d(UT1 - UTC)$: $0.012^2 \text{ ms}^2/\text{hour}$;
- for dX and dY : $0.16^2 \text{ mas}^2/\text{hour}$.

Clock parameter and wet zenith delay at each observing site have been reset as soon as new session has started. Therefore it has not been assumed continuity in behaviour of these parameters at the boundaries of sessions. But Earth rotational parameters have not been reset and these parameters have been processed as continuous series for whole interval of observations.

Nutations in longitude and obliquity have been treated as global parameters for the whole period of observations, because numerical experiments have shown that there are not significant variations in these parameters and there is bias in Celestial Pole only defined by solution EOP(IERS)90C04 and derived from these data. We have obtained the following magnitudes for this bias: $d\psi = 0.887 \pm 0.094 \text{ mas}$ and $d\epsilon = 0.002 \pm 0.038 \text{ mas}$.

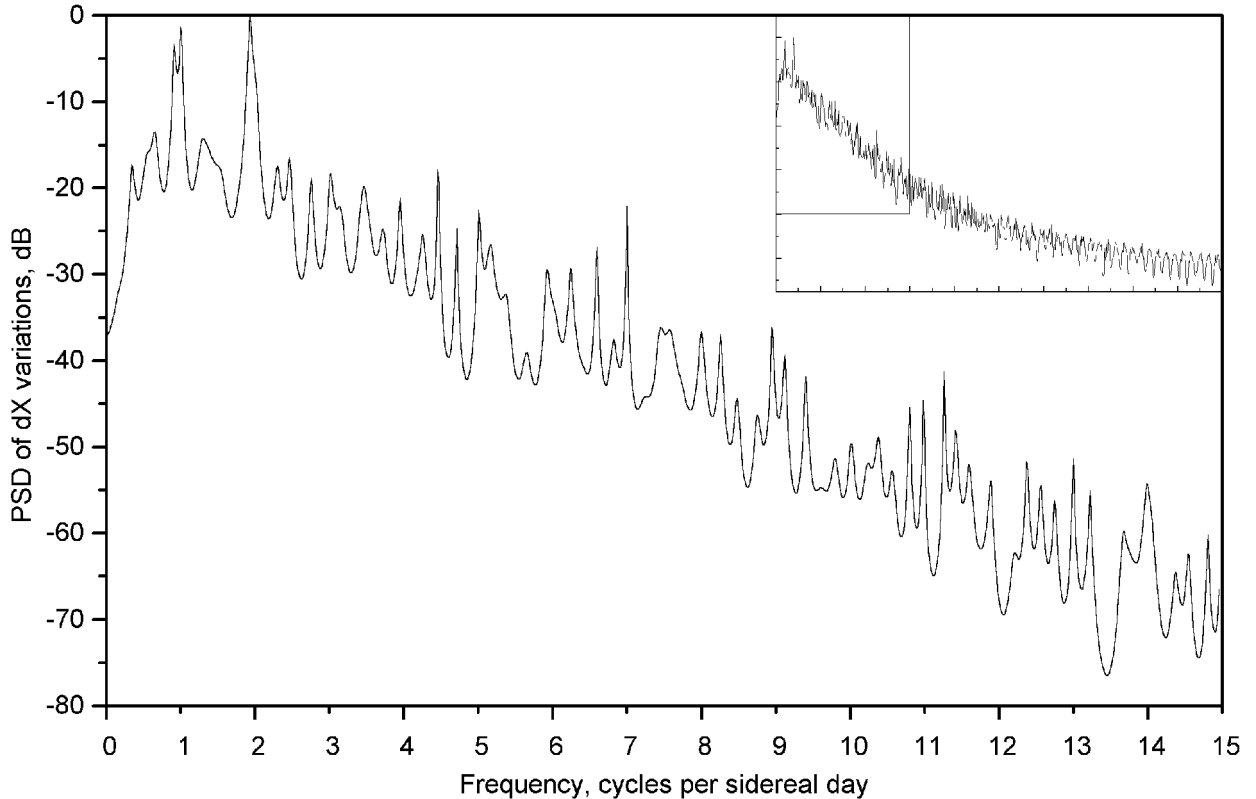


Figure 4. The PSD of variations in dX (see Fig. 3 for details).

Results

Altogether 27,975 group delays with quality factor 0 only have been processed. The final weighted rms post-fit residual is 10.30 ps.

Long periodical variations of Earth orientation parameters have been eliminated by performing cubic spline smoothing. As an example, Fig. 1 illustrates the estimates of $d(UT1 - UTC)$ and its long periodical variations, and Fig. 2 illustrates variations of $d(UT1 - UTC)$ at subdaily time scales and its comparison with theoretical (Gross [1993]) and empirical (Herring and Dong [1993]) models of diurnal and semidiurnal variations in $d(UT1 - UTC)$.

It is easy to see that the Earth orientation parameters defined by solution EOP (IERS)90C04 and derived from processed set of data have both biases and long periodical variations.

We have interpolated the EOP variations at subdaily time scales to uniformly spaced series using cubic spline with slight smoothing. These series have had 0.01 day spacing.

We have calculated the power spectral densities of uniformly spaced $d(UT1 - UTC)$, dX and dY series for the whole interval of observations. For this purpose we have used spectral analysis technique described in Marple [1980]. The results are plotted in Fig. 3 – Fig. 5 for Earth rotation parameters. The diurnal and semidiurnal bands are clearly visible for all estimated EOP. The power at these frequencies is 20 dB higher than at other frequencies. However, obtained spectra are different from spectra of above mentioned tidal models with additive noise for the same time series. It is possible that signals distinctive from tidally coherent ones are present in Earth rotation variations and polar motion.

Atmosphere calibrations obtained are available in form of ASCII files through e-mail: maouas@gluk.apc.org (S. Bolotin).

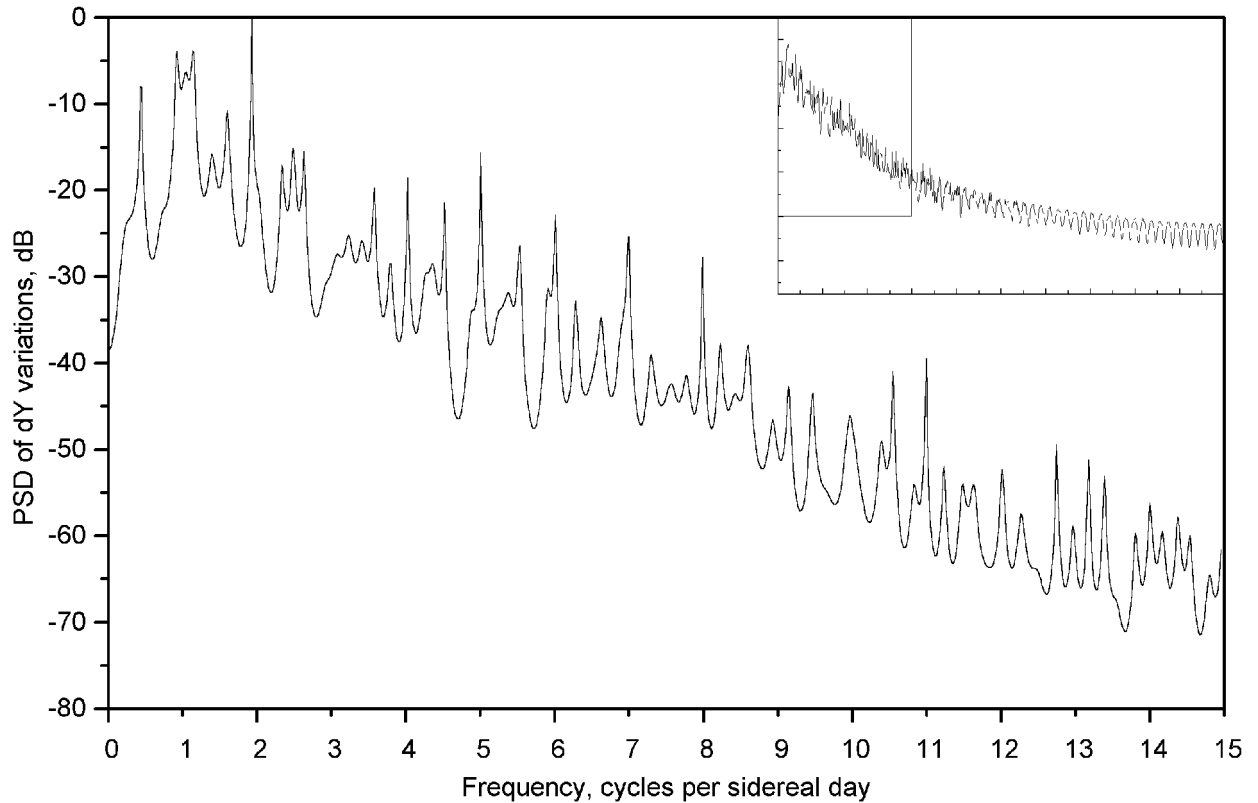


Figure 5. The PSD of variations in dY (see Fig. 3 for details).

Acknowledgments: This work was partly supported by the International Science Foundation under grant **V4S000**. I am very grateful to J.W. Ryan of NASA/GSFC for providing me with VLBI-observations data. Also, I thank K.Kh Nurutdinov for useful discussions.

References

- [1] Bierman, G.J., 1977, Factorization Methods for Discrete Sequential Estimation, V128, Mathematics in Science and Engineering Series, Academic Press.
- [2] Gross, R.S., 1993, The effects of ocean tides on the Earth's rotation as predicted by the results of an ocean tide model, *Geophys. Res. Letters*, **20**, 293–296.
- [3] Herring, T.A., Davis, J.L., Shapiro, I.I., 1990, “Geodesy by Radio Interferometry: The Application of Kalman Filtering to the Analysis of Very Long Baseline Interferometry Data”, *J. Geophys. Res.*, **95**, No. B8, pp. 12561–12581, August 10, 1990.
- [4] Herring, T.A., 1992, *Proceedings of the symposium on Refraction of Transatmospheric Signals in Geodesy*, ed. by J.C. De Munch and T.A.Th. Spoelstra, Netherland Geodetic Commision, Delft, Netherlands, *Publications on Geodesy*, No 36, 157–164.
- [5] Herring, T.A, and Dong, D., 1993, “Measurement of Diurnal and Semidiurnal Rotational Variations and Tidal Parameters of the Earth”, (submitted to *J. Geophys. Res.*, July, 1993, revised December, 1993).
- [6] International Earth Rotation Service, IERS Standards, *IERS Technical Note 13*, ed. D.D.McCarthy, Paris, France, 1992.
- [7] Marple S.L., Jr., 1980, A New Autoregressive Spectrum Analysis Algorithm., *IEEE Trans. Speech Signal Process.*, vol. ASSP-**28**, 441–454, August, 1980.

A New Approach to the Analysis of Interferometric Data

D. FRAIX-BURNET, V. DESPRINGRE, E. ANTERRIEU and A. LANNES

Laboratoire d'Astrophysique de Toulouse
Observatoire Midi-Pyrénées
14 Avenue Edouard Belin, F-31400 Toulouse, France

Abstract

We present a new technique for Fourier synthesis referred to as FIRST or WIPE depending on what is emphasized, FIRST for the principle (Fourier Interpolation and Reconstruction via Shannon-type Techniques), and WIPE for the corresponding reconstruction method (WIPE being reminiscent of CLEAN). This method, developed by A. Lannes and E. Anterrieu, is now operational for calibrated data. We illustrate the main features of WIPE on Plateau de Bure data of the jet in M87 at 89 GHz (construction of the object representation space, control of robustness at each step, critical eigenmodes to identify artefacts, etc.). This technique is about to be incorporated into a self-calibration procedure for VLBI, and current developments include multiresolution and multispectral Fourier synthesis.

Introduction

In aperture synthesis, the data are complex quantities corresponding to a *finite* and *irregular* sampling of the Fourier transform of some *object brightness distribution*. More precisely, the data are blurred values of the Fourier transform of the *object* function (multiplied by the incoherent point-spread function of the pupil elements of the array, i.e., the *antenna reception pattern*) on a given *experimental frequency list*. In general this information is partly completed by the expertise of the observer. The problem is to reduce the overall input information to a more compact form, directly interpretable in terms of object representation.

The guiding idea of the method presented in this paper is based on the *Shannon sampling formula*, whence the name of the principle: FIRST (Fourier Interpolation and Reconstruction *via* Shannon-type Techniques). To cope with the difficulties arising from the finite and irregular character of the data sampling, this elementary reference must of course be enriched by other theoretical considerations. In particular, very powerful tools are to be found in *approximation theory* and in *multiresolution analysis*. For example, the concept of “regularization” proves to play an important role in practice. Likewise, as most of the images of physical interest have features at different levels of resolution, multiresolution analysis is a key related topic (Mallat 1989; Wickerhauser and Coifman 1992). It is intuitively clear that the study of the reliability of a Fourier synthesis operation requires a few tools of this type, in particular when reconstructing large fields.

The motivation at the origin of this work was to apply these general concepts to aperture synthesis, and thereby to make the link with the experience of radioastronomers in aperture synthesis. This is why the widely-used technique in astronomy, CLEAN, appears in counterpoint. We will even adopt its terminology for describing the corresponding deconvolution method of FIRST: WIPE.

In its global approach to Fourier synthesis, the regularization principle of FIRST, and its implementation through WIPE, allows us to cope with the following difficulties (Lannes, Anterrieu and Bouyoucef 1994a, 1994b):

- 1) the finite and irregular character of the Fourier data sampling: its relation to the *field* and the *resolution* of the reconstructed images;
- 2) the choice of a *continuous finite representation* of the images to be reconstructed;
- 3) the need to find a way of incorporating the *expertise of the observer* into the methodology, as flexibly as possibly;
- 4) control of the *robustness* of the corresponding reconstruction procedures;
- 5) provision of basic tools for further developments towards *mosaic image reconstruction in multiresolution Fourier synthesis*;
- 6) the use of the *Fast Fourier Transform* in such a framework (“non-Cartesian Fourier sampling”).

General review of FIRST

The regularization principle of FIRST is based on the definition of three Hilbert spaces: the *object workspace*, the *Fourier data space* and the *object representation space* which is included in the first one. The corresponding regularization parameters are related to the *field* of the object workspace, to the *frequency coverage to be synthesized* and to the *synthesized field*. The parameters characterizing the multiresolution structure of the object representation space can also be regarded as regularization parameters. All these parameters, which are interpretable in terms of object representation, can be modified throughout the image reconstruction procedure. FIRST is therefore very flexible and particularly well suited to incorporating the expertise of the observer.

In the absence of any *a priori* information on the support of the original object, the field of the object workspace must contain the effective support of the antenna diffraction pattern. The choice of the frequency coverage to be synthesized of course depends on the experimental frequency coverage, but also on the quality of the data. The *resolution scale* of the object workspace is selected, *via* an *oversampling parameter*, as a fraction of the resolution limit corresponding to the frequency coverage to be synthesized. In general, the density of the experimental frequency coverage is too low for reconstructing, within the resolution limit, an image that would cover the entire field of the object workspace. Finally, the choice of the synthesized field therefore depends on this density and on the multiresolution structure of the object as it is revealed by the reconstruction process (*field aliasing effects* may then blur the reconstructed image). All these choices are controlled through an appropriate analysis of the error propagation. The *condition number*, which is an increasing function of the amount of interpolation to be performed both in the object and Fourier domains, must be relatively small (say < 5); otherwise the reconstruction process is slow and in practice unstable. This is the basic reason why the reconstruction methods are necessarily limited in their objectives, and that the notions of field and resolution should explicitly appear in their principle.

The reconstructed image is defined as the function minimizing an objective functional of the form $\|\Psi - A\phi\|^2$ where ϕ is the image variable; A is some regularized Fourier sampling operator, acting from the object workspace into the Fourier data space; Ψ represents the regularized Fourier data, i.e., the experimental Fourier data damped by the Fourier transform of the apodized point-spread function. This function, the *neat beam*, which results from the choice of the frequency coverage to be synthesized, is the analogue to the *clean beam* in CLEAN. The objective functional corresponds to a hybrid criterion in the sense that it can be decomposed into two components: an experimental criterion

plus a regularization criterion. The first one constrains the image to be consistent with the regularized Fourier data, whereas the second one is of course related to the resolution properties of the reconstruction process.

The objective functional of CLEAN, which only refers to the experimental frequency list, is not regularized. To circumvent this difficulty, CLEAN *implicitly* proceeds as follows. The choice of the object representation space is defined *via* the localization of the main components of the object map: a series of delta functions on a grid having some level of oversampling. To this end, CLEAN uses, implicitly, the old method of Southwell (Schwartz 1978). This technique also gives an approximation to the solution of the corresponding normal equation. This image is unstable; indeed, in general, the corresponding field constraint is not sufficient for regularizing the results: the problem must be stated in terms of Fourier interpolation. This is why CLEAN smoothes the unstable image in question by a given point-spread function: the *clean beam*. The latter is most often chosen to be a Gaussian with half-amplitude width equal to that of the dirty beam. This regularization process, which yields the *clean map*, is thus performed *a posteriori*. The clean map is therefore not defined as the function minimizing a given objective functional. The reconstructed image of this *ad hoc* method must be accepted *as it is*. In other words, the heuristic approach adopted in CLEAN cannot provide any further results concerning, for instance, the study of the error propagation (in short, no error bars with CLEAN).

It is of course preferable to define the image to be reconstructed from the outset, to complete the general regularization scheme, and then to reconstruct the image *directly* by solving the regularized normal equation $A^*A\phi = A^*\Psi$ (with the aid of the conjugate-gradient method for example). Then, the reconstruction process is stable, faster and perfectly controlled. Moreover, the study of the error propagation can then be developed on the grounds of the Singular Value Decomposition of the regularized Fourier sampling operator (A) restricted to the object representation space.

General review of WIPE

WIPE, the imaging kernel of FIRST, is the *constructive process* minimizing the objective functional. The domain of this functional is the object representation space, or a more general convex set when dynamic-range constraints are imposed. For simplicity, and without any loss of generality, let us consider the special case where the image is simply confined to a linear space such as the object representation space. WIPE is then led to solve the normal equation, in which the *dusty map* ($A^*\Psi$) proves to be the discrete convolution of the traditional *dirty map* by the *neat beam*. The dusty map, which can be obtained through a sort of *back Fourier sampling* operation, is a blurred version of the object within the level of resolution determined by the choice of the frequency coverage to be synthesized. The frequency gaps, the systematic errors and the noise limit the quality of this representation. To improve this image, one must inject some *a priori* information (here, the choice of the object representation space, i.e. for instance the support of the object), and then solve the normal equation with an appropriate iterative method. The *neat map* is then obtained as the function minimizing a well defined objective functional. This point is essential for the interpretation of the results in terms of field, resolution and brightness.

At each iteration of the selected constructive process, the experimental dusty map is compared with the *dusty map of the current image*. The corresponding operation, $A^*A\phi$, proves to be a *truncated discrete convolution*, in which the discrete point-spread function, the *dusty beam*, has two components: the traditional *dirty beam* and the *regularization beam*. Their discrete Fourier transforms are the *dirty transfer pattern* and the *regulariza-*

tion transfer pattern, respectively. The speed of the Fast Fourier Transform (FFT) is a major advantage in computing large maps. This algorithm is therefore used for calculating this truncated discrete convolution.

The *object gridding operations* concerning the dusty map and the dirty beam can be performed without any loss of accuracy through back Fourier sampling operations. To save computer time, these quantities can equally well be obtained “directly”. The approximations induced by the related *Fourier gridding operations* can be perfectly controlled. Let us finally note that the calculation of the regularization transfer pattern does not present any difficulty.

Example: Plateau-de-Bure data on M87

We are currently finishing the first test of WIPE on real data. We discuss in this paper preliminary results. A more complete description will appear elsewhere (Despringre *et al.* 1994). The data were obtained with the Plateau-de-Bure (IRAM) interferometer at 89 GHz. They consist of two sets, one with three antennas and the other with four antennas. These data were calibrated with the GILDAS package; we deconvolved them with CLEAN, as implemented in GILDAS, and with WIPE. The error analysis provided by WIPE shows that the stability of the reconstruction process is quite good for this type of object with an isotropic neat beam, even though the frequency coverage is anisotropic. The resolution level of the reconstruction process can therefore be chosen higher than that of the clean map. The stability is also good down to faint levels indicating that the reconstructed structures are not merely noise. However, because of the input errors (which also plays an important role in the study of the reliability of the final map), these structures can also be due to metrology or calibration errors. It is possible to “back-calibrate” the metrology with FIRST and we are currently investigating this point on the data set obtained with four antennas.

In summary, this real-data test seems to indicate that we can effectively extract more information with WIPE.

Concluding remarks

FIRST cannot be simply regarded as an updated version of CLEAN. In its conception, as well as in its technical developments, FIRST actually leads to a better understanding of what constitutes an image reconstruction procedure in Fourier synthesis.

In the implementation of FIRST, the regularization parameters are selected in an interactive way. The expertise of the observer can thus be easily incorporated into the reconstruction process. FIRST can be useful even when other Fourier synthesis methods are used (for example those based on a probabilistic approach). By simple examination of their results, it is possible to exhibit the corresponding regularization parameters of FIRST. By using these parameters, WIPE provides a neat map which is in general very close to that given by the particular technique thus tested. The robustness and the reliability of this neat map can then be examined on the grounds of the error analysis of FIRST. By using the triangle inequality, it is thus possible to verify *a posteriori* whether the implicit choices of the alternative approach are satisfactory. This deterministic aspect of FIRST is perhaps the most attractive.

FIRST is now about to be incorporated into a self-calibration procedure, so that we are keen on applying this new approach to VLBI data. Preliminary results on Plateau-de-Bure data on M87 give us confidence in that FIRST could become a widely used and appreciated technique for interferometric data.

References

- Despringre V., Fraix-Burnet D., Anterrieu E., Davoust E., Lannes A. 1994, in preparation.
Lannes A., Anterrieu E., Bouyoucef K. 1994a, *J. Mod. Opt.* 41(8), 1537.
Lannes A., Anterrieu E., Bouyoucef K. 1994b, *J. Mod. Opt.*, in preparation.
Mallat S. 1989, *IEEE Trans. on Pattern Analysis and Machine Intelligence*, 11(7), 674.
Schwartz U.J. 1978, *A&A* 65, 345.
Wickerhauser M.V., Coifman R.R. 1992, *IEEE Trans. on Information Theory*, 32, 712.

DISCUSSION

T. Krichbaum (Q): How is it possible to decide whether a “feature” in the map is real, due to calibration errors or sidelobes?

D. Fraix-Burnet (A): The condition number tells you whether the structure you try to deconvolve is due to noise or not. If it is not noise, it can be real or due to input errors. Metrology errors can be corrected by FIRST. But I do not think we could discriminate between real features and features due to calibration errors simply by using any software. The observer’s expertise is certainly needed as well as self-calibration procedures.

P. Wilkinson (Q): What is the speed of the programme compared with CLEAN and MEM? It’s important to have fast algorithms if the method is to be incorporated into the self-calibration loop.

D. Fraix-Burnet (A): The speed of WIPE is comparable to that of CLEAN. But of course the longest part is the interactive choice of parameters. Then the deconvolution is very quick.

L. Bååth (Q): What is your platform and data structure for the program?

D. Fraix-Burnet (A): Currently, there is no platform for our software but we have contacts to include it within AIPS++, and we are working on its implementation within the Caltech Package.

Status of the Space VLBI User Assistance Software Being Developed at the Satellite Geodetic Observatory, Hungary

I. NOSZTICZIUS

FÖMI Satellite Geodetic Observatory, Penc, Hungary
H-1373 Budapest, P.O. Box 546

Abstract

The Satellite Geodetic Observatory (SGO) has been involved in space VLBI related research since 1987. One of the main objectives of this research was to develop an assistance software to help the user community to prepare observing proposals for both planned space VLBI missions. (The Japanese VSOP and the Russian RadioAstron satellites are expected to be launched at the end of 1996 and in the first half of 1997 respectively.) The current version of the the Space VLBI Assistance Software (SPAS) is being developed since 1993. The software can be used to give some insight to the complex geometry of space VLBI missions, and for approximate scheduling of space VLBI observations taking various restrictions into account. The state of the development and some of its preliminary results will be presented.

Introduction

The SGO participation in VLBI research has been going on since 1987. The research includes both geodetic and astronomical aspects of Space VLBI. Part of this research is to develop a software tool to visualize the complex geometry of Space VLBI missions, (useful for the two VLBI satellites: VSOP and RadioAstron, to be launched in 1996 and 1997 respectively) check the technical restrictions posed by the satellite and the ground based telescopes and give some insight into the scheduling process and optimization of ground based tracking and radio astronomy networks. This tool called SPAS (Space VLBI Assistance Software) will replace an earlier program written at the observatory, and it will not only unify but will also expand the features of its progenitor. It will do all this in a very user friendly manner, by using a graphical user interface with menus and windows wherever possible, and a mouse as the main input device.

Software design

For the SPAS development project a team has been set up, which consists of three astronomers and two software engineers. This team is responsible for the design and development of the software, for which we have decided to follow the software engineering standards of the European Space Agency (ESA) [1]. We also have a cooperative project with the Agency, in which they agree to participate at the review meetings to supervise our development that the standards are satisfied. These standards do not only assure software quality, but also by following them one can easily trace the development (through heavy documentation) and make needed changes easier.

The software life cycle

According to the ESA software standards [1] the “evolutionary” approach of the Software Life Cycle has been adopted, which seems to fit best our design. This approach is characterized by planned development of multiple releases. All phases of the life cycle are executed to produce a release and each release incorporates the experience of earlier releases. This approach is justified because some of the requirements are difficult to meet within the planned time frame of the delivery. This decision was made in the Software Management Plan [6], where the project deliverables, responsibilities and managerial processes were also laid down.

Phases of the development

The development of the software – after the first version of the Software Management Plan – started with laying down the user requirements in the User Requirements Document [2]. The document is the output of the “problem definition phase”, where the users’ expectations of the software are collected. This was achieved by carrying out consultations and interviews to state the specific requirements of possible users. The users included people who may interact with the software (see Table 1).

Table 1. Possible users and applications of SPAS.

Possible group of users	Possible application
Scientists interested in VLBI and space VLBI research	Observation proposals
Students and trainees interested in space VLBI	Education and demonstration
Satellite operation and research groups	Operational research
Other users with special interest in orbit dynamics, space communication or remote sensing	Satellite orbit determination, modelling optimization

From the User Requirements and earlier software developed at the observatory we concluded what the software should be capable of, and came up with the following functions (see Table 2). These functions were specified in more detail in the Software Requirements Document. This document describes what the software should be capable of doing, without going into fine details about how it should accomplish those goals. Of course, not all user requirements were planned to be implemented in the current software, but they might be included in future versions (as well as requirements that arise during the development).

The next step in the software design was the Architectural Design, which resulted in the Architectural Design Document [4]. This document describes the physical model of the main components of SPAS based on the logical model. It also describes the structure of the whole program with top-down decomposition as well as the structure of the databases used by SPAS. For user program control we have chosen a nowadays common and widespread method: an event oriented environment (like MS Windows) where the user is “in charge” and the sequence of events (e.g. starting/aborting each subprogram) depends on her/him. The only exceptions are the tools to be included with the package, these will handle database conversions and archivation, and will be based on the DOS command line philosophy.

Table 2. SPAS main functions.

Module name	Purpose
UVPlot	Plot the baselines on the uv -plane, that is project the ground-to-ground, ground-to-space and space-to-space baselines on the plane perpendicular to the direction of the radio source.
3DView	Produce a 3-dimensional movie of the rotating Earth and the satellites orbiting around it as seen from a specified direction. This direction is the direction of the radio source, but can be modified.
SpaceView	Produce a 3-dimensional movie of the rotating Earth as seen from one of the selected satellites. Also display the telemetry stations and the subsatellite track on the surface.
SubSat	Plot the subsatellite track on the Earth map. Indicate if telemetry connection is active or not by using a different plot color.
SatVis	Display visibility diagrams of the satellites vs. time from selected telemetry stations. Satellite rise and set times are also available in written output (in file or on printer)
ObsInt	Display the visibility diagram of a given radio source vs. time from selected VLBI stations and satellites. Source rise and set times are also available in written output (in file or on printer)
TopoPos	Plot the topocentric coordinates (elevation vs. azimuth) of a given radio source and the selected satellites as seen from a VLBI station.
SkySurv	Create a survey for a specified area of the sky deciding if certain parts are observable from ground VLBI stations and satellites (a network) or not at a given time.
Access	Create a long term survey for a sky area. It shows how long (in percent) certain parts are observable from ground VLBI stations and satellites (a network) during a time interval.
CheckArc	Give information about the possible attitudes of a space VLBI satellite (taking on-board constraints into account) when observing a selected radio source during a time interval.
Beam	Select radio sources within the primary beam of a space VLBI antenna, for phase referencing purposes.
Sensitivity	Plot the RMS sensitivity of baselines as a function of integration time; plot the minimum detectable brightness temperature and the signal to noise ratio for the baselines as a function of time.
Cone	Select radio sources in special geometric configurations with respect to the satellite orbit normal.
Calculator	Perform basic calculations, unit conversions and coordinate transformations. (These calculations are also used by the other modules.)

Current status and some preliminary results of the project

Currently the project is in the Detailed Design phase, where the inner workings of the software is described in detail, and also the coding is done. For each module the document [5] contains a flow chart a pseudo code, and information about where the computer code can be found for that module. Flowcharts make it easy to follow and understand how

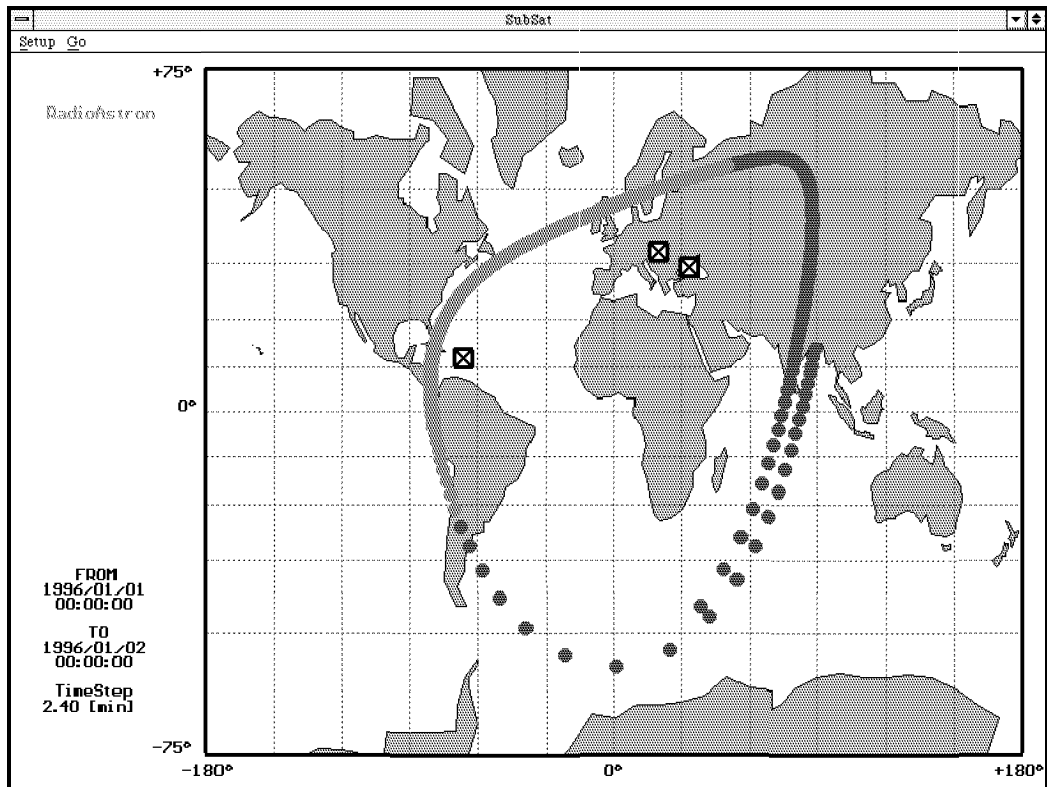


Figure 1: The SubSat output window — lighter color indicates when the satellite is trackable from the telemetry stations, indicated by a rectangle with a cross on the map.

each subprogram works, while the pseudo code — which is written with basic English words — gives a very good basis for programmers to code.

The coding of the program is currently about 50% finished, and it should be ready for first comparison testings by the first quarter of 1995. The following parts of the program are partially or fully completed :

- Graphical user interface
- Database management
- ObsInt, SubSat, SatVis, Sensitivity, TopoPos modules (see Figures 1-3)

Hardware and software requirements

SPAS is originally being designed for MS-DOS based IBM compatible machines, but future enhancements may include a version for the widely available UNIX system.

SPAS requires at least a 80386 (DX-33 MHz recommended) with 4 MB of RAM. A mathematical coprocessor is advised to increase the speed of calculations. An SVGA board with 1 MB is also recommended for producing really impressive graphics outputs. Although it is hard to estimate at this point of the development it is a good guess to say that the package will need about 2 Megabytes of disk space (excluding external databases, e.g. radio source catalogues).

A mouse as an input device — although not necessary — is required to take full advantage of SPAS' graphical user interface.

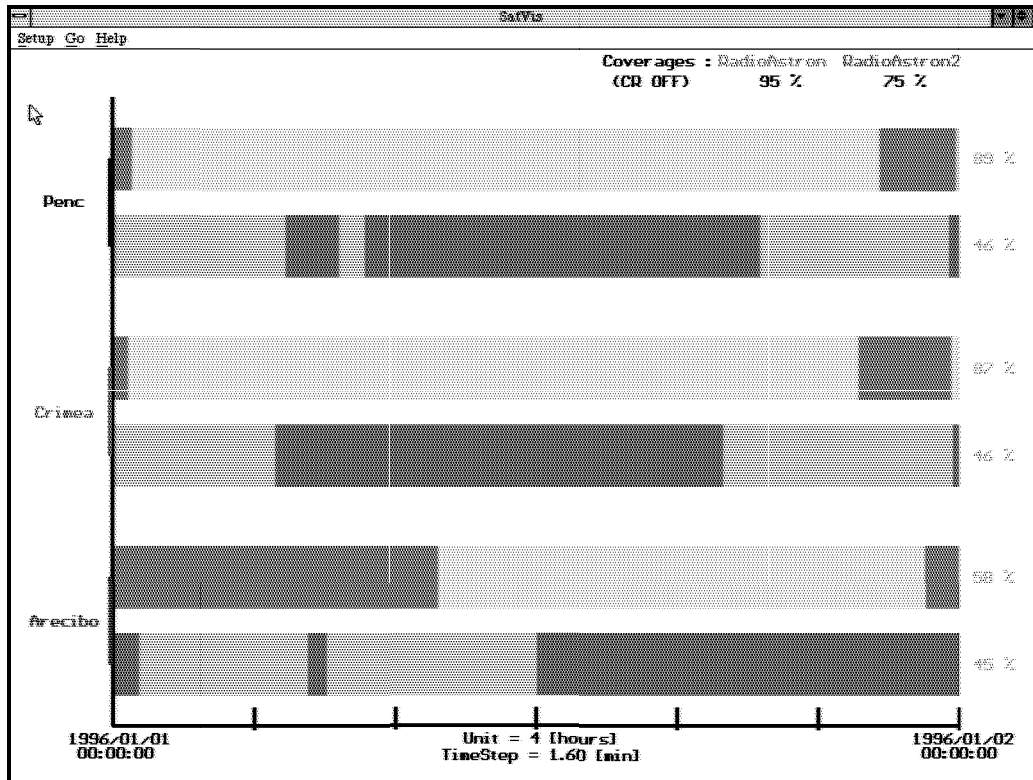


Figure 2: The SatVis output window — lighter color indicates when a given satellite is visible from a given telemetry station.

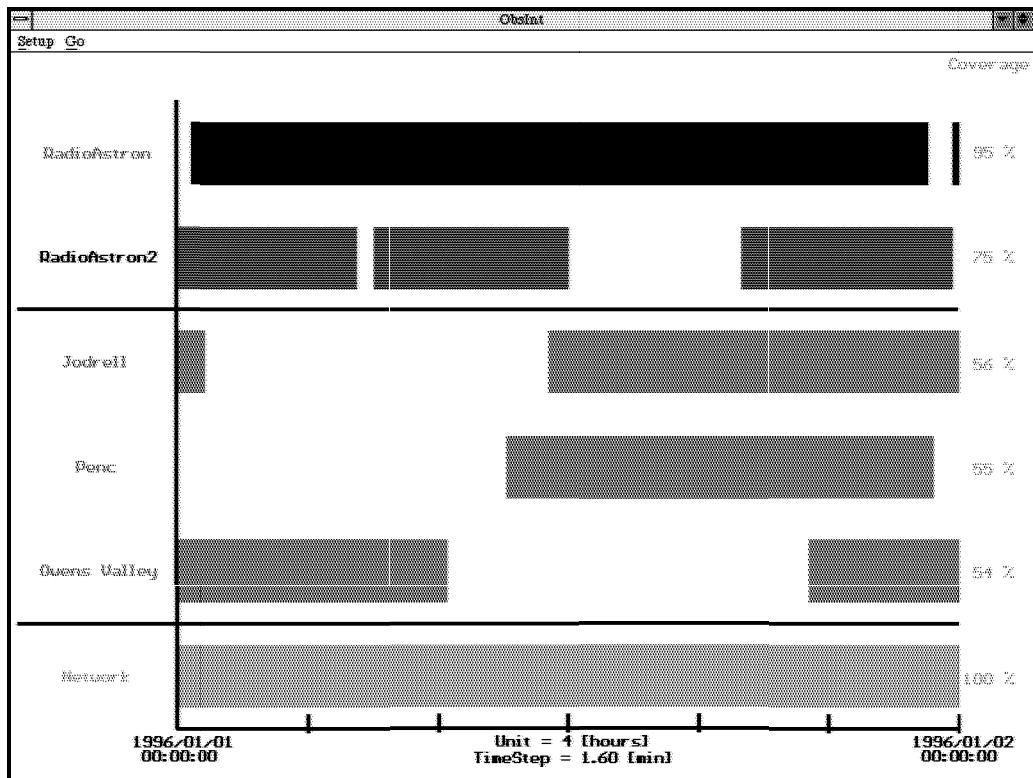


Figure 3: The ObsInt output window — shows when a given source is observable from the satellites, VLBI stations and the network (defined as a minimum of 2 stations or satellites).

Printer output will be available on a variety of models, but to produce the highest quality a HP LaserJet is recommended with at least 1.5 MB memory to achieve 300 DPI resolution.

Table 3. SPAS resource requirements.

	Minimum	Recommended
Operating System	MS-DOS V3.0	MS-DOS or DR-DOS V5.0, V6.0
Processor	80386	80386 DX-33MHz
CoProcessor	none	80387
Free Disk Space	about 2MB	about 2MB + catalogues
Memory (RAM)	2 MB (?)	4 MB
Graphics card	EGA/VGA/Hercules Mono	SVGA with 1MB VRAM
Printer	Epson compatible 9-pin matrix	HP-LaserJet (compatible)
Input device	Keyboard	Keyboard + Mouse

Development tools

SPAS is being developed using *Borland Pascal 7.0*, *Borland C++ 3.1*, and the *TEGL Windows Toolkit V3.1* for Borland Pascal (Protected mode). The Borland compilers proved to produce one of the smallest and fastest executable code and Borland Pascal is also able to compile to protected mode which gives the programmer more memory not only during compilation time but also inside his/her own programs by using the 16 bit linear address space. Also both languages come with a user friendly integrated development environment, command line compilers and various utilities.

The *TEGL Windows Toolkit V3.1* provides a perfect tool for creating a graphical user interface, but it also helps in a lot of more things (e.g. virtual memory, mouse and keyboard handling, icons, fonts, etc.)

Acknowledgements: This work is being supported by the Hungarian Space Office under contract MEC 93-0054 and by the Joint Institute for VLBI in Europe (JIVE) under contract with the Commission of European Communities (CHGECT920011).

References

- [1] ESA Software Engineering standards, ESA PSS-05-0 Issue 2, February, 1991, Paris, France.
- [2] *S. Frey*, SPAS User Requirements Document V2.1, May, 1993, Penc, Hungary.
- [3] *S. Frey*, SPAS Software Requirements Document V1.3, August, 1993, Penc, Hungary.
- [4] *G. Heitler*, SPAS Architectural Design Document, V3.0, February 14, 1994, Penc, Hungary.
- [5] *G. Heitler*, (ed.) SPAS Detailed Design Document, V2.2, August 24, 1994, Penc, Hungary.
- [6] *I. Fejes*, SPAS Software Management Plan, April, 1993, Penc, Hungary.

DISCUSSION

R.T. Schilizzi (Q): How many of the features of SPAS are needed to be used by a simple non-expert user?

I. Noszticzius (A): As with a lot of software, more functions are integrated into SPAS than an average user would use, but what seems important for one user might not be used by another, and vice versa. So I would say there are some basic functions that most radio astronomers interested in space VLBI could and would use (like UVplot and ObsInt) and there are some that are more “fun” functions (like 3DView and SpaceView) but create a good background for understanding the complex geometry of space VLBI experiments.

A.A. da Costa (Q): SPAS is DOS-based. What do you plan about a WINDOWS based SPAS, as DOS/WINDOWS seems to go to be substituted by CHICAGO?

I. Noszticzius (A): As SPAS is developed according to ESA standards — which include language and operating system independent design up to the coding phase — the software can be (and might be at a later stage) rewritten for other systems, like WINDOWS. Until then one must use the DOS compatibility box in CHICAGO; hopefully it works.

GPS QSO 2022+171 - A Possible Target for VLBI Detection of Gravitational Waves

S. POGREBENKO¹, M. MINGALIEV², S. MONTEBUGNOLI³,
S. NEIZVESTNY², N. BORISOV² and V. STOLYAROV²

¹ Joint Institute for VLBI in Europe, The Netherlands

² Special Astrophysical Observatory, Zelenchukskaya, Russia

³ CNR/IRA, Radio Astronomical Station Medicina, Italy

Introduction

The radio source 2022+171 (RA₁₉₅₀ = 20:22:39.54, Decl₁₉₅₀ = +17:08:25.0) was first discovered in the MG survey (Bennet *et al.*, 1986) and identified with $m_B = 17.5$ and $m_R = 19.5$ star-like object with the POSS (Lawrence *et al.*, 1986).

The source is of interest because it is at the angular distance of only 30 arcsec from a close binary star CM Del ($m_V = 13.4$, orbital period 3.9 h, (Shafter, 1985), finding chart — Vogt and Bateson, 1982) and may reveal an effect of phase modulation of an electromagnetic wave by a gravitational wave generated by the close binary (Laberie, 1993; Pogrebenko, 1994). The effect is potentially detectable with the global VLBI network if the radio source has a bright compact core with the sub-milliarcsecond angular size.

A study of the 2022+171 was started by us in order to determine an existence of the VLBI-detectable compact core, suitable for the future use of 2022+171 and CM Del pair as the observational target for the VLBI detection of gravitational waves.

Radio observations of the 2022+171

A 6-cm VLA snap-shot map of the 2022+171 (Lawrence *et al.*, 1986) presented in Fig. 1 shows a barely resolved quasi-point structure and about 90% of the total 5 GHz flux of the source is collected in this central region with the scale of 1.5 – 2 arcsec.

Observations of the 2022+171 at radio frequencies of 0.96, 2.3, 3.95, 7.7, 21.7 GHz were carried out by M. Mingaliev and V. Stolyarov with the RATAN-600 (Parijskij, 1993) and at 0.408 GHz by S. Montebugnoli with the Bologna Cross (Ficarra *et al.*, 1985) telescopes at June-August 1994 in order to obtain the radio spectrum and to classify the source more definitely.

To calibrate flux density measurements we used 3C138 as a calibrator for the RATAN and PKS 2021+168 and PKS 2024+171 for the Bologna Cross observations. Adopted flux densities of the calibrators available from literature (Kuhr *et al.*, 1981; PKSCAT90, 1990; Bennet *et al.*, 1986) are listed in Table 1.

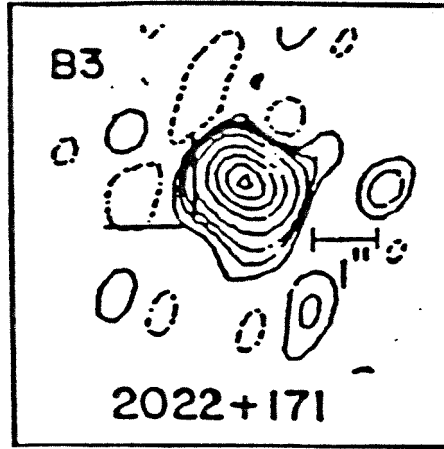


Fig. 1. The 6-cm VLA snap-shot map of the 2022+171 (Lawrence *et al.*1986).

Table 1. Flux densities of the calibration sources

<i>Frequency</i> (GHz):	0.408	0.960	2.300	3.950	7.700	11.200
<i>Source name</i>	<i>Flux</i> (mJy)					
3C138	–	11.300	6.700	4.150	3.000	2.100
PKS2021+168	2.610	–	–	–	–	–
PKS2024+171	2.420	–	–	–	–	–

The radio spectrum of the 2022+171 (see Table 2 and Fig. 2) observed at a broad wavelength region together with the data available from the literature (Bennet *et al.*, 1986; Lawrence *et al.*, 1986; Condon and Broderick, 1986; Gregory and Condon, 1991) show a GPS-like shape with a turnover frequency of 6–7 GHz and spectral index 0.1 in a 8 GHz – 11 GHz band and -0.6 in a 0.4 GHz – 5 GHz band. The cut-off of the spectrum at low frequency exhibits some slow-down.

Table 2. Radio spectrum of 2022+171

N	Frq (GHz)	BW (MHz)	Flux (mJy)	Err (mJy)	Epoch (Y)	Telescope	Ref
1	0.408	2.4	175	50	1994.6	BoCross	This paper
2	0.960	120.0	195	20	1994.5	RATAN	This paper
3	1.400	60.0	250	10	1983.8	GB-300	2
4	2.300	250.0	359	34	1994.5	RATAN	This paper
5	3.950	500.0	485	24	1994.5	RATAN	This paper
6	4.775	580.0	480	15	1982.8	GB-300	1
7	4.850	600.0	586	80	1987.8	GB-300	4
8	4.885	580.0	446	25	1982.8	VLA-B	7
9	7.700	600.0	582	36	1994.5	RATAN	This paper
10	11.200	1000.0	553	26	1994.5	RATAN	This paper

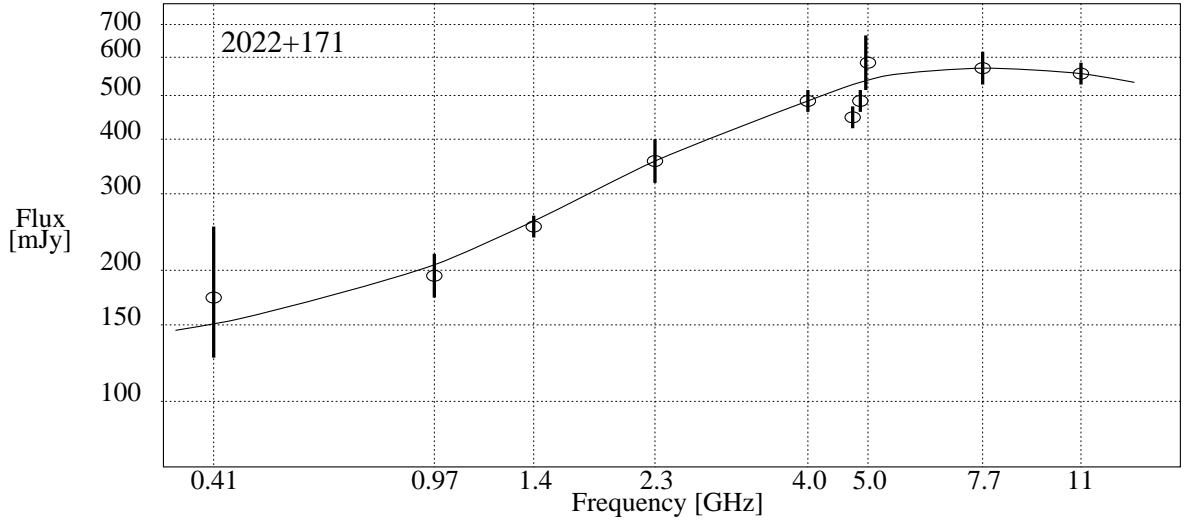


Fig. 2. The radio spectrum of the 2022+171

Optical identification

To prove 2022+171 is extragalactic, its optical spectrum was observed with the 6-meter telescope BTA by S. Neizvestny and N. Borisov in August 1994 using the 2*1024 channel photon counting spectrometer (Zinkovsky *et al.*, 1994). To observe the source, the POSS optical identification and VLA coordinates from Lawrence *et al.*(1986) were used.

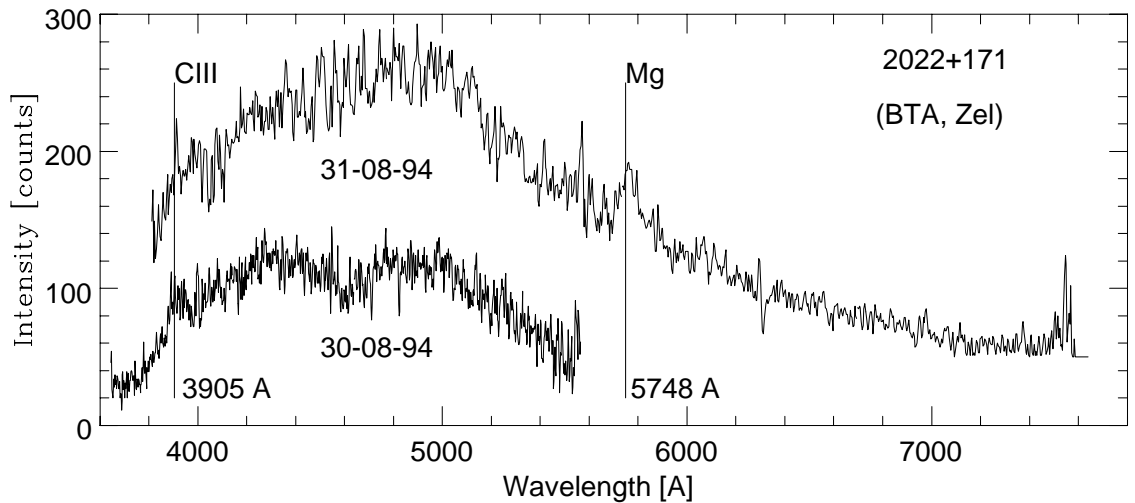


Fig. 3. Optical spectrum of the 2022+171

The spectrum observed is presented in Fig. 2. At optical wavelengths, the object shows a very blue continuum. Two emission lines at 5748 Å and 3905 Å are identified with those of Mg and CIII at $z = 1.05$, so, it is almost definitely a QSO.

Conclusions and further steps

The VLA data, the GPS-like radio spectrum and the QSO-like optical identification at $z = 1.05$ lead us to expect a core of 200 to 400 mJy, well suitable for the possible use with gravitational wave VLBI detectors.

An additional astronomical study of the 2022+171 (including MERLIN and EVN observations) is planned in order to obtain high resolution and high dynamic range radio maps. The monitoring programme, currently running at RATAN and Bologna Cross radio telescopes, will measure any variability in the source strength.

Also, it is necessary to re-observe CM Del in order to determine more accurately the orbital period, components' masses, the orbit inclination and the distance from the Earth.

Acknowledgement

Observations with the RATAN-600 radio telescope and the 6-meter optical telescope were carried out within the frame of the INTAS project #94-4010 coordinated by the Joint Institute for VLBI in Europe.

References

1. Bennet *et al.*, 1986, ApJS, 61, 1.
2. Condon & Broderick, 1986, A 1400 MHz sky atlas, NRAO.
3. Ficarra *et al.*, 1985, A&AS, 59, 255.
4. Gregory and Condon, 1991, ApJS, 75, 1011.
5. Kuhr *et al.*, 1981, A&AS, 45, 367.
6. Laberie, 1993, A&A, 268, 823.
7. Lawrence *et al.*, 1986, ApJS, 61, 105.
8. Parijskij, 1993, IEEE A&P, 35(4), 7.
9. PKSCAT90, 1990, ATNF.
10. Pogrebenko, 1994, XXII GA IAU Astronomy posters abstr., 105.
11. Shafter, 1985, AJ, 90, 643.
12. Vogt & Bateson, 1982, A&AS, 48, 383.
13. Zinkovsky *et al.*, 1994, Spectroscopic complex for Nasmyth-1 focus of the 6-m telescope. Manual guide. SAO RAN Library.

DISCUSSION

J.-F. Lestrade (Q): How are you going to discriminate between the intrinsic variability of the quasar and this effect caused by the gravitational wave radiated by the binary.

S.V. Pogrebenko (A): The modulation effect has an exactly known frequency — twice the frequency of the binary star rotation. Thus, a periodicity analysis will be a suitable tool.

A. Ipatov (Q): Would the influence of the atmosphere be on short wavelength observations of your effect?

S.V. Pogrebenko (A): The modulation effect is stronger at shorter wavelengths, but all external phase degradation effects, like those caused by the atmosphere, are stronger too. It may be that an optimum exists at some wavelength.

T. Krichbaum (Q): Would the gravitational waves, besides the flux density variability, also cause a position shift of the QSO, which can be measured with phase referencing VLBI? How large would be such a position shift?

S.V. Pogrebenko (A): I think that the gravitational wave may change the observed position of the source, but it would need to be very a strong gravitational wave to produce a detectable shift.

A. Stepanov (Q): What wavelength is optimal for VLBI observations of the gravitational lens effect?

S. Pogrebenko (A): As short as possible to observe with a good SNR.

L. Bååth (Q): This looks like an antenna-based effect. Once you have done your image with selfcal you will lose that information. How can you see it in the map?

S.V. Pogrebenko (A): The effect is much more clearly detectable in the uv -plane. I have used the image plane only as an illustration.

R. Porcas (Q): What is the size of the effect? What is the period of the binary?

S.V. Pogrebenko (A): For this particular pair of CB+QSO, the expected effect is $1 \div 2 \mu\text{Jy}$. The orbital period of CM Del is 4 hours.

Fringe Finding for 3 mm-VLBI: Application to 3C111

S. DOELEMEN¹, A.E.E. ROGERS¹ and J.M. MORAN²

¹MIT–Haystack Observatory, Westford, MA, USA

²Center for Astrophysics and Harvard University, Cambridge, MA, USA

Abstract

When coherence losses limit the integration time in mm-VLBI, detection thresholds rise and weak sources cannot be detected. Coherence problems in our 3 mm data have led us to reformulate detection methods and measurements of visibility in terms of incoherent averages. These techniques are outlined with examples and results from a 1993 global VLBI campaign.

Introduction

The 3 mm-VLBI effort recorded its first fringes in 1981 on the OVRO-HatCreek baseline (Readhead *et al.*, 1983). Since then, as receiver sensitivity and number of antennas have increased, the list of detections has grown to include some 33 sources. This list consists of quasars, BL Lac objects and cores of active galaxies, all characterized by copious mm emission, and some by large flux variations and X-, γ -ray emission. Table 1 shows sources detected at 3 mm with VLBI along with redshifts and the size scales probed by the observations.

The motivation to mm- λ VLBI starts with the increased resolution which, on long baselines, can approach $\sim 50\mu$ as. More importantly though, the higher frequency VLBI can look deeper into those sources whose cores are optically thick at lower frequencies. As evidence of this effect consider the inverted cores seen in many cm-VLBI maps. Also convincing is the evidence presented through multi-frequency flare monitoring of 3C273 by Robson *et al.*(1991). Their light curves of a 1990 flare show increased emission at all wavelengths shortward of 3.3 mm but *none* at 8.1 mm. At 3 mm we begin to see emission during the flare from regions which are invisible at longer wavelengths due to self-absorption. 3 mm-VLBI also reduces the effects of scattering by the interstellar medium in our galaxy. The scattering size of a point source near the galactic plane is proportional to λ^2 . Observations of the galactic center Sgr A* (Rogers *et al.*, 1994a) are limited by this scattering as are data on all sources at low galactic latitudes such as Cyg A (Carilli *et al.*, 1991).

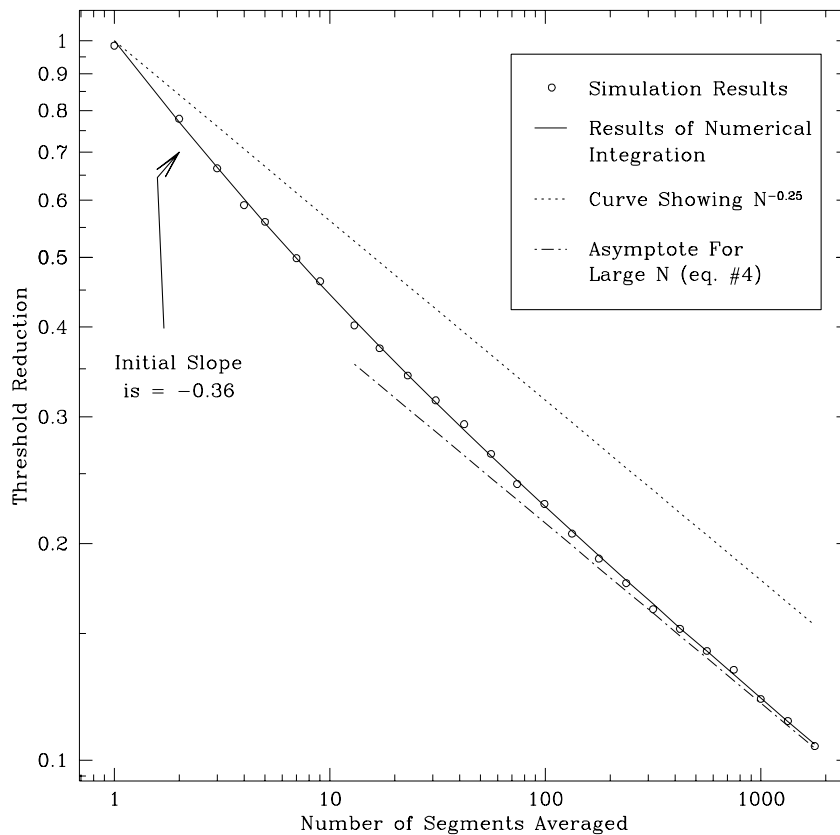


Figure 1: Reduction in the flux detection threshold obtained by searching over an incoherent average of many segments. The open circles show results of a simulation in which a maximum in segmented and averaged amplitude was found in a search of 100 points in (delay – delay-rate) space. 2000 of these searches were made and the threshold was defined as the dividing line between the top 1% and lower 99%. The solid line is calculated by numerical integration of the probability density for A^2 .

Fringe detection

Traditional methods of VLBI fringe detection have neglected the systematic coherence losses due to atmospheric turbulence and local oscillator instability. At lower frequencies this is forgivable since a VLBI interferometer can be phase stable during a 6–13 minute integration. But, at mm-wavelengths, the interval over which the visibility can be coherently integrated (τ_{coh}) is usually much shorter than the scan time. If baseline sensitivity is low, then amplitude losses due to phase noise may raise the flux detection threshold and the source will go undetected. To deal with this specific problem we have reformulated the fringe detection process to use an incoherently averaged best-estimator of the amplitude which is immune to phase noise. A VLBI scan is divided into N segments of length τ_{seg} and we define (Thomson, Moran, Swenson, 1986)

$$A^2 = \sum_i (a_i^2 - 2) \quad (1)$$

where a_i is the amplitude of the i th segment in units of SNR. The 2 is included to subtract the noise bias in the amplitude. The SNR of A^2 can be written ($s = \text{SNR}/\text{segment}$)

$$\text{SNR}_A = \frac{1}{2} s^2 \sqrt{N} \quad (2)$$

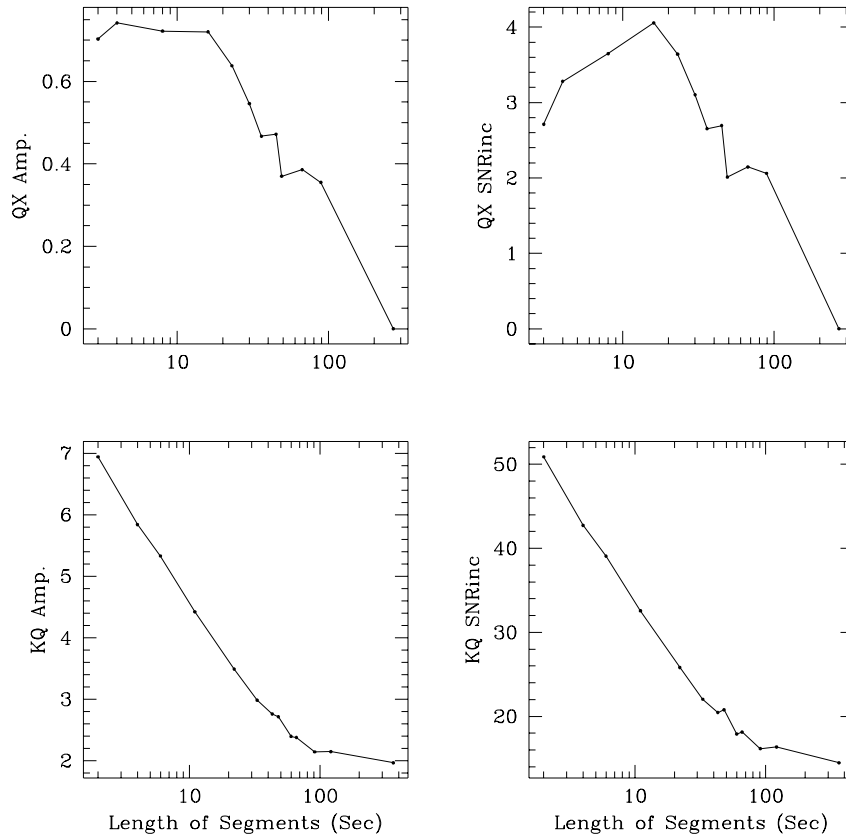


Figure 2: Incoherently averaged amplitudes and SNR as functions of segmentation length. The top two panels show a low SNR scan of 3C111 on the Quabbin-PicoVeleta (QX) baseline whose SNR_{inc} peaks near $\tau_{coh} = 12\text{sec}$. The amplitude increases as segment length decreases to τ_{coh} and reaches a limit for smaller segments. Lower panels show the same quantities for a Haystack-Quabbin (KQ) scan on 3C273. Here the SNR is higher but the coherence is much worse : even at a segment length of 2 sec. there is no peak in SNR_{inc} and we have not recovered all the amplitude.

($s = \text{SNR}/\text{segment}$) with the result that in a search of n points in delay and rate, the probability of false detection will be (Rogers, *et al.*, 1994b)

$$\text{PE} = \frac{n}{\sqrt{2\pi} \text{SNR}_A^2} e^{-\text{SNR}_A^2/2} \quad (3)$$

We can compare this method of searching for a fringe to the coherent case by computing the ratio S_{inc}/S_{coh} where S_{coh} is the flux threshold for coherent detection in the coherence time and S_{inc} is the threshold for detection using the average of many segments, each of length τ_{coh} . We find that for large N

$$\frac{S_{inc}}{S_{coh}} = (0.53)N^{-\frac{1}{4}} \quad (4)$$

where we have assumed a PE of 10^{-6} in both the coherent and incoherent search. Fig. 1. shows the behavior of S_{inc}/S_{coh} where the small N regime has been examined using Monte Carlo simulations and numerical integration of an analytic expression for $p(A^2)$.

Calculation of visibilities

After a search, the visibility amplitude of a scan is computed by segmentation and incoherent averaging. The choice of τ_{coh} comes after consideration of how amplitude varies with

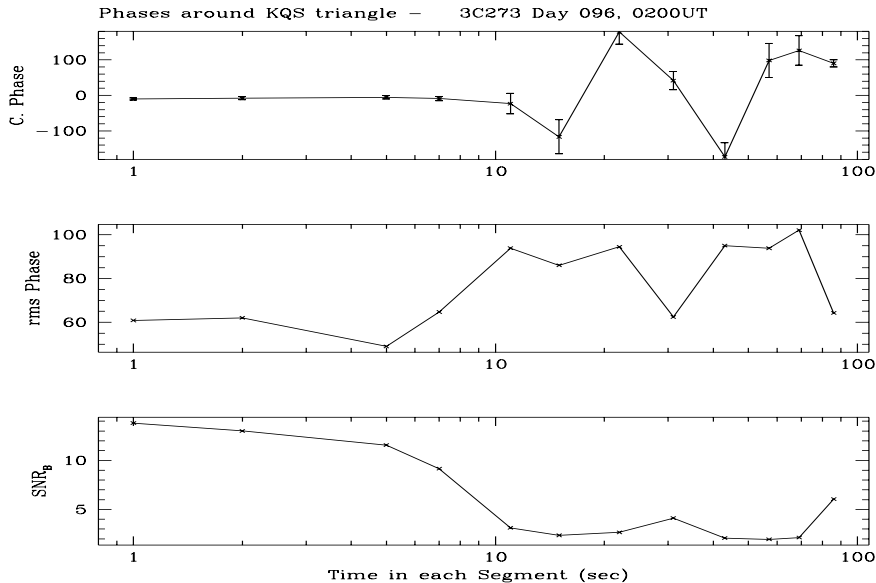


Figure 3: Top panel shows closure phase on the Haystack-Quabbin-Onsala triangle a scan on 3C273. Errors are $1\text{-}\sigma$, determined empirically by comparing noise and signal contributions from each segment in the bispectral sum (Rogers, *et al.*, 1994b). Last two panels are the rms phase of all segments in bispectral sum and the SNR_B .

segmentation. Too short a segment reduces the $\text{SNR}/\text{segment}$ and SNR_A decreases. If too long a segment is chosen then SNR_A suffers from coherence losses. This behavior is seen in the plots of amplitude and SNR_A vs. segments in Fig. 2. For the Quabbin-PicoVeleta baseline a clear peak in SNR shows that the optimum segmentation time for detection is 12 seconds. When τ_{seg} becomes comparable with τ_{coh} , each segment is essentially coherent and we get a good estimate of the amplitude. On the Quabbin-Haystack baseline the phase noise on this particular observation was due to an unstable buffer from the station's H-maser. Since $\tau_{coh} < 2$ sec, the SNR and amplitude do not turn over for this scan and keep increasing with smaller segment size.

We treat the interferometric phase on each baseline as random and glean all phase information from closure around triangles of stations. In the estimation of closure phase, segmentation can boost SNR. It can be shown that averaging the complex triple product of visibilities around a triangle (known as the bispectrum) will increase phase SNR if coherence losses are a problem. We define the averaged bispectrum as:

$$B = \frac{1}{N} \sum a_1 a_2 a_3 e^{i\theta_c} \quad (5)$$

where the a_i are amplitudes of each segment and θ_c is the corresponding closure phase. For low SNR

$$\text{SNR}_B = \frac{1}{2} s^3 \sqrt{N} \quad (6)$$

In Fig. 3, the closure phase derived from the averaged bispectrum is shown as a function of segment length.

Application to 3C111

As part of the April 1993 3 mm-VLBI campaign we made a 1.5 hour observation of the source 3C111. 3C111 was chosen as a mm-VLBI target primarily for its high mm flux

(4.4 Jy in 1993) and the compact core seen at lower wavelengths. Optically, the core is identified with an N-galaxy at $z = 0.049$ and is difficult to image due to low galactic latitude ($b = -9^\circ$). VLA maps at 1.4 GHz show a highly collimated kpc-scale jet that points towards the NE lobe but with no detected counter jet to the SW (Linfield, 1987). Recent monitoring of the pc-scale jet with VLBI at 5 GHz (Preuss, *et al.*, 1990) shows the jet to be superluminal with a speed of $\sim 3.4h^{-1}c$. At 3 mm, detection on our longest baseline (Kitt Peak-Pico Veleta), provides information on scales of $0.06h^{-1}$ pc assuming $H_o = 100h$ km/s/Mpc and $q_o = 0.5$.

Observations ran from 17:30 to 19:00 UT on April 9 with u, v -coverage shown in Fig. 4. Fringes were detected using the coherent search technique on 25 scans; after constrained searches using incoherent averages, the source was detected in 37 scans. Calibration of amplitudes with system temperatures and gain curves gave correlated fluxes to within 20% and a flux vs. baseline plot is shown in Fig. 5.

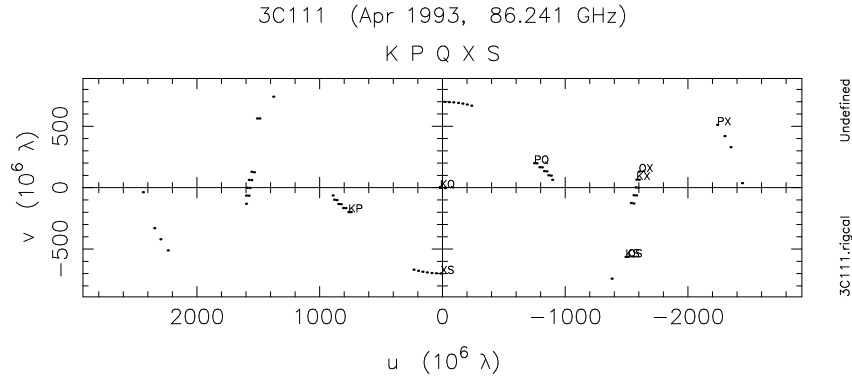


Figure 4: u, v -coverage for 1.5 hour observation of 3C111.

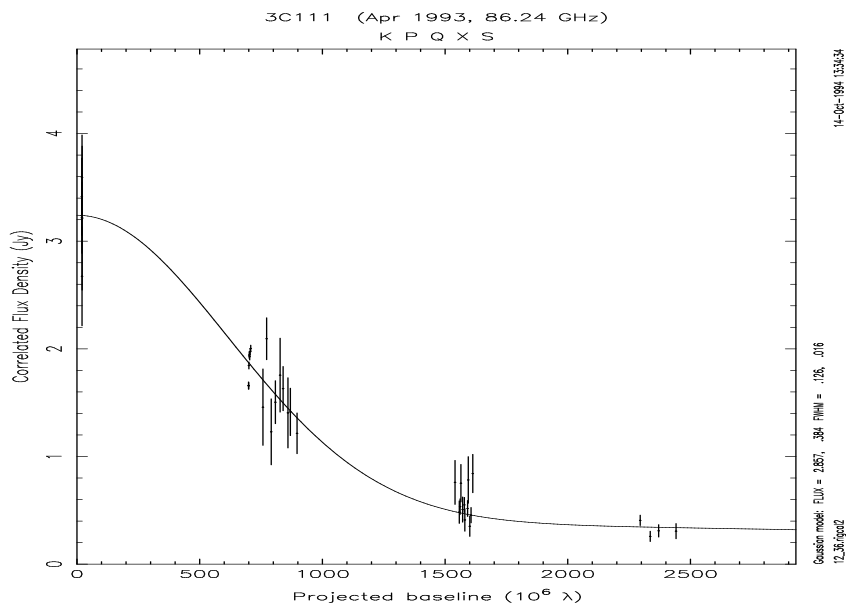


Figure 5: Plot of correlated flux density vs. projected baseline. The solid line shows the visibility amplitude for a model consisting of two circular gaussian components.

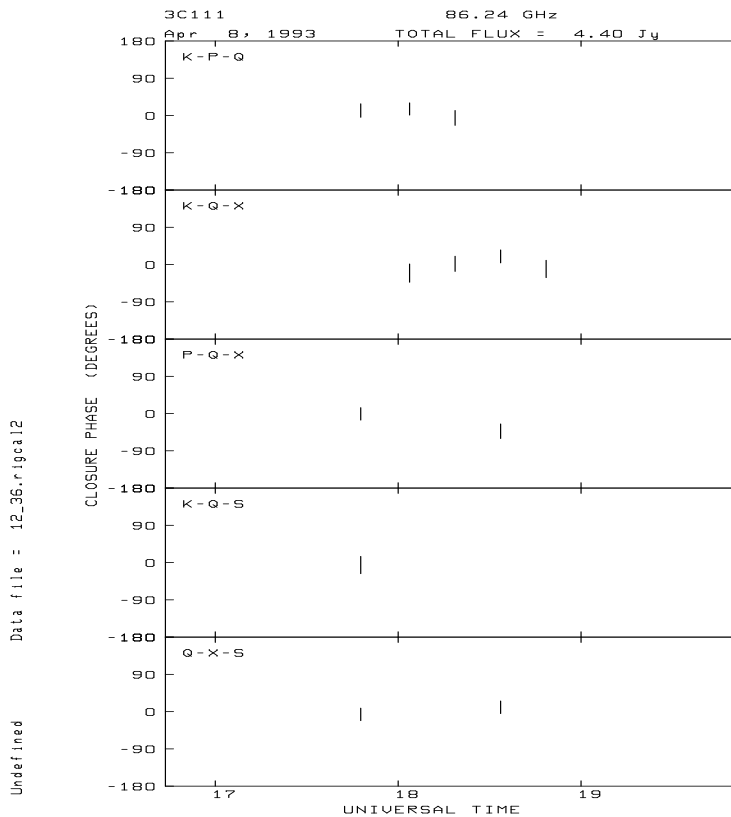


Figure 6: Closure phases for triangles in 3C111 observation.

Also shown (Fig. 6) are closure phases on the 5 triangles present which do not significantly deviate from zero. Given the possible calibration errors, we modeled the source with circular gaussians and the visibility amplitude of the best-fit two component model is shown as a solid line in Fig. 5. The 300 mJy detection on the long Kitt Peak-Pico Veleta baseline implies a slight core-halo interpretation to the model. Most of the flux (2.9 Jy) is found in a component with FWHM = 0.126 mas and a second component with a flux of 0.38 Jy and FWHM of 0.016 mas accounts for the flux on long baselines.

The smaller component boosts the maximum T_{bright} of the model to 2.75×10^{11} K. Convolution of the model with an interferometer beam of $0.3 \text{ mas} \times 0.09 \text{ mas}$ reduces this maximum to 1.9 Jy/Beam or $T_{bright} = 1.2 \times 10^{10}$ K.

With these limited observations there is no evidence for asymmetry on sub-parsec scales - no continuation of the kpc and pc-scale jet to the high frequency core. One possibility for this may be the timing of our observation. The lifetime for synchrotron electrons emitting at 86 GHz can be written as :

$$\tau_{synch} = 0.092B^{-\frac{3}{2}} \text{ years.} \quad (7)$$

Assuming an order of magnitude magnetic field of ~ 1 Gauss extrapolated from 5 GHz data (Linfield, 1987), the τ_{synch} is about 1 month. Observations within a month of 86 GHz flux changes may show the innermost jet structure just as material is ejected from the core. Better u, v -coverage observations will also help search for small-scale structure (flaring and quiescent). 3C111 is a relatively high-declination source and longer observations with the same stations will fill out the u, v -coverage considerably.

Table 1: Sources detected with 3 mm VLBI. B — BL Lac objects, Q — quasar, G — galaxy. The scale column shows the linear size at source redshift assuming a $100 \mu\text{as}$ beam with $q_o = 0.5$ and $H_o = 100h \text{ km s}^{-1} \text{ Mpc}^{-1}$

Source	Alias	90 GHz Flux (Jy)	Type	z	Scale ($h^{-1}\text{Pc}$) $\theta \sim 100\mu\text{as}$
0212+735	–	1.4	B	2.367	0.39
0224+67	4C67.05	2.3	Q	–	–
0235+164	OD 160	1.9	B	0.94	0.42
0316+413	3C84	7.3	G	0.0172	0.24
0415+379	3C111	2.6	G	0.049	0.066
0528+134	–	4.7	Q	2.06	0.41
0552+398	DA 193	1.9	Q	2.365	0.39
0642+449	OH 471	1.1	Q	3.406	0.35
0716+714	–	1.5	Q	–	–
0748+126	–	2.9	Q	0.889	0.42
0836+710	4C71.07	1.0	Q	2.16	0.40
0851+202	OJ 287	2.6	B	0.306	0.28
0923+392	4C39.25	6.2	Q	0.699	0.40
1055+018	OL 093	2.3	Q	0.888	0.42
1226+023	3C273B	22.5	Q	0.158	0.18
1228+126	3C274	7.3	G	0.004	0.006
1253–055	3C279	24.2	Q	0.538	0.37
1334–127	–	7.8	Q	0.541	0.37
1641+399	3C345	4.8	Q	0.595	0.38
1730–130	NRAO 530	6.0	Q	0.902	0.42
1742–289	Sgr A*	3.0	G	0.0	4e-6
1749+096	4C09.57	5.1	B	0.321	0.29
1803+784	–	1.3	B	0.68	0.40
1823+568	–	2.7	B	0.664	0.39
1921–293	OV 236		Q	0.352	0.30
1928+738	4C73.18	1.8	Q	0.302	0.28
1957+405	CYG A		G	0.056	0.07
2007+777	–	1.1	B	0.342	0.30
2145+067	DA 562	5.7	Q	0.990	0.43
2200+420	BI Lac	1.7	B	0.0695	0.09
2223–052	3C446	2.0	B	1.404	0.43
2230+114	CTA 102	2.7	Q	1.037	0.43
2251+158	3C454.3	12.8	Q	0.859	0.42

Acknowledgements: 3 mm-VLBI experiments always require the efforts and special attention of many people. We thank all those who were involved with this global campaign. The quality of high frequency VLBI data depends heavily on good calibration at each antenna. Some 3 mm flux values given in Table 1 were taken from Standke *et al.* (1994) which also contains a good discussion of coherence. A good overview of 3 mm VLBI as well as an explanation of a global fringe searching technique can be found in Bååth *et al.* (1992).

References

- Bååth, L.B., *et al.*, 1992, VLBI observations of active galactic nuclei at 3 mm, *A&A*, **257**, 31–46.
- Carilli, C.L, Bartel, N. and Linfield, R.P., 1991, VLBI Observations of the Nuclear Jet in Cygnus A, *AJ*, **102**, 1691–1695.
- Linfield, R.P., 1987, VLBI Observations of the 3C 111 Jet, *Ap. J.*, **317**, 121–127.
- Preuss, E., *et al.*, 1990, 3C111 and 3C390.3: Beaming in Nearby Radio Galaxies, in *Parsec-scale radio jets*, J.A. Zensus, Ed., Cambridge University Press, Cambridge, pp. 120–124.
- Readhead, A.C.S., *et al.*, 1983, Very long baseline interferometry at a wavelength of 3.4 mm, *Nature*, **303**, 504–506.
- Robson, E.I., *et al.*, 1993, The infrared-millimetre-centimetre flaring behaviour of the quasar 3C273, *M.N.R.A.S.*, **262**, 249–272.
- Rogers, A.E.E., *et al.*, 1994a, Small Scale Structure and Position of SGR A* From VLBI at 3 mm Wavelength, *Ap. J. Let.*, **434**, L59–L62.
- Rogers, A.E.E., Doeleman, S.S., Moran, J.M., 1994b, Fringe Detection Methods for Very Long Baseline Arrays, *AJ*, submitted.
- Standke, K.J., *et al.*, 1994, “High sensitivity” VLBI at 86 GHz: First Fringes with the 100m Radio Telescope in Effelsberg, in *URSI/IAU Symp. on VLBI technology, progress and new observational possibilities*, M. Inoue, T. Sasao, S. Manabe and O. Kameya, ed., Kyoto, in press.
- Thompson, A.R., Moran, J.M. and Swenson Jr., G.W., 1986, *Interferometry and Synthesis in Radio Astronomy*, John Wiles & Sons, New York, p. 268.

DISCUSSION

R.T. Schilizzi (Q): Your segmented coherence approach reminded me (as an old-timer) of a programme called BCA (Broken Coherence Averaging) written, I think, by Barry Clark in the early 70’s, and used for detection of fringes.

S. Doeleman (A): Incoherent averaging has been used for a long time to obtain better estimates of amplitude. We are incorporating this technique into the search process to reduce the minimum flux threshold and estimate the amplitude.

J.-F. Lestrade (Q): Have you used this detection technique at smaller wavelengths than 3 mm?

S. Doeleman (A): 1 mm fringes have been detected with low SNR using coherent averaging. This technique of searching on the incoherent average can be applied to 1 mm data and we hope to re-analyse 1 and 3 mm data from past experiments.

Jets of Blazars at Sub-mas Scales: a Status Report on mm-VLBI

T.P. KRICHBAUM¹, K.J. STANDKE^{1,6}, A. WITZEL¹,
C.J. SCHALINSKI^{2,1}, M. GREWING^{2,3}, A. GRAVE^{2,3}, R.S. BOOTH⁴,
L.B. BÅÅTH⁴, A.E.E. ROGERS⁵ and J.A. ZENSUS⁷

¹Max-Planck Institut für RadioAstronomie, Bonn, Germany

²Institut de Radio Astronomie Millimétrique, Grenoble, France

³Instituto de Radio Astronomia Millimetrica, Granada, Spain

⁴Onsala Space Observatory, Onsala, Sweden

⁵Haystack Observatory, Westford, Massachusetts, USA

⁶Geodätisches Institut der Universität Bonn, Germany

⁷National Radio Astronomy Observatory, Socorro, New Mexico, USA

Introduction

At millimetre wavelengths VLBI-imaging with an angular resolution of a few tenths of micro-arcseconds allows to investigate compact radio sources in unsurpassed detail. Stretching the technical possibilities of some observatories to their extremes, one hopes that in the near future VLBI observations at 3 mm & 1 mm and eventually sub-millimetre wavelengths will improve our knowledge of the energy production in blazars (and compact galactic objects, as e.g. radio emitting X-ray binaries or the Galactic Center source Sgr A*), helping to understand more details of the still mysterious processes in the ‘central engines’.

Since the early eighties, when first fringes at mm-wavelengths were detected, considerable improvement has been made. Due to better system- and antenna performances *AND* due to the addition of large and sensitive antennas to the existing arrays (e.g. the VLBA at 43 GHz, the 30 m-MRT at Pico Veleta and the 100 m-RT at Effelsberg at 43 & 86 GHz), the detection sensitivity has improved considerably, and the number of sources accessible for mm-VLBI observations increased drastically (see Krichbaum *et al.*, 1994c, Standke *et al.*, 1994). By now, sources with correlated flux densities of $S_{corr} \geq 0.1$ Jy can be reliably imaged at 43 GHz (e.g. Krichbaum & Witzel, 1992). For a summary of sources detected so far at 43 GHz see e.g. Krichbaum *et al.*, 1994c. At 86 GHz typical single baseline detection thresholds are higher and range between 0.2 – 1 Jy (using antenna parameters as summarized in Table 1).

Prior to 1990/1991 reliable images from VLBI observations performed at 3 mm wavelength were still sparse (see Bååth *et al.*, 1992 for details). In order to further improve the imaging capabilities at 86 GHz we performed several VLBI observations, all of which were aimed as technical tests for at least some of the participants: in 1991 we obtained ‘first fringes’ for Pico Veleta and one VLBA antenna (Pie Town) at 43 GHz (Krichbaum *et al.*, 1993b), in 1992 we obtained for the first time fringes between Effelsberg and Pico Veleta at 86 GHz (Schalinski *et al.*, 1993), while at 43 GHz the combination of 4 VLBA antennas with the antenna at Haystack and three antennas in Europe (Effelsberg, Onsala and Pico Veleta) yielded maps with largely improved dynamic range (see e.g. Krichbaum *et al.*, 1994c).

Table 1: Antenna Specifications at 86 GHz

Station	D [m]	T_{sys} [K]	gain [K/Jy]	η_A
Effelsberg	60	350	0.13	0.13
Haystack	37	200	0.058	0.15
Nobeyama	45	400	0.17	0.29
Pico Veleta	30	180	0.14	0.55
Onsala	20	250	0.056	0.49
SEST	15	300	0.032	0.50
Quabbin	14	300	0.024	0.43
KittPeak	12	150	0.023	0.56
OVRO	4x10.4	300	0.067	0.55
Hat Creek	7x6.1	300	0.050	0.65
VLBA (PT&LA)	25	150	~ 0.09	~ 0.50
JCMT	15	300	0.038	0.60
P. de Bure	15	150	0.043	0.67
Metsähovi	14	300	0.017	0.30

Note: For the 100 m-RT at Effelsberg the illuminated diameter is given. Stations which may join in in the near future are listed in the lower part of the table. For the 4 element interferometer at Plateau de Bure participation with a single antenna is planned first.

Results

A step towards an improved performance of the VLB-interferometer at 86 GHz was obtained in an experiment performed in April 1993, in which the antennas at Effelsberg, Onsala, Pico Veleta, and Haystack participated. Aimed as a detection test 25 flat spectrum sources were observed in snap shot mode (Schalinski *et al.*, 1994, Standke *et al.*, 1994), and 23 sources were detected with VLBI at 86 GHz, 19 of these for the first time (including 3C454.3, Schalinski *et al.*, 1993 and the galactic center source Sgr A*, Krichbaum *et al.*, 1994a&b). In table 2 we summarize for each baseline the signal-to-noise ratio after standard fringe fitting (program ‘FRNGE’) and integration over the full scan length. As can be seen most sources with total flux densities $S_{86\text{GHz}} > 1\text{ Jy}$ were detected at least on one baseline.

To demonstrate the performance of mm-VLBI in some examples, we present in the following paragraph preliminary maps from VLBI observations at 43 GHz and 86 GHz and compare them with data obtained at longer wavelengths.

Specific sources

The blazar PKS 0528+134

The high redshift blazar PKS 0528+134 ($z = 2.07$), recently attracted attention due to its extreme brightness and variability in the gamma-ray regime (Hunter *et al.*, 1993) and in mm- and cm- radio bands (Zhang *et al.*, 1994). At 8 and 22 GHz the source displays a slightly bent and core-jet structure of $\sim 3\text{ mas}$ length (Zhang *et al.*, 1994). Based on a new high dynamic range map obtained from a 10 station experiment in 1992.85 at 22 GHz (see figure 1), we find several jet components ‘N’, ‘C1’, ‘C2’, ‘C3’ & ‘C4’ located at separations

Table 2: Signal-to-Noise ratios of sources observed at 86 GHz in April 1993.

Source	$S_{86\text{GHz}}$ [Jy]	BK	BX	BS	KS	KX	SX
0212+735	1.4	<7	7	<7	—	<7	—
4C 67.05	2.3	<7	<7	<7	<7	8	8
0235+164	~4.0	<7	—	8	<7	—	—
3C 84	7.3	—	<7	<7	—	—	—
0528+134	7.4	7-12	13	<7	—	—	—
DA193	2.4	<7	<7	—	—	11	—
0642+449	1.1	<7	<7	<7	<7	9	17
0716+714	1.5	<7	15	8	<7	7-26	16
0836+710	~1.0	<7	7	<7	<7	<7	10-12
4C 39.25	5.8	<7	7-12	9-10	<7	8	14
3C 273	27.0	10-12	39-73	17-27	—	149-207	—
3C 279	20.5	12	43-107	13-19	—	169	—
3C 345	5.8	<7	10-32	7-15	—	6-13	24
NRAO530	7.0	7-8	8-70	10-19	7-9	21-82	12-76
Sgr A*	8.1	—	7-20	—	—	—	—
1749+096	2.6	7	15-30	7-12	7-10	9-43	20-39
1803+784	1.8	<7	<7	<7	<7	8-10	25-31
1823+568	2.7	<7	11-17	<7	16-15	35-43	49-64
1928+738	1.8	<7	7	<7	<7	8	8-11
Cyg A	1.8	<7	<7	<7	<7	<7	10-13
2005+403	1.0	<7	<7	<7	<7	<7	<7
2007+777	1.5	<7	<7	<7	<7	<7	13-18
2145+067	4.6	<7	8-47	12	7	9-19	38-37
CTA102	1.7	<7	10-14	<7	<7	9-14	7-22
3C 454.3	10.0	8-16	12-80	12-27	10-29	10-20	28-84

—: not observed; <7: not detected

B Effelsberg; K Haystack; S Onsala; X Pico Veleta.

of 0.2, 0.6, 0.9, 3.1, and 4.9 mas relative to the core C0, respectively (Pohl *et al.*, 1995, *in preparation*). Our VLBI observations at mm-wavelengths now trace the jet down to sub-mas scales (see figure 1). 0528+134 is also included in S/X Geo-VLBI experiments, which have the potential to yield maps with a time sampling of typically 1 map every 1-3 months (Schalinski *et al.*, 1986, Britzen *et al.*, 1993&1994). First maps from such Geo-VLBI monitoring were recently obtained for 0528+134 (amongst other sources), and showed a continuously bent jet, extending to even larger core separations than those seen at 22 GHz.

The combination of our data with the observations of Zhang *et al.*, 1994, allowed to identify the jet components and to search for structural variability. We suggest an identification scheme in which the components ‘C2’, ‘C3’, and ‘C4’ remained stationary relative to ‘C0’ within the observing interval 1991.16 - 1992.85. For component ‘C1’, however, we find strong evidence for motion with $\beta_{app} = 5.3 \pm 1.4$ (see figure 2). The high frequency data (22 & 43 GHz) revealed evidence for a new component ‘N’ at $r = 0.2$ mas,

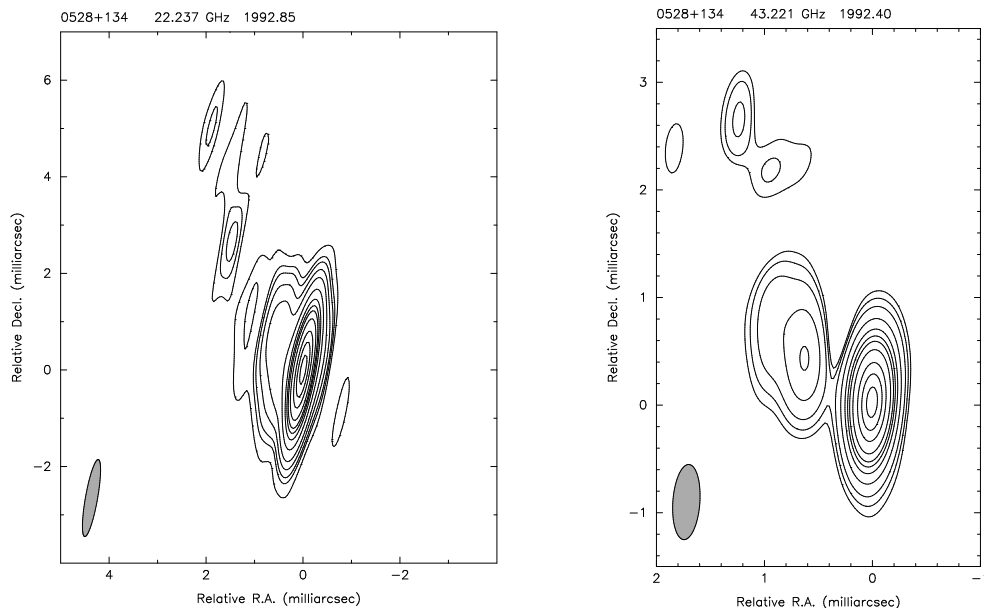


Figure 1: Left: *0528+134* at 22GHz. Contour levels are 0.1, 0.3, 0.5, 1, 2, 5, 10, 15, 20, 30, 50, 70, and 90 % of the peak flux density of 2.8 Jy beam^{-1} . The restoring beam size is $1.62 \times 0.25 \text{ mas}$, $p.a. = -10 \text{ deg}$. Right: *0528+134* at 43GHz. Contour levels are 0.5, 1, 2, 5, 10, 15, 20, 30, 50, 70, and 90 % of the peak flux density of 2.5 Jy beam^{-1} . The restoring beam size is $0.70 \times 0.25 \text{ mas}$, $p.a. = -4 \text{ deg}$.

which was not seen previously in our 8 GHz maps (epochs 1991.2 & 1992.2) nor in the data of Zhang *et al.*, 1994 at 8 & 22 GHz (epochs 1990.9 & 1991.1). This new component is also seen in a preliminary 86 GHz map obtained in 1993.3 (Standke, 1994). We tentatively determined the angular separation rate of ‘N’ to be in the range of $0.3 - 0.5 \text{ mas/yr}$ ($\beta_{app} = 12 - 20$), which is about a factor of 2 to 4 faster than the apparent velocity of ‘C1’ (see figure 2; another component registration is indicated by a dashed line in the figure, but seems inconsistent with results obtained at 86 GHz). At 22 GHz *0528+134* showed a large flux density outburst with a preceding smaller peak near ~ 1992.2 and a prominent peak near ~ 1993.5 . Back-extrapolation of the motion of ‘N’ yields $t_0 \simeq 1992.1$ for its zero-separation epoch. This and the observed considerable flattening of the total spectrum of *0528+134* (Zhang *et al.*, 1994) strongly indicates that ‘N’ was ejected during the first maximum of the outburst and now becomes visible at high frequencies. Future observations should allow to relate the ejection of ‘N’ with this outburst more clearly.

The blazar PKS 0420–014

The strongly variable flat spectrum radio source PKS 0420–014 ($z = 0.915$) shows superluminal motion with $\beta_{app} \leq 8c$ (Wagner *et al.*, 1994). The detection of quasi periodic optical variability, which presumably correlates with variations seen at 100 MeV – 5 GeV with EGRET (Wagner *et al.*, 1994, and references therein) can be explained by a helical jet model, similar to the one suggested for 3C 345 (Steffen *et al.*, 1993, Schramm *et al.*, 1993). In figure 3 we show the first high resolution map of PKS 0420–014, obtained in May 1992, during a global 43 GHz VLBI campaign. The source structure is of core-jet type and shows considerable bending (by more than 90 deg) on mas- to sub-mas scales. Combination of the maps achieved from mm-VLBI observations with images obtained

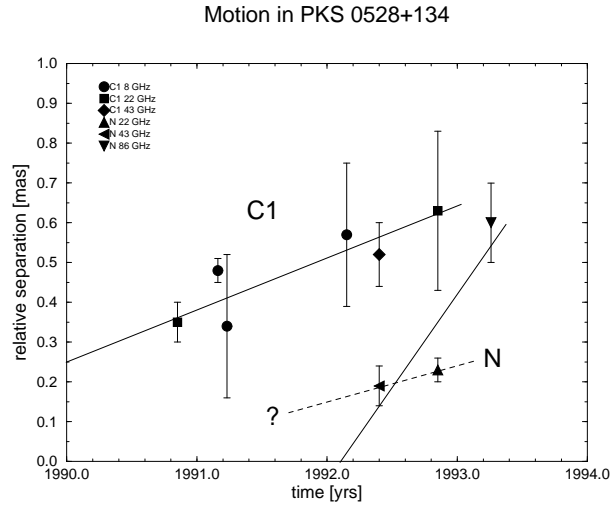


Figure 2: Motion of two new jet components in PKS 0528+134. The two solid lines represent fits to the data using the most plausible cross identification between components at different frequencies and epochs. The dashed line indicates an alternative identification scheme, which we regard as less plausible due to mismatching component at 86 GHz. The slope of the solid lines corresponds to apparent velocities of $\beta_{app} = 5.3 \pm 1.4$ for ‘C1’, and $\beta_{app} \simeq 20 \pm 4$, for ‘N’, (using $H_0 = 100 \text{ km s}^{-1} \text{ Mpc}^{-1}$, $q_0 = 0.5$).

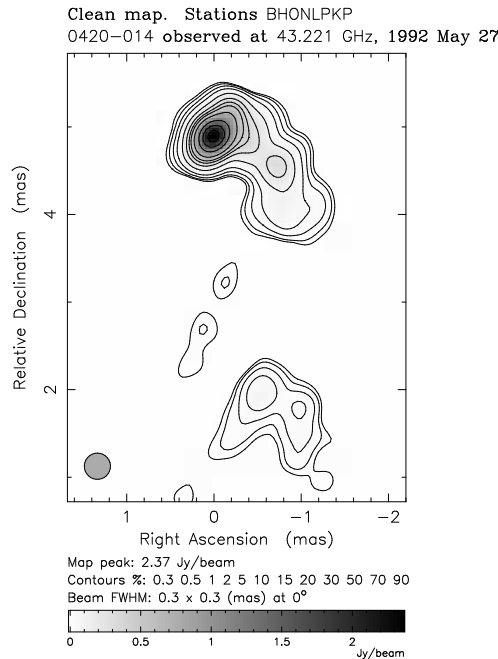


Figure 3: Hybrid map of the quasar PKS 0420-014 at 43 GHz; epoch 1992.40. Contour levels are: 0.3, 0.5, 1, 2, 5, 10, 15, 20, 30, 50, 70, 90 percent of the peak flux density of $2.37 \text{ Jy beam}^{-1}$. The map is restored with a superresolving beam of size $0.3 \times 0.3 \text{ mas}$. The true observing beam has a size of $0.9 \times 0.25 \text{ mas}$, oriented at $p.a. = -8 \text{ deg}$.

from the geodetic VLBI-monitoring at S/X-bands (Britzen *et al.*, 1994) will allow to see, if the jet components move along bent paths, as expected from the helical model.

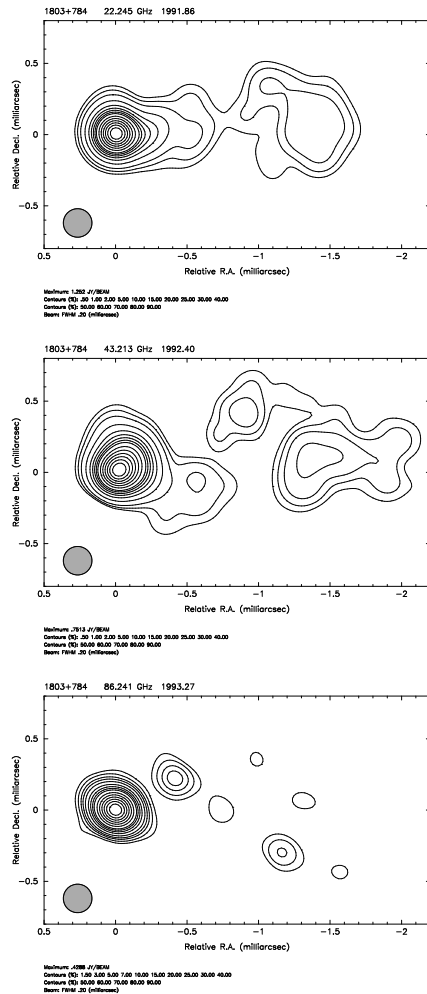


Figure 4: The sub-mas structure of the BL Lac 1803+784. From top to bottom we show maps obtained at 22 GHz, 43 GHz and 86 GHz. Although still of low dynamic range, the map at 86 GHz is in good agreement with the maps obtained at longer wavelengths and represents the basic source structure correctly. The high quality of the 43 GHz images now allows to produce spectral image maps, if combined with data obtained at longer wavelengths (e.g. at 22 GHz). Frequent monitoring with sufficient time sampling will therefore allow to determine spectral index changes in the source structure, which are expected from merging of moving and stationary components.

The BL Lac object 1803+784

The S5-source 1803+784 ($z = 0.684$) shows a pronounced core jet structure with embedded moving and stationary components. The misalignment between pc- and kpc-scales indicates large scale jet curvature of ≥ 90 deg. On mas- to submas scales the mean ridge-line of the jet is ‘quasi-sinusoidally’ bent and the apparent component velocities vary systematically, strongly indicating motion along spatially curved paths (cf. Krichbaum *et al.*, 1993a & 1994b&c). Within this scenario one would expect component acceleration in the region $0.4 \text{ mas} < r < 0.8 \text{ mas}$ from $\mu \simeq 0.05 \text{ mas yrs}^{-1}$ to $\mu \simeq 0.3 \text{ mas yrs}^{-1}$. A comparison of the 22 GHz map from 1991.9 with the new (but still preliminary) map obtained at 43 GHz in 1992.4 indeed supports these expectations (see figure 4): between both epochs a component seems to have moved from $r = 0.5 \text{ mas}$ to $r = 0.8 \text{ mas}$, while a component located at $r = 1.1 \text{ mas}$ (in 1991) merged with the stationary component at $r = 1.4 \text{ mas}$ in 1992. A first 86 GHz map of 1803+784 (epoch 1993.3) shown in figure 4 represents the basic source structure quite well (core and stationary component at $r = 1.2 \text{ mas}$) and furthermore reveals evidence for structural variability near $r = 0.5 \text{ mas}$. Future monitoring at 43 GHz and 86 GHz will allow to test the helical motion model for 1803+784 also in the vicinity of the VLBI-core (at $r \leq 0.5 \text{ mas}$).

Summary and conclusion

Considerable progress has been achieved with VLBI imaging at millimetre wavelengths: at 43 GHz the maps now have dynamic ranges comparable to those from cm-VLBI observations, allowing detailed investigations of the sub-parsec scale structures in AGN, and galactic compact radio sources. In many cases the 43 GHz images revealed increasing jet curvatures when approaching the VLBI-cores, sub- or superluminal motion along bent paths, and evidence for motion along spatially bent (helical) trajectories. All this indicates a common physical process for most of the superluminal radio sources, which might be explained by taking the coupling of the rotating accretion disk with the jet into account (cf. Camenzind, 1994, Hardee *et al.*, 1994).

At 86 GHz compact sources with total flux densities of 1 – 2 Jy are now accessible for VLBI-imaging. First models and maps for sources like 0528+134, 4C39.25, 1803+784, and 3C454.3 are now obtained, tracing the jets down to micro-arcsecond scaled regions. With its high angular resolution VLBI imaging at millimetre wavelengths ($\nu \geq 43$ GHz) provides a unique tool to investigate the morphology and kinematics of the jets in AGN in much more detail.

Combined with flux density monitoring programs (at all accessible wavelengths), mm-VLBI observations can significantly contribute to the understanding of the physical processes of jet generation, in particular with the early detection (and subsequent monitoring) of new jet components, which are ejected after phases of enhanced activity of the ‘central engines’.

Acknowledgements: We especially like to thank the staff of the observatories for their efforts making mm-VLBI possible. Without the continuous engagement of Dave Graham the observations presented here would have been less successful. T.P.K. appreciates the support of the German BMFT-Verbundforschung.

References

- Bååth, L., *et al.*, 1992, *A&A*, **257**, 31.
- Britzen, S., Gontier, A.-M., Witzel, A., and Campbell, J., 1993, in: *Proceedings of the 9th Working Meeting on European VLBI for Geodesy and Astrometry*, Mitteilungen aus den Geodätischen Instituten der Rheinischen Friedrich-Whilhelms-Universität No. 81, ed. J. Campbell and A. Nothnagel, p. 157.
- Britzen, S., Krichbaum, T.P., Steffen, W., Witzel, A., and Schalinski, C.J., 1994, in: *Compact Extragalactic Radio Sources*, ed. J.A. Zensus and K.I. Kellermann, NRAO-workshop, Socorro, p. 251.
- Camenzind, M., 1994, in: *IAU 159: Multi-Wavelength Continuum Emission of AGN*, ed. T.J.-L. Courvoisier and A. Blecha, (Kluwer, Dordrecht), p. 257.
- Hardee, P.E., Cooper, M.A., and Clark, D.A., 1994, *ApJ*, **424**, 126.
- Hunter, S.D., Bertsch, D.L., Dingus, B.L., *et al.*, 1993, *ApJ*, **409**, 134.
- Krichbaum, T.P., and Witzel, A., 1992, in: *Variability of Blazars*, ed. E. Valtaoja and M. Valtonen (Cambridge University Press), p. 205.
- Krichbaum, T.P., *et al.*, 1993a, in: *Sub Arcsecond Radio Astronomy*, ed. R.J. Davis and R.S. Booth, Cambridge University Press, p. 181.
- Krichbaum, T.P., *et al.*, 1993b, *A&A*, **275**, 375.

- Krichbaum, T.P., *et al.*, 1994a, in: *The Nuclei of Normal Galaxies: Lessons from the Galactic Center*, ed. R. Genzel (Kluwer, Dordrecht), in press.
- Krichbaum, T.P., *et al.*, 1994b, in: *IAU 159: Multi-Wavelength Continuum Emission of AGN*, ed. T.J.-L. Courvoisier and A. Blecha, (Kluwer, Dordrecht), p. 187.
- Krichbaum, T.P., *et al.*, 1994c, in: *Compact Extragalactic Radio Sources*, ed. J.A. Zensus and K.I. Kellermann, NRAO-workshop, Socorro, p. 39.
- Schalinski, C.J., Alef, W., Schuh, H., Witzel, A., and Campbell, J., 1986, in: *Die Arbeiten des SFB 78 Satellitengeodäsie der TU München 1984 & 1985*, ed. M. Schneider, Bayrische Akademie der Wissenschaften (München), p. 292.
- Schalinski, C.J., *et al.*, 1993, in: *Sub Arcsecond Radio Astronomy*, ed. R.J. Davis and R.S. Booth, Cambridge University Press, p. 184.
- Schalinski, C.J., *et al.*, 1994, in: *Compact Extragalactic Radio Sources*, ed. J.A. Zensus and K.I. Kellermann, NRAO-workshop, Socorro, p. 45.
- Schramm, K.-J., *et al.*, 1993, *A&A*, **278**, 391.
- Standke, K.J., 1994, PhD-thesis, University of Bonn.
- Standke, K.J., *et al.*, 1994, in: *URSI/IAU Symp. on VLBI technology, progress and new observational possibilities*, ed. M. Inoue, T. Sasao, S. Manabe and O. Kameya, Kyoto, in press.
- Steffen, W., *et al.*, 1993, in: *Sub Arcsecond Radio Astronomy*, ed. R.J. Davis and R.S. Booth, Cambridge University Press, p. 363.
- Wagner, S.J., *et al.*, 1994, *A&A*, in press.
- Zhang, Y.F., *et al.*, 1994, *ApJ*, in press.

DISCUSSION

R.T. Schilizzi (Q): Is 3C345 the only example you can use for this detailed analysis of component expansion and flux density evolution?

T. Krichbaum (A): For 3C345 the most complete set of data is available. However, in the BLLac 1803+78 (Krichbaum *et al.*, 1994, IAU 159) and in the QSO 4C39.25 (e.g. Alberdi *et al.*, 1993, *A&A*, 271, 93) also some good evidence for motion along spatially curved paths is found from VLBI at cm- and mm-wavelengths.

VLBI Study of Circumstellar Masers: Status Report

FRANCISCO COLOMER

Centro Astronómico de Yebes, Apartado 148. E – 19080 Guadalajara, Spain
and
Onsala Space Observatory, S – 439 92 Onsala, Sweden

Abstract

We discuss the European effort in the study of millimeter-wave circumstellar masers with very long baseline interferometry.

Present status

We have undertaken the study of the silicon monoxide (SiO) maser emission in the circumstellar envelopes of late-type stars with European VLBI telescopes since 1990. We obtained the first detection of compact SiO maser features with interferometric baselines up to 1750 km, providing fringe spacings as small as $0''.0004$ (Colomer *et al.*, 1992).

The first attempt to map the distribution of the SiO masers, performed in April 1991, confirmed the detection and the estimated maser sizes. The study of the supergiant μ Cep showed two spots separated ~ 5 mas (Colomer, 1993).

We observed the Mira star R Cas for 6 hours with the Onsala–Effelsberg baseline. We have obtained a fringe-rate map (Colomer, 1995) that is consistent with previous observations of this source (Lane *et al.*, 1982; McIntosh *et al.*, 1989). We clearly distinguish four regions of emission, distributed within 40 mas. Amplitude visibilities for this source yield Gaussian sizes in the range 1 – 2 mas (4 to $8 \cdot 10^{12}$ cm at 270 pc), demonstrating the existence of structure at milliarcsecond level. These results compare well with the structure of the SiO masers obtained at 86 GHz with the Plateau de Bure interferometer (A. Baudry, *priv. comm.*).

Future work

We have performed a new set of observations with 14 VLBI telescopes (the VLBA telescopes in the USA, Onsala, Effelsberg, Yebes, and the IRAM 30-m on top of Pico Veleta) to be processed soon at the VLBA correlator. We expect to produce high quality results owing to the much improved u, v -coverage obtained.

We are also planning new observations of the SiO masers at 43 and 86 GHz. We look forward to the participation of other European telescopes (like Toruń, Metsähovi, Medicina, Noto, Cambridge, or Crimea) to enhance the geometry of the interferometer with more east–west baselines.

Acknowledgements: This project is being developed in collaboration with D.A. Graham, T.P. Krichbaum, A. Witzel, R. Booth, B. Rönnäng, P. de-Vicente, A. Barcia, J. Gómez-González, V. Bujarrabal, J. Alcolea, A. Baudry, and N. Brouillet. It would not have been possible without the expertise and help of the staff crews at all participating observatories.

References

- [1] Colomer, F., Graham, D.A., *et al.*: 1992, ‘Detection of compact SiO maser emission at 43 GHz with a European very long baseline interferometer’, *A&A* **254**, L17.
- [2] Colomer, F.: 1993, ‘The study of SiO masers with VLBI’. Technical Report No. 144L, Chalmers University of Technology, Göteborg (Sweden).
- [3] Colomer, F.: 1995, ‘VLBI Study of the SiO maser emission at 43 GHz in the circumstellar envelope of R Cas’. Proceedings of the ‘Circumstellar matter’ conference held in Edinburgh (Scotland), on August 29th – September 2nd 1994. G.Watt, P.Williams (Eds), Kluwer Academic Publ. (in press).
- [4] Lane, A.P.: 1982, ‘Observations of SiO masers in the circumstellar envelopes of late-type stars’, PhD Thesis, University of Massachusetts.
- [5] McIntosh, G.C., Predmore, C.R., *et al.*: 1989, ‘VLBI and polarimetric observations of the SiO masers in R Cassiopeiae’, *Ap J* **337**, 934.

Towards Stellar Proper Motions in the Galactic Center

LORÁNT SJOUWERMANN

Onsala Space Observatory, 439 92 Onsala, Sweden *and*
Leiden Observatory, P.O.Box 9513, 2300 RA Leiden, The Netherlands

Prologue

At the Galactic Centre (GC) a large sample of OH/IR stars has become available (Habing *et al.*, 1983; Lindqvist *et al.*, 1992a; Van Langevelde *et al.*, 1992a). These stars are outstanding tracers of the gravitational potential in the inner 100 parsecs of the Galaxy. We have searched for H₂O maser emission in all the (known OH masering) stars and for SiO maser emission in a subsample. The results of such a survey will be valuable for the study of the maser emission mechanisms and the stellar population of the GC. *Most importantly, it will enable future VLBI measurements of stellar proper motions at the GC within a few years.*

Introduction

Because the OH masers in the circumstellar envelopes of the OH/IR stars directly reveal the radial velocity, these objects can be used for studies of the dynamics of the inner Galaxy (Fig. 1). In a first analysis the results have been modelled using a spherical potential and isotropic velocity distribution (Lindqvist *et al.* 1992b). Further work on more realistic models is in progress (Sevenster and Habing, private communication). But in all approaches it is clear that the interpretation is limited by the fact that only two components of the true position and one component of the velocity of the stars are measured. This is frustrating, because already there is some evidence that there is interesting structure in the stellar dynamics near the GC; stars with peculiar high velocity are present and apparently different populations of OH/IR stars can be distinguished near the GC. In particular it is of great importance to know the velocity distributions, not only in the *radial* (line-of-sight) direction, but in the *transverse* directions as well. Only knowledge of the true velocity distribution can reveal the true mass distribution in the GC (Binney & Tremaine, 1987) and therefore measurements of proper motions of these stars are required.

A VLA survey

A typical velocity of 100 km/s at the GC corresponds to about 2.5 mas/yr. Unfortunately, such a motion cannot be detected with VLBI observations of the OH maser close to the GC, because of heavy interstellar scattering at decimeter wavelengths (e.g.

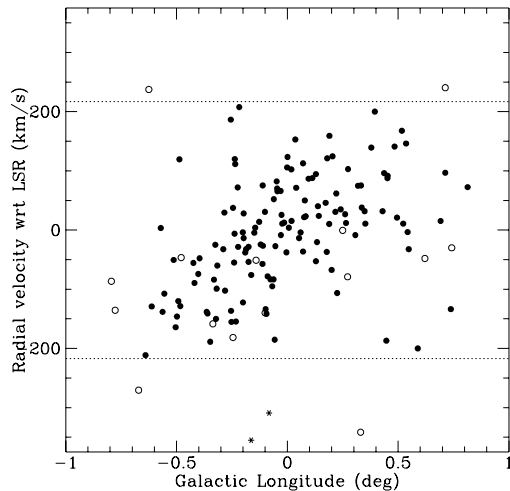


Figure 1: Radial velocities of OH/IR stars close to the GC as a function of Galactic Longitude. The dotted lines show the velocity limits of Lindqvist et al. (1992a). Open circles taken from Habing et al. (1983) and asterisks from Van Langevelde et al. (1992a). The correlation between the velocity and longitude is commonly explained by a net galactic rotation.

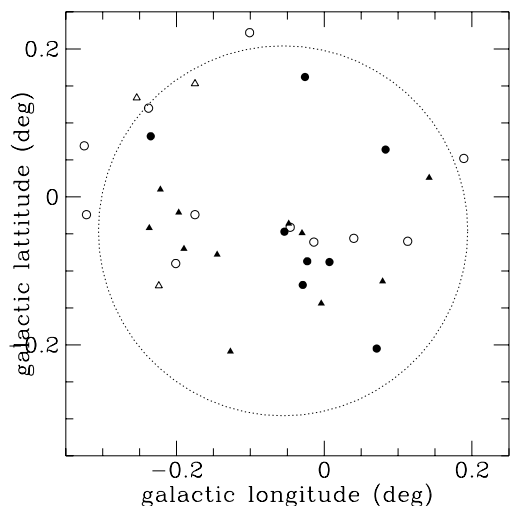


Figure 2: SiO emission from OH/IR stars close to Sgr A*. The circle is drawn at $14'$ from Sgr A*. Triangles are tentative detections; open symbols taken from Lindqvist et al. (1991), filled symbols are detections from our VLA survey.

Van Langevelde *et al.*, 1992b; Frail *et al.*, 1994). Therefore we have embarked on a project to search for H₂O maser emission in all 150 OH/IR stars and for SiO maser emission in a subsample of 50 OH/IR stars closest to Sgr A*. In the H₂O line this has been moderately successful, with a 15% detection rate. However, it is clear that SiO masers are even more promising in this respect. Not only would SiO observations yield even higher resolution (≈ 1 mas), allowing a 10 km/s accurate proper motion *measurement* within a year. But the SiO masers have the advantage that they originate very close to the star (Diamond *et al.*, 1994; Miyoshi *et al.*, 1994), making it easier to interpret VLBI data in terms of proper motions.

From our first VLA SiO observations we were already able to detect 7 out of 24 sources.

The future

The total sample of strong SiO masering OH/IR stars, together with the ones that show H₂O maser emission, should be enough to model the distribution of proper motions of OH/IR stars in the GC. Up till now we have good quality, strong (over 300 mJy) detec-

tions of 19 SiO and 9 H₂O stellar masers. We are still extending the list with our latest VLA observations and hope to confirm about 10 detections each in SiO and H₂O in the next months (Fig. 2).

In addition to the study of the stellar dynamics at the GC, a direct comparison of radial and transverse velocities and velocity dispersions would provide us with a direct geometrical value of R_0 , the distance to the GC (Reid *et al.*, 1988).

In particular the VLBA characteristics for these frequencies are most suited to detect these high brightness maser proper motions. With the full VLBA being operational, we proposed to observe three epochs of the H₂O and SiO masering OH/IR stars within the next year. Because we also have some stars that show both SiO and H₂O maser emission we will be able to check the resulting proper motions (referenced to Sgr A*) independently and start to build a catalogue of accurate relative proper motions ($\lesssim 1$ mas/yr or 40 km/s at 8 kpc).

This should enable us to reach our final goal: to model the mass distribution of the immediate environment of Sgr A*; the dynamical center of our Galaxy.

References

- Binney, J., Tremaine, S., 1987, Galactic Dynamics, Princeton Univ. Press, Princeton.
- Diamond, P.J., Kemball, A.J., Junor, W., Zensus, A., Benson, J., Dhawan, V., 1994, ApJ 430, L61.
- Frail, D.A., Diamond, P.J., Cordes, J.M., Van Langevelde, H.J., 1994, ApJ 427, L43.
- Habing, H.J., Olmon, F.M., Winnberg, A., Matthews, H.E., Baud, B., 1983, A&A 128, 230.
- Lindqvist, M., Ukita, N., Winnberg, A., Johansson, L.E.B., 1991, A&A 250, 431.
- Lindqvist, M., Winnberg, A., Habing, H.J., Matthews, H.E., 1992a, A&A Suppl. 92, 43.
- Lindqvist, M., Habing, H.J., Winnberg, A., 1992b, A&A 259, 118.
- Miyoshi, M., Matsumoto, K., Kamenno, S., Takaba, H., Iwata, T., 1994, Nature 371, 395.
- Reid, M.J., Schneps, M.H., Moran, J.M., Gwinn, C.R., Genzel, R., Downes, D., Rönnäng, B., 1988, ApJ 330, 809.
- Van Langevelde, H.J., Brown, A.G.A., Lindqvist, M., Habing, H.J., de Zeeuw, P.T., 1992a, A&A 261, L17.
- Van Langevelde, H.J., Frail, D.A., Cordes, J.M., Diamond, P.J., 1992b, ApJ 396, 686.

DISCUSSION

T. Krichbaum (Q): Will the regions of emission in the SiO stars be longlived enough to follow their motion?

L. Sjouwerman (A): We know the lifetime of individual SiO maser spots in these stars is about a few months. But the general SiO variability (integrated over all spots) is much less. We are confident that, if we might resolve some of the ring-like structures of the SiO maser spots, the average SiO maser spot is well defined — enough to keep the positional error of the star within 1 mas (which is the diameter of the SiO masering ring).

P.S.: We redetected 50 % of previously known (= 1990) SiO masering stars.

P. Wilkinson (Q): How close to the dynamical centre do you have to measure velocities to be within the sphere of influence of the central massive object?

L. Sjouwerman (A): The SiO masers we have looked for all are well within 50 pc of the GC. The expected circular velocity at 1 parsec is about 65 km/s for a 1 million solar mass Black Hole. The line-of-sight velocity dispersion of the OH/IR stars in the GC is already larger than this. So we really are interested in the type of stellar orbits (which probably are strongly elliptical). An interesting object we have found to show SiO maser emission is located at 0.3 pc projected distance of Sgr A* (which we believe is the dynamical center). We have high expectations for this source (for which the radial velocity is only -27 km/s) to show a large transversal motion.

22 GHz VLBI Survey: Status Report and Preliminary Results

G. MOELLENBROCK¹, K. FUJISAWA², R. PRESTON³, L. GURVITS^{4,5,6},
 R. DEWEY^{3,7}, H. HIRABAYASHI², M. INOUE⁸, D. JAUNCEY⁹,
 V. MIGENES⁹, D. ROBERTS¹, R. SCHILIZZI^{4,10}, S. TINGAY^{3,11}
 and A. ZENSUS¹²

¹ Brandeis University, Waltham, MA, U.S.A.

² Institute of Space and Astronautical Science, Sagamihara, Japan

³ Jet Propulsion Laboratory, California Institute of Technology, Pasadena, CA, U.S.A.

⁴ Joint Institute for VLBI in Europe, Dwingeloo, The Netherlands

⁵ Netherlands Foundation for Research in Astronomy, Dwingeloo, The Netherlands

⁶ Astro Space Center of P.N.Lebedev Physical Institute, Moscow, Russia

⁷ Princeton University, Princeton, NJ, U.S.A.

⁸ Nobeyama Radio Observatory, Nobeyama, Japan

⁹ Australia Telescope National Facility, Canberra, ACT, Australia

¹⁰ Leiden Observatory, Leiden, The Netherlands

¹¹ Mount Stromlo and Siding Springs Observatories, Weston Creek, ACT, Australia

¹² National Radio Astronomy Observatory, Socorro, NM, U.S.A.

Abstract

A ground-based VLBI survey to measure the visibilities and correlated flux densities in continuum at 22 GHz of more than 140 extragalactic radio sources has been conducted with baselines up to ≈ 11000 km. The project has been designed to help in preparation of target lists for VSOP and RadioAstron Space VLBI missions as well as providing observational data for statistical study of structural properties at 22 GHz on sub-milliarcsecond scales for this large sample of extragalactic sources.

Introduction

Space VLBI missions will provide baseline lengths up to 30000 km (VSOP) and 85000 km (RadioAstron). In order to make efficient use of observing time with two orbiting antennas, multifrequency estimates of correlated flux densities on these baselines are needed. To some extent, these estimates can be based on parameters which can be determined with single dish observations: total flux density, spectral and variability indices. However, two much more representative parameters are the correlated flux density and source visibility on long ground baselines (8000 – 10000 km). Sources with large correlated flux densities and/or high visibilities are almost certain to be visible over at least some of the range of VSOP baselines, and are the best candidates for observations with RadioAstron.

Extensive ground-based VLBI surveys of more than 900 extragalactic radio sources with intercontinental baselines have been performed at 2.3 and 8.4 GHz (Preston *et al.* 1985, Morabito *et al.* 1986). More than 200 extragalactic radio sources have been imaged with VLBI at 5 GHz in recent years (*e.g.* Eckart *et al.* 1987, Pearson and Readhead 1988, Taylor *et al.*, Thakkar *et al.* 1994). Successful detections on baselines of 1 – 2.4 Earth

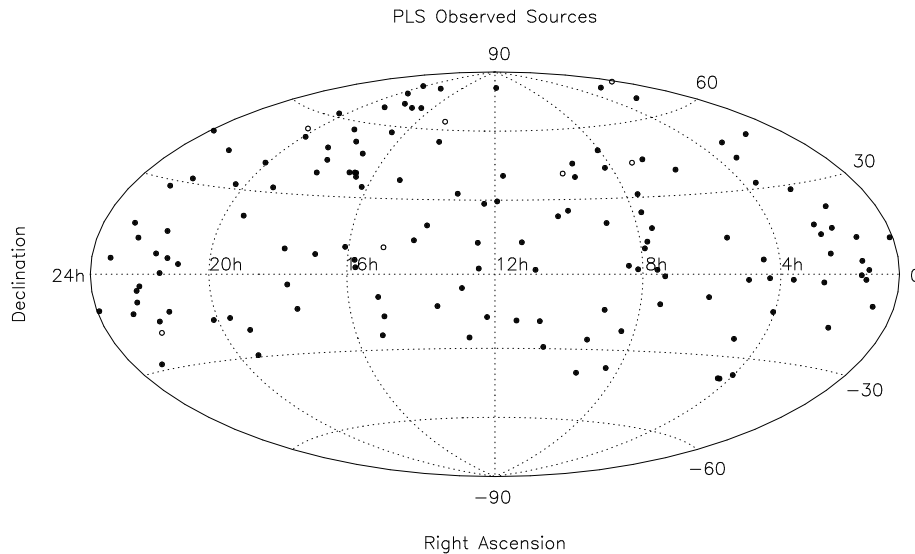


Figure 1: Sky distribution of sources observed in VLBI survey at 22 GHz. Filled circles show detected sources, open circles – non-detected.

diameters were made on 23 of 24 sources in the first Space-Ground VLBI experiment using an antenna on a TDRSS satellite at 2.3 GHz (Linfield *et al.* 1989). At 15 GHz, the detection rate in TDRSS Space-Ground demonstration VLBI experiment was lower, but so was the sensitivity of a small (5 m diameter) antenna. This indicates that sources can be detected on baselines of at least 40000 km (Linfield *et al.* 1990).

Much less extensive ground-based VLBI observations have been performed at 22 GHz. Lawrence *et al.* (1985) have detected 25 of 26 sources observed with baselines up to $\approx 5 \times 10^8 \lambda$ (≈ 7000 km). Only a few strongest sources (*e.g.* 3C84, 3C273, 3C345) which were well studied at lower frequencies have also been extensively imaged with VLBI at 22 GHz. Recently a sample of 15 bright AGN has been observed at 22 GHz with a global VLBI network (Wiik *et al.*, this Symposium).

The discussed survey allows a substantial enlargement to the list of sources suitable for follow up VLBI observations at 22 GHz with ground and space-ground VLBI.

It also has been shown that data from a non-imaging VLBI survey of a large enough sample of optically identified extragalactic sources can be used in order to conduct a cosmological study (Gurvits 1994).

Sample selection, observations, and data reduction

Selection of sources for the survey was based upon spectral flatness at 22 GHz. As of March 1993, 211 sources had published 22 GHz total flux densities and $\alpha > -0.5$ at 22 GHz. These sources constituted the primary target list. In order to reduce a bias toward northern sources, sources with $\alpha > -0.5$ at higher or lower frequencies (22 GHz total flux density unknown) were added. In accomodating finite observing time, scheduling priority was given to the strongest sources.

The sample contains all 26 sources from the previous 22 GHz VLBI survey (Lawrence *et al.* 1985) and all 47 suggested sources for mm and Space VLBI (Valtaoja *et al.* 1992).

The observations have been carried out in 8 sessions in 1993. The following antennas have been used (although not always all in each session): Goldstone (70 m), Tidbinbilla

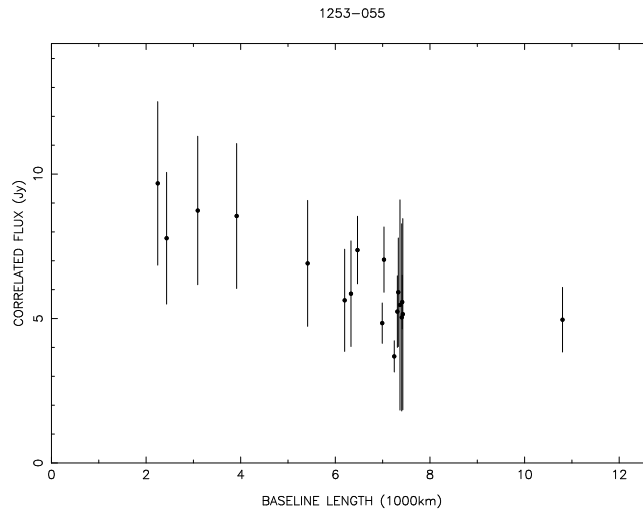


Figure 2: Correlated flux density versus projected baseline for the source 1253-055.

(70 m), Nobeyama (45 m), Kashima (34 m), VLBA Brewster (25 m), VLBA Mauna Kea (25 m). Nobeyama radio telescope was also used for total flux density measurements of all observed sources. Data had been recorded in Mk3A mode B format (28 MHz bandwidth), using high-density (narrow-track) terminals, and correlated at the 4-station Caltech/JPL correlator in Pasadena.

Preliminary results and conclusions

The allocated amount of time allowed observation of 142 sources, each source at at least 3 hour angles. A total of 135 sources has been detected ($SNR > 7$ with an integration time of 4 minutes). Fig. 1 shows the distribution of the observed 142 sources over the sky.

Table 1 represents distribution of detected and non-detected sources over various types of optical counterpart objects according to classification of Véron-Cetty and Véron (1993). Redshifts are known for 122 out of 135 detected sources.

Table 1. The distribution of observed 142 sources over optical counterpart types

	Quasars	BL Lacs	Other AGN	Empty fields
Detected	99	23	7	6
Non-detected	4	1	1	1
Total	103	24	8	7

Fig. 2 shows a typical example of the available data. As a general statement we note that almost all detected sources show decreases in correlated flux density with increasing projected baseline. However, at least 30% of the observed sample is composed of sources which have high enough correlated flux density to be primer candidates for observations with VSOP and RadioAstron. Further analysis will allow better specification of these sources.

Acknowledgements. The authors thank staffs of the NASA DSN, NRAO VLBA, NRO and Kashima stations for support of the project. The Netherlands Foundation for Research in Astronomy is supported by the Netherlands Foundation for Scientific Research (NWO). The National Radio Astronomy Observatory is operated by Associated Universities, Inc. under a Cooperative Agreement with the National Science Foundation.

Part of this research was carried out at the Jet Propulsion Laboratory under contract to NASA.

References

- Eckart A., Witzel A., Biermann P., Johnston K.J., Simon R., Schalinski C., and Kühr H. 1987, *A&AS* 67, 121.
- Gurvits L.I. 1994, *ApJ* 425, 442.
- Lawrence C.R., Readhead A.C.S., Linfield R.P., Payne D.G., Preston R.A., Schilizzi R.T., Porcas R.W., Booth R.S., and Burke B.F. 1985, *ApJ* 296, 458.
- Linfield R.P., Levy G.S., Ulvestad J.S., Edwards C.D., DiNardo S.J., Stavert L.R., Ottenhoff C.H., Whitney A.R., Cappallo R.J., Rogers A.E.E., Hirabayashi H., Morimoto M., Inoue M., Jauncey D.L., and Nishimura T. 1989, *ApJ* 336, 1105.
- Linfield R.P., Levy G.S., Edwards C.D., Ulvestad J.S., Ottenhoff C.H., Hirabayashi H., Morimoto M., Inoue M., Jauncey D.L., Reynolds J., Nishimura T., Hayashi T., Takano T., Yamada T., Barrett J.W., Conner S.R., Heflin M.B., Léhar J., Burke B.F., Roberts D.H., Whitney A.R., Cappallo R.J., Rogers A.E.E., Pospieszalski M.W., DiNardo S.J., Skjerve L.J., Stavert L.R., and Maher M.J. 1990, *ApJ* 358, 350.
- Morabito D.D., Niell A.E., Preston R.A., Linfield R.P., Wehrle A.E., and Faulkner J. 1986, *AJ* 91, 1038.
- Pearson T.J., and Readhead A.C.S. 1988, *ApJ* 328, 114.
- Preston R.A., Morabito D.D., Williams J.G., Faulkner J., Jauncey D.L., and Nicolson G.D. 1985, *AJ* 90, 1599.
- Taylor G.B., Vermeulen R.C., Pearson T.J., Readhead A.C.S., Henstock D.R., Browne I.W.A., and Wilkinson P.N. 1994, *ApJS*, in press.
- Thakkar D.D., Xu W., Readhead A.C.S., Pearson T.J., Polatidis A.G., and Wilkinson P.N. 1994, *ApJS*, in press.
- Valtaoja E., Lähteenmäki, and Teräsranta H. 1992, *A&AS* 95, 73.
- Véron-Cetty M.-P., & Véron P. 1993, *A Catalogue of Quasars and Active Nuclei*, 6th Edition, ESO Sci. Report No. 13.
- Wiik K., Valtaoja E., & Leppänen K. 1994, these Proceedings.

DISCUSSION

E. Valtaoja (Q): Do you see any dependence between the length of the baseline and the detection rate? In other words, can you extrapolate to RadioAstron/V SOP baselines and estimate how many of the sources you would be able to detect?

L. Gurvits (A): That is exactly the aim of the project. I present here very preliminary results. Further elaborations should answer the question.

I. Fejes (Q): What percentage of the 135 sources would you be able to observe with the sensitivity of RadioAstron and VSOP?

L. Gurvits (A): PLS sample selection criteria have been chosen to match expected sensitivity of the space VLBI missions. Therefore, we expect that a substantial part of the presented sample could be detected with the space VLBI, given that about 50 % of the sources observed demonstrate high enough correlated flux density at baselines $\sim 10\,000$ km.

Global VLBI Observations of Bright AGN

KAJ WIIK, ESKO VALTAOJA and KARI LEPPÄNEN

Metsähovi Radio Research Station, Finland

Abstract

A sample of 15 bright AGN has been observed at 22 GHz with two epoch global VLBI observations. The sample consists of all sources in the complete 2 Jy catalogue of Valtaoja *et al.* (1992) previously unmapped at 22 GHz. The aims of the survey are 1) to obtain basic high frequency data in preparation for the space VLBI missions, 2) to explore connections between continuum and VLBI data, and 3) to test unified models for AGN by estimating viewing angles and Lorentz factors from v/c (VLBI) and T_b (continuum).

The observing sample

For several years we have been monitoring the continuum flux densities of over 100 bright AGN with $\delta > -25^\circ$ using the Metsähovi (22, 37 and 90 GHz) and SEST (90 and 230 GHz) telescopes (Teräsraanta *et al.* 1992), with additional surveys of complete samples of radio sources (Wiren *et al.* 1992; Tornikoski *et al.* 1993). With the exception of a few steep-spectrum radio galaxies, virtually all important present-day VLBI sources as well as the most likely future millimeter and space VLBI candidates are included in our monitoring sample.

Although high resolution 22 GHz space VLBI observations are just a couple of years in the future, our knowledge of the mas structure of even the brightest AGN remains very fragmentary and hampers the planning of the complicated space programs. Using the results of our monitoring, we have constructed a complete Northern hemisphere sample of compact AGN (Valtaoja *et al.* 1992). The sample is the first one based on the high-frequency characteristics of AGN, using the selection criteria $S(22 \text{ GHz}) > 2 \text{ Jy}$ and $\alpha(2.7\text{--}5 \text{ GHz}) > -0.5$. Being the brightest and the most compact (from spectral flatness) of sources, the 2 Jy sample of 47 AGN is likely to include most of the main targets of mm and space VLBI. Our lack of basic data is well illustrated by the fact that of these 47 sources 15 had no published 22 GHz VLBI observations. These 15 sources formed our sample.

Our approach differs from that of the 22 GHz pre-launch survey (Moellenbrock *et al.*, these proceedings) in that instead of measuring one-epoch visibilities of a large sample our aim is to obtain high resolution multiepoch maps of some of the brightest and most compact sources. The basic difficulty with all non-mapping snapshot surveys is that the correlated 22 GHz flux density is almost completely dependent on whether the source is having a radio outburst at the time of the VLBI observation, since most of the the correlated flux comes from the compact new shock. Thus, the 'compactness' of a source, as derived from correlated and total VLBI flux density, is as time-variable as the total flux density, and therefore not a very good indicator of compactness at some future date (Valtaoja 1991; Valtaoja *et al.* 1992).

The continuum/VLBI connection

Total flux density measurements are often used just to calibrate VLBI data. However, they can be of much more use in trying to unravel both the structure and the evolution of the innermost regions in AGN. According to shock models, new shocks in the relativistic jets are responsible both for the major continuum flux density variations and for the creation of new VLBI components. We have begun to investigate, to which extent continuum monitoring can be used as a predictor of what will be seen in an upcoming VLBI observation, how much structural information can be derived just from continuum monitoring, and other ways of using continuum data to complement VLBI (for example component identifications and zero separation epochs).

The basic principle is simple. At 22 GHz (or higher), the lifetime of an outburst is usually less than the time interval between successive bursts, and only one bright shock component is visible at a given time. In the first approximation, a simple structure is then seen: either just the core (i.e., the base of the jet), or the core and the most recent shock propagating along the underlying jet. With well-sampled continuum monitoring the contributions of these two components can be separated, and the variability timescales associated with the shock flux changes can be used to get an estimate of the shock's physical size. New components are also 'seen' much earlier as total continuum flux changes, enabling the determination of zero epochs for the emergence of new VLBI components. In the few cases where sufficient 22 GHz continuum and VLBI data are available, the correspondence between continuum- and VLBI-derived source parameters is quite good (Valtaoja 1994; Valtaoja and Teräsranta 1993). (Abundant lower frequency data is not suitable for the comparisons, since the shocks remain visible for a long time, and the source structures become quite complex, as amply demonstrated by cm-VLBI maps.)

Since all the 15 sources in our sample are being monitored with Metsähovi and SEST telescopes, our multiepoch observations will enable us to evaluate the usefulness of continuum support for high resolution VLBI. Of high interest would also be the finding of total flux changes without the emergence of new VLBI components (or vice versa). These might indicate that other mechanisms than shocks are important, for example changes in the jet direction followed by Doppler (de)boosting of the components.

Unified models and viewing angles

The central tenet of unified models is that the orientation of a source is a crucial parameter for its observed properties and classification. As the viewing angle, the angle between the outflow and the line of sight, cannot be measured, various indirect estimates have been attempted. We have proposed a very direct method, which has not been previously used. In the simplest case, a relativistic outflow can be defined by just two parameters, the viewing angle Θ and the intrinsic Lorentz factor Γ of the flow. These are directly related to two at least in principle measurable quantities, the expansion speed β_{app} , and the Doppler boosting factor D . Taking the conventional view that apparent high brightness temperatures in excess of 10^{12} K are due to Doppler boosting, D can be estimated from T_b , which in turn can be calculated from the continuum flux variability timescales.

We have applied this method to all sources with known VLBI expansion speeds and sufficient monitoring data (Teräsranta and Valtaoja 1994). We found that the different classes of sources do indeed occupy different regions of the (Γ, Θ) -space in accordance with the unified model predictions. For examples, radio galaxies have, on the average,

larger viewing angles than 'normal' low polarization quasars, and the 'blazar-type' highly polarized quasars have the smallest viewing angles, while all three classes have similar Lorentz factors indicating that they belong to the same population of sources.

However, these conclusions are based on only 2–5 sources in each class, and at the very least a complete sample of radio sources should be observed for β and T_b . We hope to get expansion speeds for the majority of our 15 sources. Since we can estimate the zero epochs from continuum monitoring, we can calculate upper limits to β even for unresolved sources.

The observations

The first epoch observations were made in November 1992 and the second epoch observations in September 1993 (not yet correlated) at 22 GHz. We applied MK III for both epochs but got MK III mode E only for the latter. Because of this the first epoch data is quite noisy. 14 telescopes participated in the first epoch observations but due to wrong coordinates used in correlation, VLA (W1) data was lost. Furthermore there were problems with Green Bank baselines, phase oscillated during the whole session with a period of about 38 minutes and amplitude of even 180 degrees, possibly a receiver phaselock problem.

Fifteen sources (plus two calibrators) were observed during the 48 hours of total allocated time. Observations were split to EVN, US and global networks to keep all telescopes observing most of the time. One source was observed only a half or one hour at a time and scans for the same source were spread to cover the allocated observing time as evenly as possible and also to minimise the slewing time of the telescopes. Despite the snapshot nature of this observation, the uv -coverages are reasonable and even enable making high-resolution maps of some of the brightest sources.

Data reduction

Fringe fitting, calibration and combining of the data was made using the AIPS software. Editing, self calibration, model fitting and hybrid mapping were done using the Caltech VLBI software package.

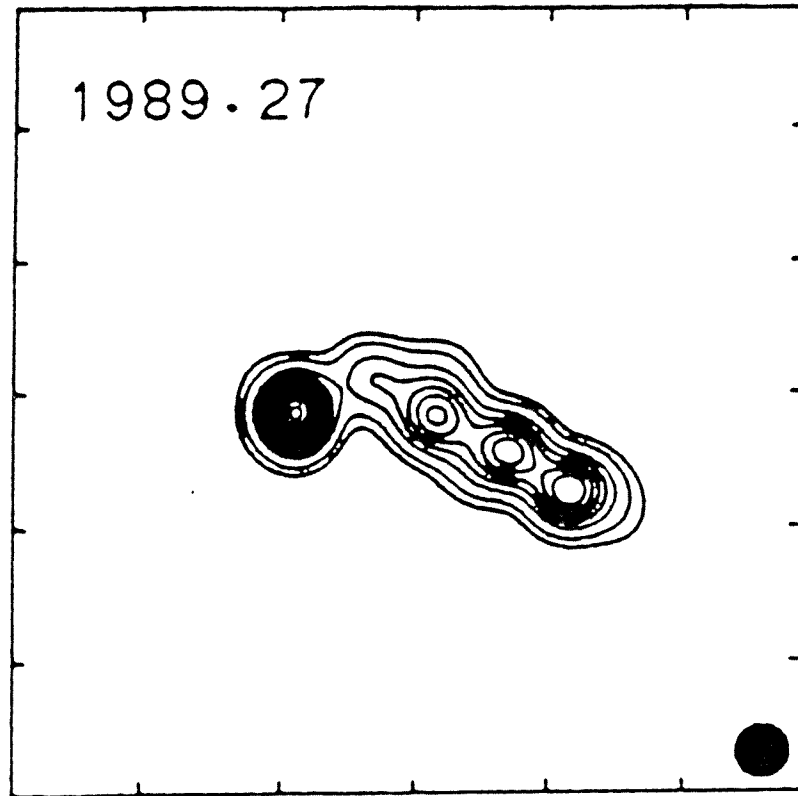
The system temperature information from the telescopes (except VLBA) were edited heavily as it seems that usually the first T_{sys} figure in a scan is taken before the antenna reaches the correct elevation.

First five sources were reduced using NRAO AOC Sun workstations but all the further work is done in Metsähovi using x486 and Pentium based Linux workstations.

Examples of the preliminary results

2134+004 (OX 057)

When compared to the previous VLBI observations at 10.7 GHz (Pauliny-Toth *et al.* 1990) the component separation is virtually constant and only the relative positions of the sources are changed. Furthermore Metsähovi continuum data shows a nearly constant flux of 5 Jy with very slight variation for nearly a decade. This supports the suggestion that the observed components represent quasi-stationary shocks in an underlying relativistic jet.



2134+004 at 10.7 GHz.

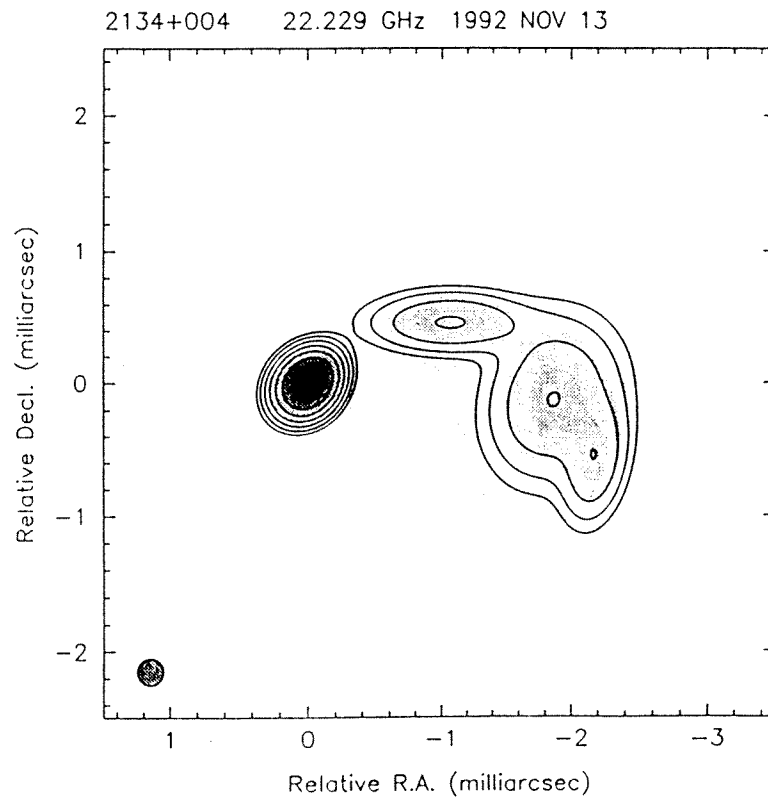


Figure 1: VLBI maps of 2134+004 at 10.7 GHz (Pauliny-Toth *et al.* 1990) and 22 GHz. The component separation is virtually constant and only the relative position has changed.

2145+067

This source was observed previously at 5 GHz (Wehrle *et al.* 1992) in 1986. There are no higher resolution/high frequency maps available although the source is quite strong (9 Jy during the observation).

0202+149

The flux of 0202+149 showed two peaks before the first epoch observations. If these peaks correspond to the components seen in the VLBI map, the velocity of the components would be $4c$ ($z = 0.8$) indicating a new superluminal source. Comparing the flux curve with also the second epoch map will be most interesting.

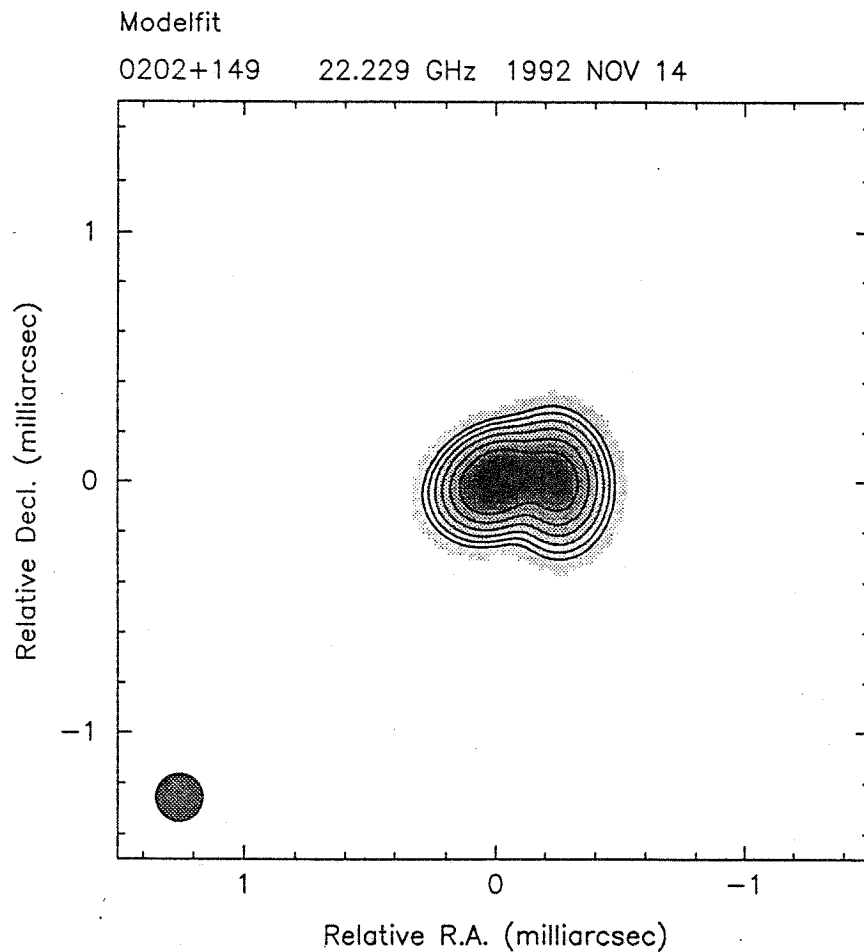


Figure 2: VLBI map of 0202+149 at 22 GHz. If the flux variations correspond to the VLBI components, this source is a new superluminal source

References

- Teräsraanta, H., *et al.*, 1992, *Astron. Astrophys. Suppl.* **94**, 121.
- Wiren, S., *et al.*, 1992, *Astron. J.* **104**, 1009.
- Tornikoski, M., *et al.*, 1993, *Astron. J.* **105**, 1680.
- Valtaoja, E., *et al.*, 1992, *Astron. Astrophys. Suppl.* **95**, 73.
- Valtaoja, E., 1991, in *Frontiers of VLBI*, ed. H. Hirabayashi *et al.*, Universal Academy Press, Tokyo, p. 209.
- Valtaoja, E., 1994, in *Astronomy with Millimeter and Submillimeter Wave Interferometry*, eds. M. Ishiguro and Wm.J. Welch, ASP Conference Series **59**, p. 54.
- Valtaoja, E., Teräsraanta, H., 1994, *Astron. Astrophys.* **289**, 35.
- Teräsraanta, H., Valtaoja, E., 1994, *Astron. Astrophys.* **283**, 51.
- Pauliny-Toth, I.I.K., *et al.*, 1990, in *Parsec-scale radio jets*, eds. J.A. Zensus and T.J. Pearson (Cambridge: Cambridge University Press), p. 55.
- Wehrle, A.E., *et al.*, 1992, *Astrophys. J.*, **391**, 589.

DISCUSSION

A. Alberdi (Q): Which explanations could you give to the case where you find a flare not associated with a component ejection?

K. Wiik (A): Good question! This is in fact one phenomenon we would like to study. One possibility is the too low resolution at lower frequencies.

Investigation of a Unique Sample of Faint Peaked Spectrum Sources

IGNAS SNELLEN¹, RICHARD SCHILIZZI^{1,2}, GEORGE MILEY¹,
GER DE BRUYN³ and MALCOLM BREMER¹

¹ Leiden Observatory, The Netherlands

² Joint Institute for VLBI in Europe, The Netherlands

³ Netherlands Foundation for Radio Astronomy, The Netherlands

Objects with radio spectra peaked near 1 GHz are a separate important but relatively rare category of radio source. These powerful radio sources are thought to be confined within their host galaxies, with spectral turnovers due to synchrotron self absorption caused by their high electron densities. It is thought that their host galaxies have particularly dense ISM which causes the radio source to be confined, to dimensions of typically 100 pc. It is not clear if they are small in linear size because they are very young radio sources (Mutel and Phillips 1988) or because they are confined by a very dense interstellar medium (O'Dea *et al.* 1991).

Until now, published studies (Fanti *et al.* 1990, O'Dea *et al.* 1991) have only concentrated on the bright members of the class, due to the lack of a significant sample of peaked spectrum sources at low flux densities. We have selected a sample of 119 peaked spectrum candidates with inverted spectra from two regions from the Westerbork Northern Sky Survey (WENSS). Additional 20 and 6 cm observations with WSRT and 3.5 and 2 cm observations with the VLA have been undertaken to select a sample of 52 truly peaked spectrum sources. The peaked spectrum sources in this sample have peak frequencies between 0.5 and 10 GHz and peak flux densities between 50 and 1000 mJy. The median peak flux density of our sample is 100 mJy, more than an order of magnitude lower than published samples.

We have already made considerable progress in the optical study of this sample. Of the 25 sources observed with the Jacobus Kapteyn Telescope (in June 1994), about half are galaxies and half are stellar objects (probably quasars). The magnitude distribution is similar to that for the bright peaked spectrum sources (O'Dea *et al.* 1991), so they very probably have the same optical luminosity distribution. Observations to determine the redshift for the sources in this sample have been proposed. If indeed our sample is similar to O'Dea *et al.*, we expect to find a wide range of redshift; this in turn should ensure good sampling of intrinsic peak frequency.

With this sample we hope, for the first time, to be able to investigate peaked spectrum sources over a wide range of luminosity, peak flux density and peak frequency. VLBI observations have been proposed, and are a crucial element of this project. It is the only way to investigate the radio structure of these objects, and will serve to investigate the physical nature and cosmological evolution of peaked spectrum sources.

References

- Fanti R. *et al.*, 1990, *A&A*, 231, 333.
Mutel R. L., Phillips, R. B., 1988, *Proc. IAU*, 129, p. 73.
O’Dea C. P., Baum, S. A., Stanghellini C. 1991, *ApJ*, 380, 66.

DISCUSSION

A. Lobanov (Q): When you determine the spectral parameters of the sources, do you plan to fit your data by some physical model, or just use a mathematical approximations?

I. Snellen (A): Yes, I plan to do physical modeling for these sources.

A. Lobanov (Q): In this case, do you expect to be able to avoid confusion because of possible multiple emitting regions in the source?

I. Snellen (A): The spectra we have are very clearly and narrowly peaked, which can support physical modeling. We also hope to constrain this modeling using VLBI observations.

J. Machalski (Q): Are you sure that your faint sources are not variable?

I. Snellen (A): For each source in our sample we have 5 or 6 flux-points at different frequencies. Although taken at different epochs, the sources still have narrow cone-shape spectra, which would be unlikely if they were variable. I cannot rule out low-level variability. We have 5 GHz data at 2 epochs (WSRT + Green Bank) which can rule out the variability.

Wide-field VLBI Observations of Gravitational Lenses

M.A. GARRETT¹, A.R. PATNAIK² and R.W. PORCAS²

¹University of Manchester, NRAL, Jodrell Bank, Macclesfield, Cheshire, SK11 9DL, UK.

²MPIfR, Auf dem Hügel 69, 53121, Bonn, Germany.

Abstract

We present a new method for imaging wide-field gravitational lens systems. This method uses the strongest, most compact lensed image as a phase calibrator. The phase corrections derived from mapping this image may be applied to the entire field of view. We present a wide-field EVN map of 2016+112 which employs this method. The phase calibration method also allows maps to be made of very weak images which might otherwise go undetected. Finally we note some caveats regarding the interpretation and comparison of VLBI maps of lensed images.

Introduction

VLBI observations of large-separation ($\sim 1 - 7''$) gravitational lens systems introduce several challenging data processing problems. In particular, lensed images of comparable flux give rise to multiple responses in rate and delay space. As a result, it is often difficult to isolate the visibilities associated with any one particular image or to make a map which is big enough to encompass all the images in one large field. Porcas (1993) has examined the process of fringe-fitting such data and demonstrates the advantages of adopting delay-rate referencing in these cases. This discussion will concentrate on the problem of wide-field mapping after the fringe-fitting process has been successfully completed.

Wide-field mapping

The field of view of Global VLBI observations is usually set by the bandwidth and visibility averaging time chosen by the observer. Averaging in time and frequency reduces the noise associated with each averaged visibility and allows weaker sources to be mapped using self-calibration procedures. However, the larger the bandwidth and the integration time, the smaller the field of view. The typical field of view is $\lesssim 300$ mas for MkIII mode A (56 MHz) $\lambda 18$ cm Global VLBI observations. This is usually more than sufficient for VLBI observations of compact, extragalactic radio sources since most of these show structure on scales $\lesssim 150$ mas. However, for gravitational lenses the separations are often considerably larger than this and most of the known systems are relatively weak. Hence a clear conflict exists between these two opposing constraints. On one hand the observer must average in time and frequency in order to have enough signal-to-noise for the self-calibration process; on the other hand, this reduces the field of view to such an extent that it no longer encompasses all the lensed images.

The traditional solution

Previous VLBI observations of gravitational lenses have pursued the following (partial) solution. The fringe-fitted data are rotated to the position of one of the lensed components and then averaged severely in frequency and in time (subject to the usual coherence restrictions). By doing this for each component, multiple data sets are generated (usually one for each image) and these are then mapped and self-calibrated in the normal way. The main drawback of this procedure is that it only works well for the largest separation lens systems (*e.g.* 0957+561). Even in this case one still finds that the response of both images is present on the shortest baselines (*e.g.* Effelsberg-Westerbork, $\lambda 18$ cm). This produces artefacts in the maps and usually the only solution is to delete the offending baselines (often the baselines with the highest sensitivity!). Nevertheless, this method has been able to produce reasonable results (Porcas *et al.* 1981, Gorenstein *et al.* 1988, Campbell *et al.* 1994 & Garrett *et al.* 1994).

The phase calibration solution

This new method uses the brightest, most compact lensed image as a phase calibrator in order to determine the phase corrections for the entire field. The data are averaged severely (as in the traditional method) and a map is made of the chosen calibrator image in the usual way. The phase corrections thus obtained (in the form of an AIPS CL table) are applied to the original unaveraged data and these are then transformed and CLEANed.

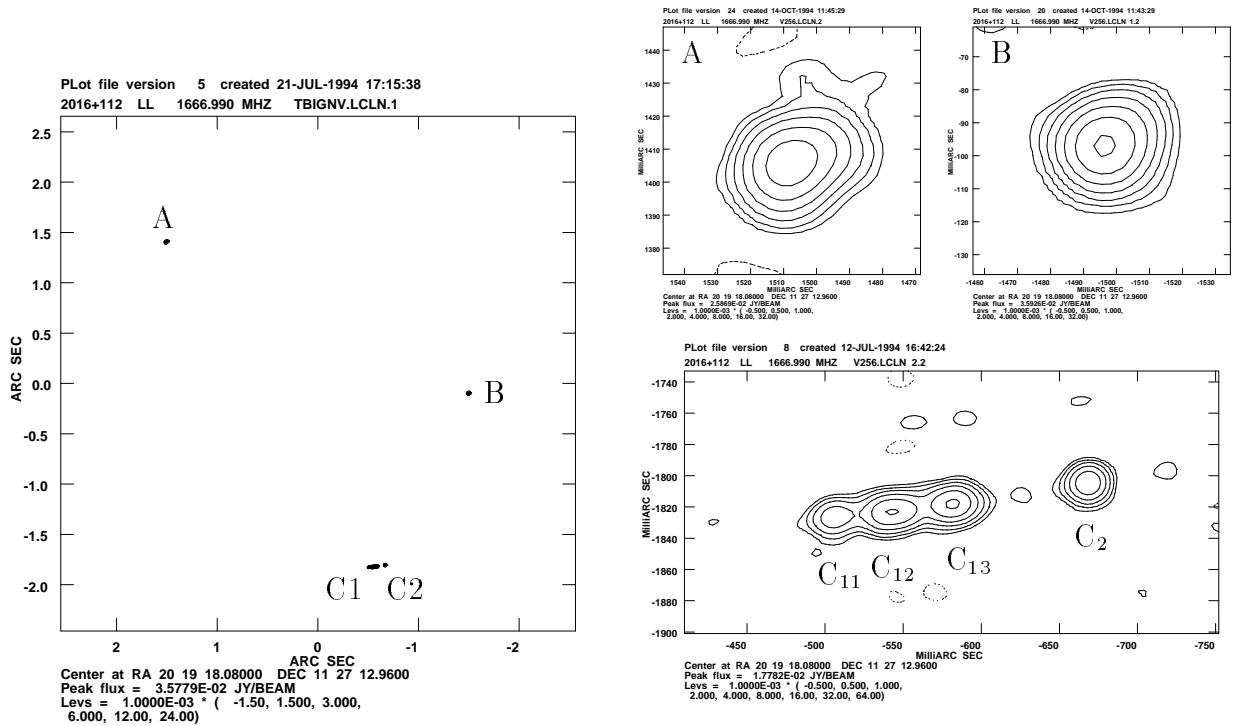


Fig. 1: The $\lambda 18$ cm wide-field EVN hybrid maps of 2016+112 A,B,C1,C2.

Figure 1 shows a wide-field EVN map of the remarkable gravitational lens system 2016+112 A,B,C. The map is 4 arcsec^2 in extent and in order to avoid smearing effects the data are stored as 7 adjacent (but independent) frequency channels (IFs) within which the visibility averaging time ranges from 30 to 5 seconds, depending on the baseline length. The circular restoring beam has a FWHM of 15 mas. The data were self-calibrated but the first phase correction was determined by using 2016+112B as a phase calibrator. This is an important first step, as it is very difficult to generate an accurate starting model for the first self-calibration procedure and a point source model is simply inadequate.

Mapping weak lensed images

The phase calibration method (previous section) has also been used to obtain the first global $\lambda 18 \text{ cm}$ VLBI map of a lensed image which was previously considered too weak to map with global VLBI - 2016+112C (see Figure 2). Again 2016+112B was chosen as the phase calibrator and the phase corrections were applied to the averaged 2016+112C data set. This source is too weak for self-calibration so the corrected data are simply transformed and cleaned. The resulting map is shown in Figure 2. The peak flux is only 4 mJy/beam and the extended double structure is strongly suggestive of gravitational lensing. C_2 is almost certainly a third lensed image of the same source which gives rise to the lensed images at A and B.

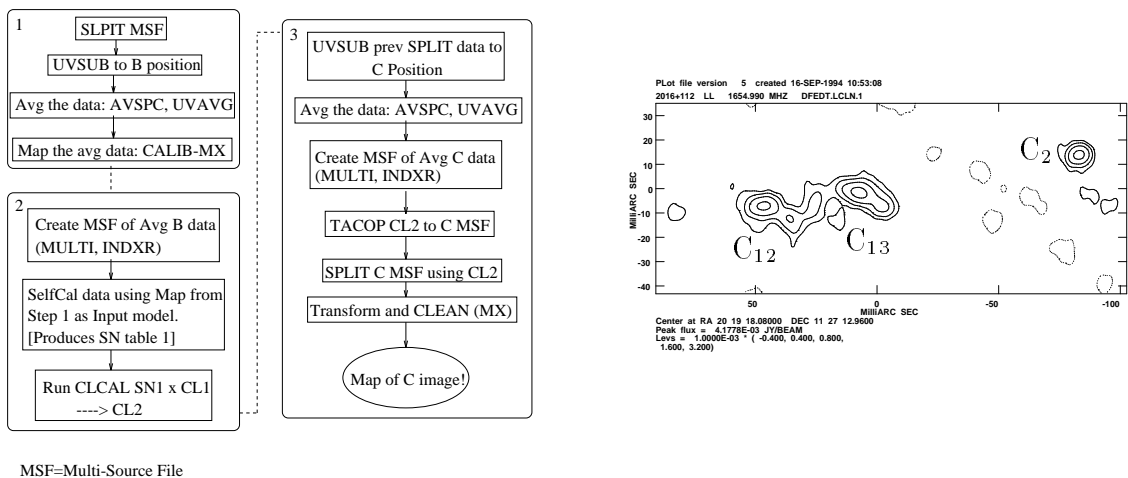


Fig. 2 Left: The phase calibration process as implemented within AIPS. Right: The phase-calibrated $\lambda 18 \text{ cm}$ Global VLBI map of the C complex. The peak flux is $\sim 4 \text{ mJy/beam}$ and the circular restoring beam $\sim 6 \text{ mas}$.

Note that with this method the position of C is known accurately with respect to the position of the phase-calibrator, 2016+112B. The success of this technique should allow other weak, demagnified lensed images to be mapped on mas scales. A similar technique was used by Rogers (1989) in order to map the weak third component (G') of 0957+561.

A similar result is obtained if the phase corrections are applied to the unaveraged Global VLBI data set (2.5 s average time, 7 IFs [Mode B]). However, the computational demands are considerable, with task completion measured on the time scale of days (for a SPARCclassic). This makes experimentation/iteration virtually impossible. The principle

advantage of using the unaveraged data is that the shortest, most sensitive baselines are now properly utilised.

Analysis details

The procedure, which is most easily implemented within AIPS, is shown schematically on the LHS of Figure 2. On the RHS the phase-calibrated map of the C complex is also shown. There are several possible pitfalls one might encounter along the way. Firstly, the offset position used for each of the images should be known to a few mas, if the data are to be severely averaged. Secondly, a CL table determined from the averaged data set (1 IF) will not be directly applicable to the unaveraged data set (multiple IFs). In this case a multi-IF CL table can be generated by self-calibrating the unaveraged phase calibrator data set using the best averaged (single IF) map as the input model. Finally, data editing can be greatly simplified by considering the strongest lensed image alone and applying its flag table to the other data sets (including the unaveraged data set). With multi-IF data it is often impractical to look at each IF individually but many of the remaining bad points can be removed with CLIP.

The interpretation of VLBI maps of lensed images

The observation that lensed images of a given system are magnified (or stretched/compressed) in different ways, coupled with the fact that VLBI can often resolve these images may lead to inconsistencies in the interpretation of the maps. This is not usually the case for the VLA (or even MERLIN) since the lensed images are often unresolved for these instruments.

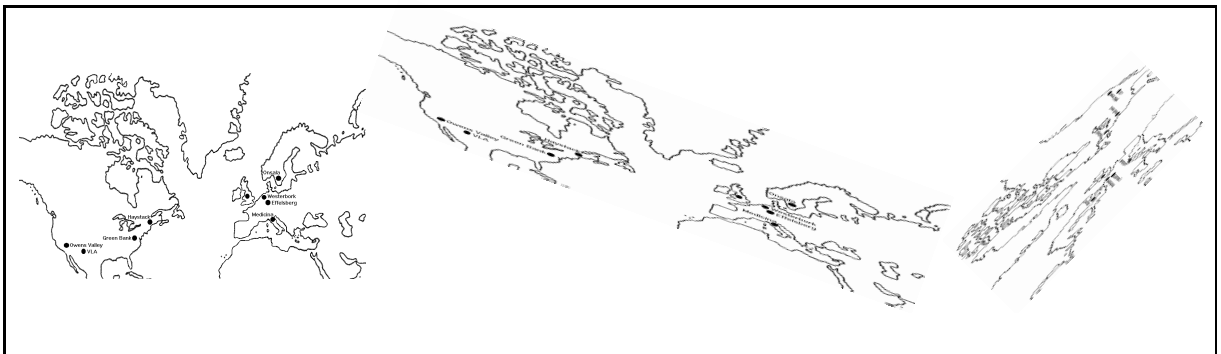


Fig. 3: Images of a VLBI array as it might appear to a source in the absence of lensing (3a) and in the presence of lensing (3b,c).

It is perhaps instructive to view the geometry of the observational process from the source’s point of view rather than the observer’s. The source “sees” multiple images of the Earth and hence multiple images of the VLBI array. Figure 3a,b,c show images of a VLBI array as it might appear to a source in the absence of lensing (3a) and in the presence of lensing (3b,c). The image shown in Fig. 3b represents a magnified image of the array while Fig. 3c represents a demagnified image of the array. The net effect is that as far as the source is concerned, multiple observations (and correlations/calibrations!)

are made with very different uv-coverage. From the observers perspective this means that a feature which is detected in one image *need not* be detected in another.

This effect can lead to different levels of missing flux in different images and may make the calculation of image flux ratios a tricky business. It would appear that sources with extended, non-discrete structure (*e.g.* 2016+112) are more likely to be affected than sources with relatively strong, barely resolved, discrete structure (*e.g.* 0957+561 A,B). Further work is required in order for these effects to be properly quantified.

Acknowledgments:

It is a pleasure to thank Sunita Nair for many useful discussions and for comments on the text of this paper.

References

- Campbell, R. *et al.* 1994, *Astrophys. J.*, **426**, 486.
Garrett, M.A. *et al.* 1994b, *Monthly Notices Roy. Astron. Soc.*, **270**, 457.
Gorenstein, M.V. *et al.* 1988, *Astrophys. J.*, **334**, 42.
Porcas, R.W. *et al.* 1981, *Nature*, **289**, 758.
Porcas, R.W. 1993, Compact Extragalactic Radio Sources, NRAO Workshop No. 23, eds J.A. Zensus and Kellermann, K.I., p. 125.
Rogers, A.E.E. 1989, in *Gravitational Lenses*, ed. J.M. Moran, J.N. Hewitt, and Lo, K.Y. (Springer-Verlag), p. 70.

DISCUSSION

A.A. da Costa (Q): Has the reversed effect of lensing on baselines you have described other effects besides the different resolution of the images?

M.A. Garrett (A): The effect is that radio structure which is mapped well in one of the (relatively demagnified) images may not be detected in another (relatively magnified image) because the VLBI array does not properly sample the larger scale size of the radio structure. This can make flux measurements inaccurate.

A Global VLBI Search for Milli-lenses

D.R. HENSTOCK¹, P.N. WILKINSON¹, I.W.A. BROWNE¹,
G.B. TAYLOR², A.C.S. READHEAD², T.J. PEARSON²,
R.C. VERMEULEN² and W. XU²

¹University of Manchester, NRAL, Jodrell Bank, Macclesfield, Cheshire, UK

²California Institute of Technology, Pasadena, CA, USA

Abstract

We have searched for milliarcsecond-scale gravitational lenses (“milli-lenses”) by examining VLBI maps of 300 flat spectrum sources from the recently completed CJ2 survey and the existing PR and CJ1 surveys. We have identified the 8 most promising lens candidates from this sample and have carried out multi-frequency follow-up observations with the VLBA. These VLBA observations allow us to rule out half the candidates; further observations are required to determine the nature of the remaining objects. If all the candidates are ruled out then the density of uniformly-distributed black holes must be less than $\sim 1\%$ of the closure density.

Introduction

Over the last few years there have been several major optical and radio surveys to search for multiply imaged quasars, including surveys with the HST (Bahcall *et al.* 1992) and the VLA (e.g. the Jodrell Bank–VLA Astrometric Survey, JVAS; Patnaik *et al.* 1992 and unpublished data). These surveys have had resolutions of 0.1 – 0.2 arcseconds and so have probed for lensing by galactic mass lenses of $\geq 10^{10} M_{\odot}$. Most of the lens systems discovered have image separations of $\sim 1''$; only a few have been found with sub-arcsecond separations. The smallest confirmed lensed system is 0218+357 (Patnaik *et al.* 1993) which was found during the JVAS; the lensing mass in 0218+357 is part of a gas-rich (hence spiral) galaxy (Carilli *et al.* 1993; Browne *et al.* 1993). A lens system with 0.45 arcsec image separation (1208+411) has been found optically (Magain *et al.* 1992; Bahcall *et al.* 1992). Finally, MERLIN observations of the compact triple source 2311+469 have shown that one of the outer lobes may be an Einstein ring with a diameter of ~ 0.2 arcsec (Polatidis 1993).

Lenses with image separations below ~ 100 mas (“milli-lenses”), corresponding to lensing masses of $\leq 10^9 M_{\odot}$, have not yet been found because they are smaller than the resolution limit of previous search techniques. In fact the only direct way to push the image separation limit below ~ 100 mas is to use VLBI. With VLBI we can look for lenses with image separations of 1 – 200 mas and hence probe for several interesting types of object which have masses in the range 10^6 to $10^9 M_{\odot}$.

The second Caltech-Jodrell VLBI survey (CJ2; Taylor *et al.* 1994, Henstock *et al.* 1994) was the first systematic search for gravitational lensing on scales of 1 – 200 mas. CJ2 was a global MkII snapshot VLBI survey of 193 flat spectrum radio sources at 5 GHz. Flat spectrum sources were chosen as the target objects because multiple imaging is much easier

to recognise in these core-dominated sources. The sources were selected from JVAS with the selection criteria: $S_{5\text{GHz}} \geq 350$ mJy; $\alpha_{8.4\text{GHz}}^{365\text{MHz}}$ flatter than 0.5; $\delta \geq 35^\circ$; $|b_{II}| \geq 10^\circ$.

CJ2 extended the Pearson & Readhead (PR; 1988) and first Caltech-Jodrell (CJ1; Polatidis *et al.* 1994, Thakkar *et al.* 1994, Xu *et al.* 1994) 5 GHz global VLBI surveys, by lowering the flux density limit and restricting the sample to flat spectrum objects. Also, the flat spectrum sources from the PR and CJ1 surveys (107 objects out of the 200 sources in the PR and CJ1 samples) have been retrospectively examined for lensing. Combining CJ2 with PR and CJ1 there is a total sample of 300 flat spectrum sources in which we have searched for millilensing.

Gravitational lensing on milliarcsecond scales

Conventional mass concentrations do produce systems with image separations of a few hundred mas and hence there is good reason to search on smaller scales. Spiral galaxies with small central bulges are obvious ~ 100 mas lens candidates. Also, the recent discovery of a large population of faint blue galaxies at $z \approx 0.5 - 1$ (e.g. Cowie, Songaila and Hu 1991; Smail *et al.* 1994), which are ideally placed for lensing, gives specific impetus to a VLBI search which is sensitive to 10 – 100 mas separations. The mass distribution in the centre of compact galaxies is, however, uncertain and this precludes a prediction of the frequency of lensing on these scales.

Searches for lensed systems with smaller image separations still, 1 – 10 mas, are of great cosmological interest. Such separations correspond to lensing masses in the range $\sim 10^6$ to $\sim 10^8 M_\odot$, comparable with the expected masses of pre-galactic compact objects (PCOs). PCOs arise in a wide range of cosmogonic scenarios with a natural mass scale, set by the Jeans mass, of order $10^6 M_\odot$ (e.g. Carr 1990). Uniformly distributed PCOs could provide a significant fraction of the closure density of the universe and can only be detected by their gravitational lensing effects. Press & Gunn (1973) first calculated the optical depth of the Universe to lensing by point masses and their calculations have been extended by Ostriker & Vietri (1986), Nemiroff and Bistolos (1990) and Kassiola, Kovner and Blandford (1991). Gnedin & Ostriker (1992) have recently suggested that radiation from an early generation of massive stars ($10^{6.5} M_\odot$), forming somewhat after decoupling, may have altered the light element abundances. Their hypothesis allows a larger amount of baryonic dark matter and does away with the need for non-baryonic forms. The massive stars collapse to black holes and with the required density, $\Omega \sim 0.15$, $\sim 5\%$ of high-redshift quasars should be milli-lensed.

The VLBI search

Observational parameters

A total of 300 flat-spectrum radio sources have been mapped in the course of the PR, CJ1 and CJ2 surveys. The typical resolution achieved with the USVN + EVN array at 5 GHz is 1 mas and the dynamic range in all the maps is $> 100 : 1$. We are confident that we can detect compact lensed components 30 times weaker than the brightest component in the map out to ± 200 mas. However, for image separations < 1.5 mas, i.e. comparable with the beam size, we are only sensitive to compact components with flux ratios $< 10 : 1$.

Redshift distribution

Redshifts for many of the PR and CJ1 sources have been determined using the Palomar 5m (e.g. Xu *et al.* 1993). More recently, we have used the 2.5m Isaac Newton Telescope on La Palma, and the Palomar 5m, to measure redshifts of many of the CJ2 sources. Hence the great majority ($\sim 80\%$) of the 300 flat-spectrum sources in the PR, CJ1 and CJ2 surveys now have measured redshifts. The current redshift distribution of the flat spectrum sources in the combined PR, CJ1 and CJ2 sample is shown in Figure 1. Further optical observations of faint CJ2 sources are planned which should increase the fraction of CJ2 objects with known redshifts to $> 90\%$.

The fraction of high redshift sources is a strong function of the limiting flux density of the sample. In the combined PR sample ($S_{6cm} > 1.3$ Jy) and CJ1 sample ($1.3 \text{ Jy} \leq S_{6cm} \leq 0.7$ Jy) only 3 objects ($\sim 3\%$) have $z > 2.5$ whereas in the CJ2 sample ($0.7 \text{ Jy} \leq S_{6cm} \leq 0.35$ Jy) 18 objects ($\sim 9\%$) have $z > 2.5$.

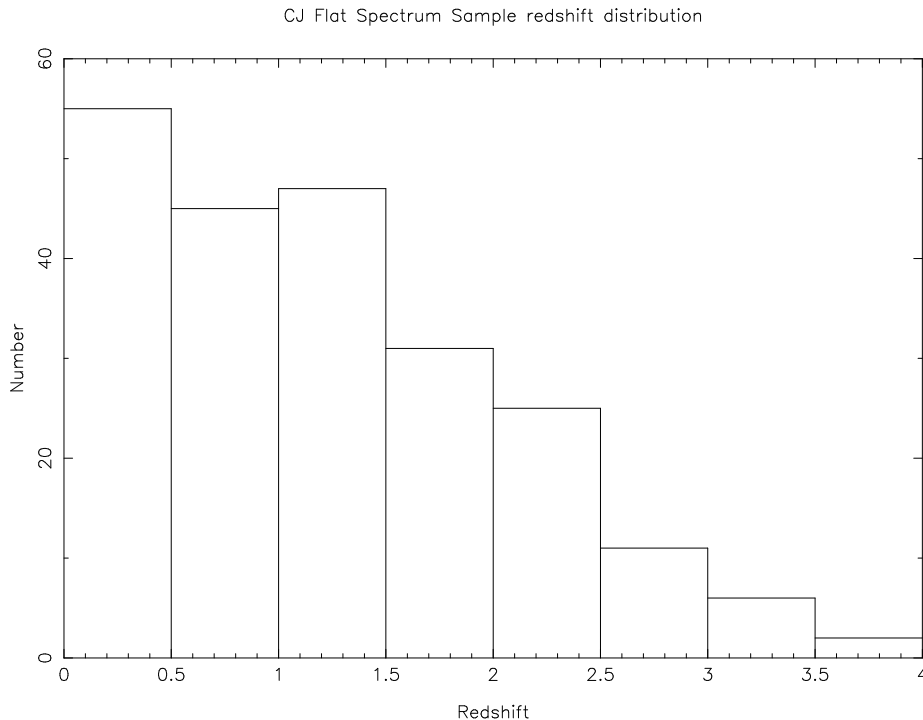


Figure 1: The redshift distribution of flat-spectrum sources in PR+CJ1+CJ2

Recognizing lens candidates

To get a feeling for the possible lensed-image configurations to be expected in the VLBI surveys we carried out simulations[†] of the lensing effect of a $10^7 M_{\odot}$ PCO on a typical core-jet source. These simulations were carried out for various impact parameters of the lens with respect to the source.

In a few cases the structure obtained was a Einstein ring-like (cf. 0218+357) or a twin core-jet (cf. 1830–211) configuration. These obviously lensed images would be easy to recognise. However, in the majority of cases the structure was much simpler, consisting of

[†]Using a program written by D. Narasimha

the core-jet primary image with the secondary image a demagnified, fainter component. When these cases were convolved with a 1 mas restoring beam the secondary image appeared to be smaller than, or comparable in size with, the primary image. Therefore, we treated any source with a compact companion component *no larger than the bright component* as a lens candidate.

Full details on the simulations are given in Henstock (1992) and are summarised in Wilkinson *et al.* (1994a).

Candidates and follow-up observations

Using the knowledge gained from our computer simulations and with the aid of model-fitting for an initial set of candidates, we identified six promising *candidate* mas-scale lens systems in CJ2 and two candidates in CJ1. No candidates were identified in PR as this sample has been well studied and the few potential candidates could be ruled out from the literature. It should be noted, however, that there are other sources with well-separated multiple components in PR, CJ1 and CJ2 but these are (or are likely to be) Compact Symmetric Sources (CSOs; Conway *et al.* 1992, 1994; Wilkinson *et al.* 1994b).

We made initial follow-up observations of these candidates with 6 telescopes of the VLBA in February and March 1994 (total observing time = 2×12 hours). To complement the existing 5 GHz images we observed each candidate at 1.6 GHz, 8.4 GHz and 15 GHz using the MkII recording system; three 20-minute snapshots were obtained per source at each frequency. The aims of the follow-up observations were twofold. First, we were interested in the appearance of components at the different frequencies/higher resolution—would they have simply related structures consistent with lensing, or would they, for example, be shown to be conventional core-jet sources with the fainter component being a knot in a previously unseen jet. Secondly, we wanted to use the multi-frequency observations to measure the radio spectra of the potentially lensed components; lensed images must have identical spectra.

The 1.6 GHz and 8.4 GHz observations were very successful, and we obtained good images of all the candidates at these frequencies. However, the 15 GHz observations were less successful as the limited sensitivity of the MkII recording system meant that reliable images were only obtained for sources with correlated fluxes of > 250 mJy. We obtained

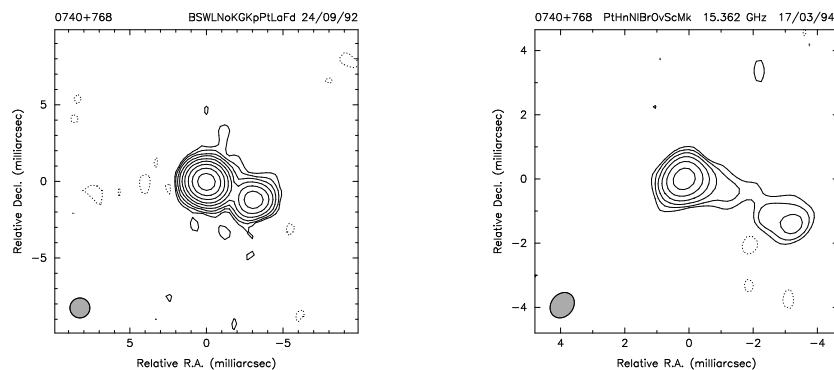


Figure 2: The lens candidate 0740+768: left—CJ2 map at 5 GHz (resolution ~ 1 mas) made with a “global” array; right—VLBA map at 15 GHz (resolution ~ 0.5 mas)

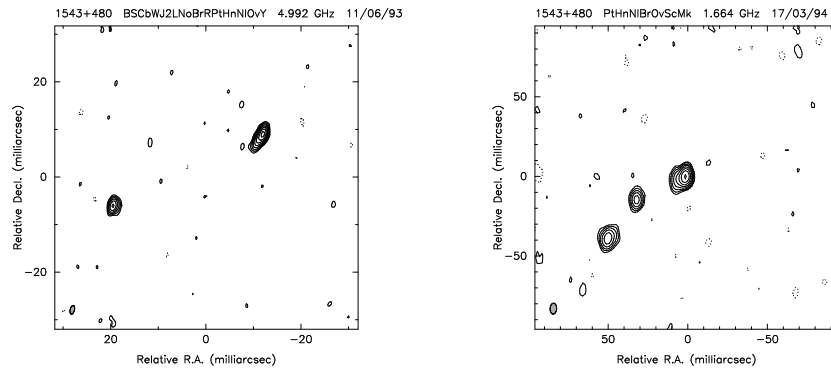


Figure 3: The lens candidate 1543+480: left—CJ2 map at 5 GHz (resolution ~ 1 mas); right—VLBA map at 1.6 GHz (resolution ~ 5 mas)

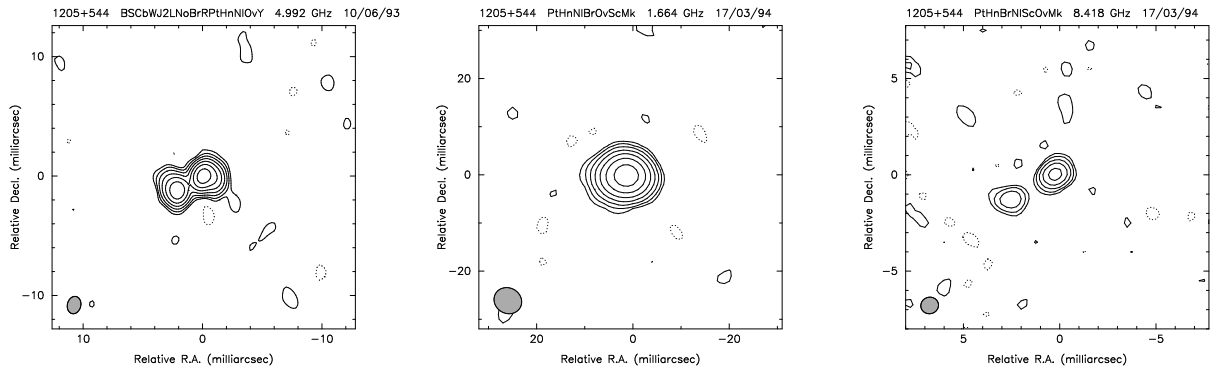


Figure 4: The lens candidate 1205+544: left—CJ2 map at 5 GHz (resolution ~ 1 mas); middle—VLBA map at 1.6 GHz (resolution ~ 5 mas); right—VLBA map at 8.4 GHz (resolution ~ 1 mas)

reliable images for only two candidates at this frequency.

The follow-up observations allowed us to rule out about half of the candidates as being conventional core-jet sources. Figure 2 shows an example of such a source, 0740+768. Our CJ2 survey map shows 0740+768 to be a good lens candidate, however the higher resolution 15 GHz VLBA map reveals the sources to be a core with a jet at a p.a. of -100° . Figure 3 shows another example, 1543+480. Here, the 1.6 GHz map shows a steep spectrum third component not seen at 5 GHz. This, coupled with the fact that the middle component has a steeper spectrum than the right-hand component, imply that this source is not a milli-lens but is instead almost certainly a core-jet source.

Most of the remaining candidates are probably ruled out because of spectral differences between the components, but the limited success of the 15 GHz observations means that we can as yet not be certain. Figure 4 shows one of the remaining candidates, 1205+544, at 5 GHz, 1.6 GHz and 8.4 GHz. For such remaining candidates, we await the results of higher sensitivity VLBA observations at 15 GHz, which are scheduled for the 1994/1995 Winter.

If any of the remaining candidates are confirmed as gravitationally lensed systems, then we will have revealed the presence of a significant population of objects in the universe with masses of $\sim 10^6 - 10^9 M_\odot$. Further observations will then be carried out to try and determine whether the lensing bodies are galaxies or black holes (e.g. is there any

evidence of gas in the lensing object?). If the lensing bodies are black holes, then we would confirm that PCOs make up a significant fraction of the closure density of the universe. Alternatively, if all the candidates are finally ruled out, we can limit the density of uniformly distributed PCOs to less than 1% of the closure density.

Note that CSOs might initially be mistaken for milli-lenses and vice versa. But CSOs are predominantly identified with galaxies, have low polarisation and low variability and also have radio spectra which steepen at high frequencies; their components are also likely to be more resolved than a system of multiple core images. Hence it should be straightforward to discriminate lensed systems from CSOs.

Conclusions

We have identified the 8 most promising milli-lens candidates from our sample of 300 flat spectrum sources. We have followed these up with multi-frequency VLBA observations and have ruled out about half of the candidates. We will follow up the remaining objects at 15 GHz with the VLBA in Winter 1994/5. If all the candidates are eventually ruled out, we can constrain the density of uniformly distributed PCOs to $\sim 1\%$ of the closure density.

However in order to place stronger constraints on the cosmological density of PCOs, and the contribution of compact galaxies to lensing on scales 10 – 100 mas, a larger sample of sources must be searched. Following the suggestion of Kassiola, Kovner and Blandford (1991) an initial goal would be to increase the sample size from 300 to ~ 1000 sources. Such a sample would be comparable in size to that of successful arcsec-scale lens searches made with the VLA. The VLBA is well-suited to this new surveying task.

Acknowledgements: We thank the many people at the observatories participating in the PR, CJ1 and CJ2 VLBI surveys for helping make them such a great success. We are very grateful to Martin Shepherd for developing and maintaining DIFMAP. Our thanks also go to D. Narasimha for the use of his lensing program.

References

- Bahcall, J. N., Maoz, D., Doxsey, R., Schneider, D. P., Bahcall, N. A., Lahov, O., and Yanny, B. 1992, *Astrophys. J.*, **387**, 56.
- Browne, I. W. A., Patnaik, A. R., Walsh, D., and Wilkinson, P. N. 1993, *Monthly Notices Roy. Astron. Soc.*, **263**, L32.
- Carilli, C. L., Rupen, M. P. and Yanny, B. 1993, *Astrophys. J. (Letters)*, **412**, L59.
- Carr, B. J. 1990, *Comments on Astrophysics*, **14**, 257.
- Conway, J. E., Pearson, T. J., Readhead, A. C. S., Unwin, S. C. Xu. W. and Mutel, R. L. 1992, *Astrophys. J.*, **396**, 62.
- Conway, J. E., Myers, S. T., Pearson, T. J., Readhead, A. C. S., Unwin, S. C., and Xu, W. 1994, *Astrophys. J.*, in press.
- Cowie, L. L., Songaila, A., and Hu, E. M. 1991, *Nature*, **354**, 460.
- Gnedin, N. Yu. and Ostriker, J. P. 1992, *Astrophys. J.*, **400**, 1.
- Henstock, D. R. 1992, PhD Continuation Report, University of Manchester.
- Henstock, D. R., Wilkinson, P. N., Taylor, G. B., Readhead, A. C. S. and Pearson, T. J., *Astrophys. J. Suppl.*, in preparation.
- Kassiola, A., Kovner, I., and Blandford, R. D. 1991, *Astrophys. J.*, **381**, 6.

- Magain, P., Surdej, J., Vanderriest, C., Pirenne, B. and Hutsemekers, D. 1992, *Astron. Astrophys.*, **253**, L13.
- Nemiroff, R. J. and Bistolos, V. G. 1990 *Astrophys. J.*, **358**, 5.
- Ostriker, J. P. and Vietri, M. 1986, *Astrophys. J.*, **300**, 68.
- Patnaik, A. R., Browne, I. W. A., Wilkinson, P. N., and Wrobel, J. M. 1992, *Monthly Notices Roy. Astron. Soc.*, **254**, 655.
- Patnaik, A.R., Browne, I.W.A., King, L.J., Muxlow, T.W.B., Walsh, D., and Wilkinson, P.N. 1993, *Monthly Notices Roy. Astron. Soc.*, **261**, 435.
- Pearson, T. J. and Readhead, A. C. S. 1988, *Astrophys. J.*, **328**, 114.
- Polatidis, A. G.: 1993, Ph. D. thesis, University of Manchester.
- Polatidis, A. G., Wilkinson, P. N., Xu, W., Readhead, A. C. S. and Pearson, T. J., 1994, *Astrophys. J. Suppl.*, in press.
- Press, W. H. and Gunn, J. E. 1973, *Astrophys. J.*, **185**, 397.
- Smail, I., Ellis, R. S., and Fitchett, M. J., 1994, *Monthly Notices Roy. Astron. Soc.*, **270**, 245.
- Taylor, G. B., Readhead, A. C. S., Pearson, T. J., Henstock, D. R., and Wilkinson, P. N., *Astrophys. J. Suppl.* in press.
- Thakkar, D.D., Xu, W., Readhead, A. C. S., Pearson, T. J., Polatidis, A. G. and Wilkinson, P. N., 1994, *Astrophys. J. Suppl.*, in press.
- Wilkinson, P. N., Henstock, D. R., Browne, I. W. A., Readhead, A. C. S., Taylor, G. B., Pearson, T. J., and Vermeulen, R. C., 1994a, in *Compact Extragalactic Radio Sources*, Proceedings of Socorro Workshop, eds. J. A. Zensus and K. .I. Kellermann (NRAO), p. 259.
- Wilkinson, P. N., Polatidis, A. G., Readhead, A. C. S., Xu, W. and Pearson T. J., 1994b, *Astrophys. J. (Letters)*, **432**, L87.
- Xu. W., Lawrence, C. R., Readhead, A. C. S., and Pearson, T. J., 1994, *Astron. J.*, **108**, 395.
- Xu. W., Readhead, A. C. S., Pearson, T.J., Polatidis, A. G., and Wilkinson, P. N. 1994, *Astrophys. J. Suppl.*, in preparation.

Sub-arcsecond Structure of the ‘Optically Quiet Quasar’, 0646+600

C.E. AKUJOR^{1,2,3}, R.W. PORCAS¹ and J.V. SMOKER³

¹Max-Planck Institut für Radioastronomie, Auf dem Hügel 69, 53121 Bonn, F.R.G.

²Chalmers University of Technology, Onsala Space Observatory, Onsala S-439 92, Sweden

³University of Manchester, NRAL, Jodrell Bank, Cheshire, SK11 9DL, England

Abstract

We report the progress on our continuing survey of Optically Quiet Quasars (OQQs) and present multi-frequency (1.6, 4.9, 8.4 and 22 GHz) VLBI and optical observations of 0646+600, a prototype OQQ. It is a ‘red’ quasar with a compact mas double/triple radio structure, which exhibits anomalous structural changes. Between 1989.79 and 1992.22, the overall separation of the two bright components at 5 GHz decreased by 0.25 mas, and a weak middle feature evident in 1989 was not detected in the later observations. We discuss these structural changes in 0646+600.

Introduction

In the last few years we have continued detailed optical and radio investigation of ‘Optically quiet quasars’ (OQQs) — objects which resemble quasars in radio structure (bright radio cores) and spectrum (flat), but are unidentified or faint optically (Akujor & Porcas 1991; Akujor *et al.* 1994 and in prep.). These observations made with the Nordic Optical Telescope (NOT), VLA, MERLIN and VLBA/VLBI do show that a majority of OQQs are ‘red’ quasars with $m_{R-V} \sim 1$ and show different structural types in their cores; core-jet, doubles/triples (Akujor *et al.* in prep.). Observations at several wavelengths also suggest that many OQQs are Gigahertz-peaked spectrum (GPS) radio sources.

The confirmed compact (mas) double/triple radio sources so far found amongst OQQs include 0218+356, 0026+346, 0646+600 (Zensus & Porcas 1985, Akujor & Porcas 1992). 0646+600 is a ≤ 1 Jy (5 GHz) variable radio source which shows no large-scale extended structure (Stanghellini *et al.* 1990). We had associated it with an ‘empty field’ on the basis of the radio position of Patnaik *et al.* (1992), but Meisenheimer & Röser (1983) report an identification with a faint 19 mag red QSO with a redshift $z = 0.455$ (Stickel & Kühr 1993). We have made deep multi-band optical images of 0646+600 with the NOT and observed it with VLBI at 1.6 (1992.87), 5 GHz (1989.79; 1992.22), 8.4 GHz (1991.17) with transatlantic baselines and at 22.2 GHz (1992.85) with the EVN.

NOT observations

The optical observations of 0646+600 were taken during 1993 April 22nd using the 2.5 m NOT using the Stockholm CCD camera. The $2.5' \times 2.5'$ field was imaged in *V* for 900 s and in *R&I* for 600 s with the seeing FWHM being ~ 0.8 arcsec. Standard CCD reduc-

Table 1: Magnitudes for QSO 0646+60

m_V	m_R	m_I	References
20.5(0.2)	19.6 (0.1)	18.9 (0.1)	This paper
	19.9		Stickel & Kühr (1993)
	19.2(0.2)		Fugmann & Meisenheimer (1988)
	18.9(0.3)		Meisenheimer & Röser (1983)

tion procedures were used to reduce these data. This included dark current subtraction, debiasing, cosmic ray removal and flatfielding using twilight flatfields. The standard star field F873–8 (Stobie *et al.* 1985) was used to calibrate the V and I filters and the R calibration was tied to stars in the 0957+561 field observed in r by Young *et al.* (1981). We estimate the uncertainty in the calibration to be less than 0.1 magnitudes.

Using the Jodrell Bank coordinate measuring machine, we measured the coordinates of 15 SAO stars of known positions and used these to calculate the position of the brightest star on the CCD image that was also visible on the Palomar Sky Survey. Unfortunately only one such star exists whose image is visible on both the CCD and POSS print; the QSO and surrounding galaxies are invisible on the POSS. This is not surprising as their magnitudes lie beneath the print limit of $m_R=18.9$ mag (Meisenheimer & Röser 1983). We note that having only one star common to the CCD and POSS print is not an ideal situation; if the star has significant proper motion between the date of the POSS plate exposure (1954 Nov 2nd) and the current CCD image exposure (1993 April 22nd) then the optical QSO position given here may be in error. With this caveat, the derived optical position agrees within the errors with the radio position given in Patnaik *et al.* (1992).

The apparent VRI magnitudes of 0646+600 were determined using FOTO within FIGARO and are listed in Table 1. The errors in our magnitudes have been calculated using the photon and readout noises and a contribution of 0.1 magnitudes due to the zero-point uncertainty. Values have not been corrected for internal absorption or galactic extinction; using the maps of Burstein & Heiles (1982) we estimate $A_V = 0.20$ mag and $A_R = 0.15$ mag. Previous measurements of the R magnitude of 0646+600 taken by Meisenheimer & Röser (1983), Fugmann & Meisenheimer (1988) and Stickel & Kühr (1993) indicate that 0646+600 is an optically variable object. Although these authors used different types of R passband for their observations, this is unlikely to account for the large spread in R magnitude observed over the last ten years which is probably intrinsic to the QSO.

As was noted by Stickel & Kühr (1993), we find that the QSO is surrounded by a number of faint galaxies. Stickel & Kühr find that one of these galaxies has a redshift $z \approx 0.45$, compared to the QSO which they find to have redshift of $z = 0.455$.

VLBI observations

All our VLBI observations were made using the MK2 recording system and correlated at the Caltech Block2 correlator. A summary of the observational details is given in Table 2.

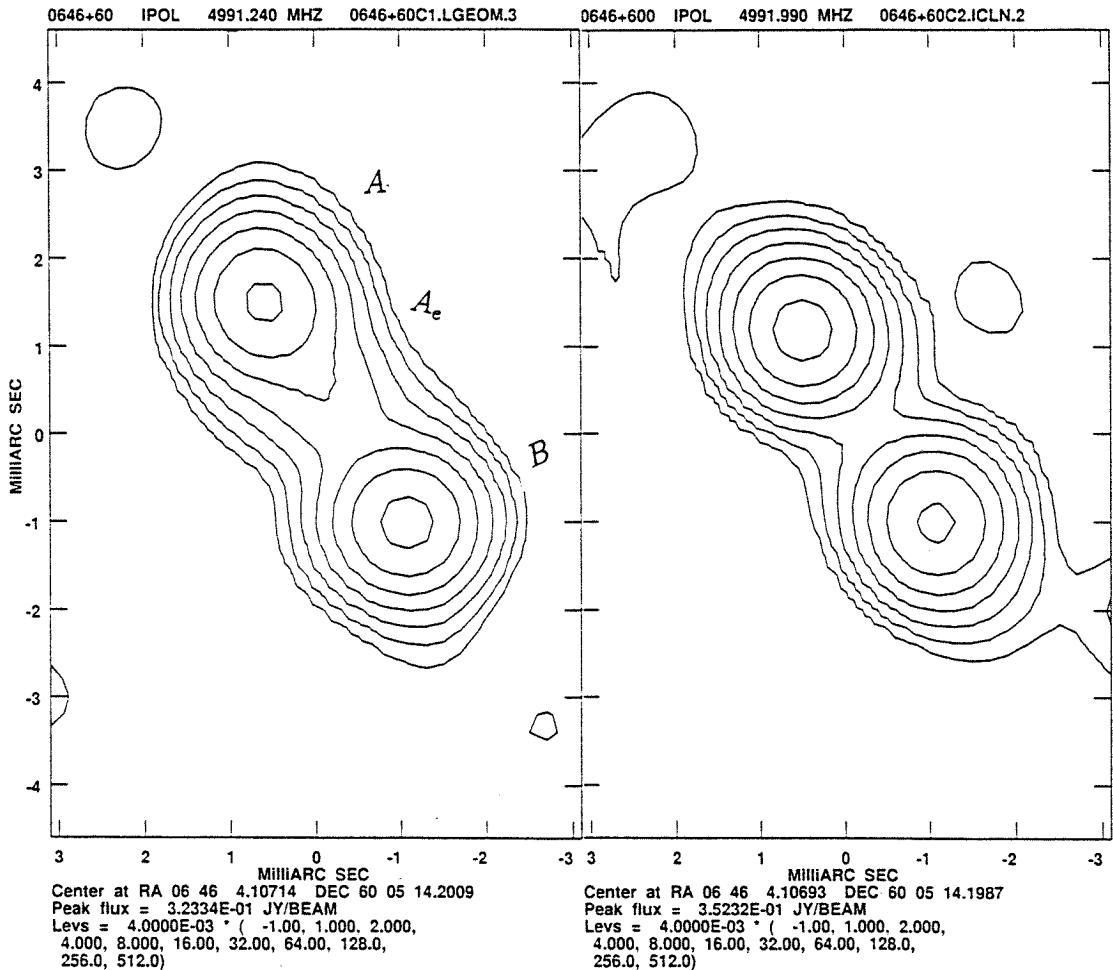
At 5 GHz (first epoch: 1989.87) the structure showed two bright components separated by 3.0 mas and there appears to be a weak component or extension, A_e with a brightness of ~ 50 mJy/beam. This feature had been confirmed independently by the Caltech-Jodrell group (A. Polatidis, private communication). Further observations were made to determine whether 0646+600 was either a double or triple, and to measure the motion, if any,

Table 2: Journal of VLBI observations

Frequency MHz	Epoch	Duration Hrs	Tels
1662	1992.87	0.5	Eb,Jb(1),Wb,On,Mc,Tr, Nt,Sh,Hh,Gb,Sm,Bl, HN,NL,PT,KP,LA,BR,OV
4995	1989.79	8.0	Eb,Jb(2),Wb,On,Mc,Hs, Gb,Vl,PT,KP,FD,Ov
4995	1992.22	3.5	Eb,On,Mc,Nt,Hs,Gb,Vl PT,KP,LA,FD,BR,OV
8414	1991.17	3.5	Eb,On,Nt,Gb,Vl,Ov
22230	1992.85	3.5	Eb,On,Mh,Mc,Nt

of the components. At all the frequencies it essentially remained a double.

A second epoch observation at 5 GHz (1992.22) indicates that the overall size decreased by 0.25 mas; while the middle feature, A_e was not detected. There is no indication of a change in size or the existence of A_e from 8.4 GHz observations made between the two 5 GHz epochs. The observations at 22 GHz show that it had apparently 'relaxed' to the

**Figure 1:** Global 5 GHz VLBI maps of 0646+600 at two epochs (1989.79; 1992.22) and 1 mas resolution

original size and decreased again at 1.6 GHz; but A_e was not detected. It is not clear how much of these apparent changes in size are the effect of different observing frequencies.

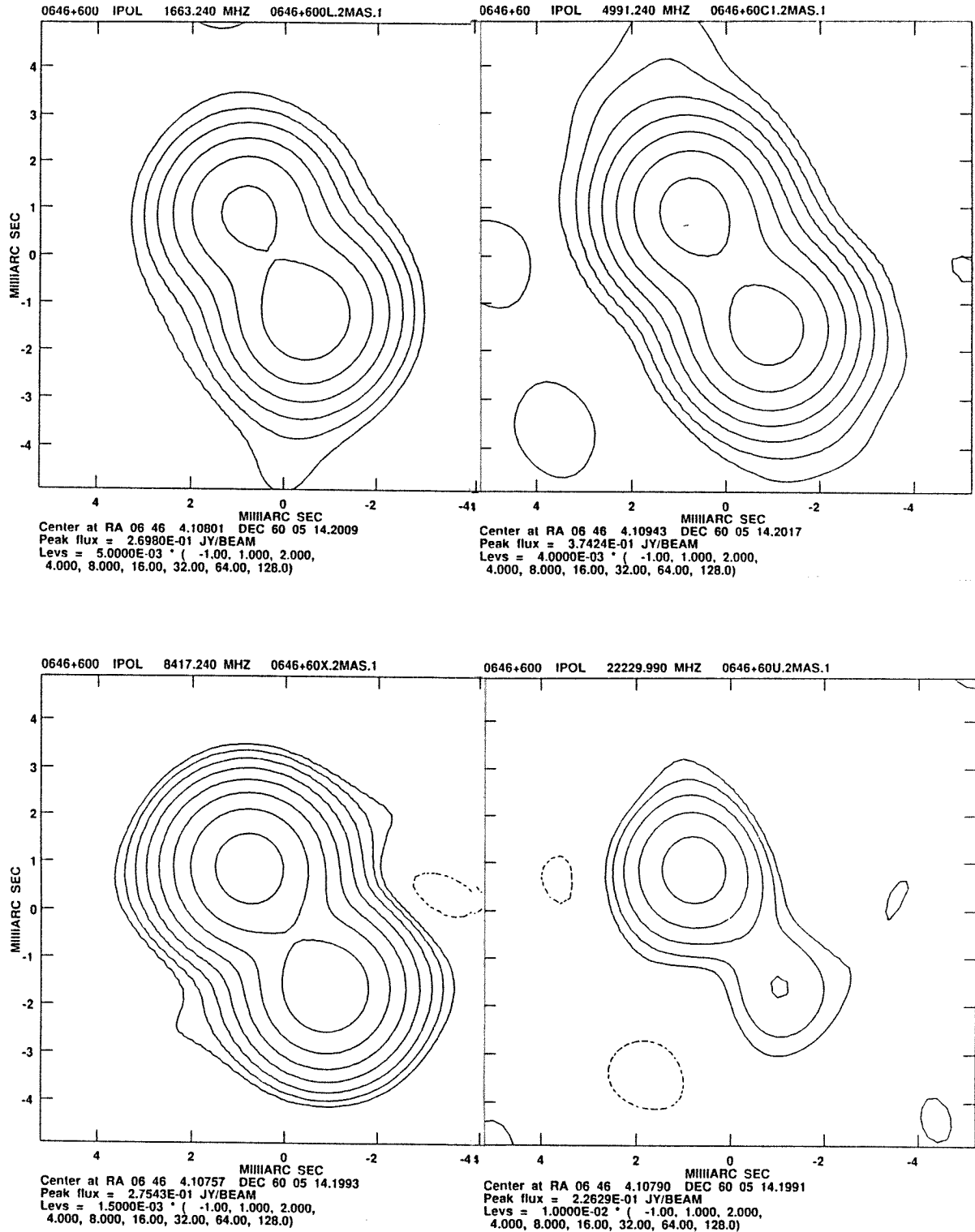


Figure 2: VLBI maps of 0646+600 at 1.66, 8.4, 5 and 22 GHz; the high frequency data are convolved to the resolution (2 mas) of 1.6 GHz data

However, the apparent contraction at 5 GHz is unusual, but appears to be transient since it is not evident in the observations at 8 and 22 GHz. If it is a result of the motion of either component, it implies a proper motion $\mu \sim 0.18$ mas/yr and $\beta_{app} \sim 2.8c$ (for $h = 1; q_o = 0.5$). One possibility is that A_e moved towards, and blended with, either component creating a new centroid of the combined component, thus resulting in an apparent decrease in overall size. In this case it is not clear which direction it would have gone since both components appear to vary in brightness. There is also no obvious change in the size of either component to support this scenario. Moreover, a motion of A_e towards the nearer component A would imply an incredibly high speed $\beta_{app} \sim 10c$. The other possibility is that the middle component has faded, but this doesn’t explain the apparent size decrease.

0646+600 is unusual because it is a Gigahertz-peaked spectrum (GPS) source with a structure resembling the compact triples/doubles (Philips & Mutel 1982), but shows structural changes not usually seen in these types of sources. Indeed, the two components, A, B also have peaked spectra around 3.8 and 3.4 GHz, which corresponds to estimated magnetic field ~ 2.8 mG and 4.2 mG, respectively. Component B has a steeper optically thin spectrum, which may imply higher synchrotron and inverse Compton losses and suggesting that A is the main centre of activity.

Although superluminal motion is common in the core of bright flat-spectrum sources, no definite separation speed has been measured in true compact doubles/triples. An apparent size contraction had been reported for one object, 4C39.25 (Shaffer & Marscher 1987), and this is explained by a bright feature moving between two stationary components (Shaffer *et al.* 1987). Marcaide *et al.* (1990) model this in terms of motion in a twisted relativistic jet. Further observations may reveal a similar phenomenon in 0646+600.

Concluding remarks

We have made deep optical images and multi-frequency VLBI observations of 0646+600 at different epochs. It is a ‘red’ object, as are many others found amongst OQQs. The radio structure is mainly a mas double of 3 mas separation; each component has a spectrum peaked at very high frequencies. The overall size appears to have temporarily contracted corresponding to an apparent motion $\beta_{app} \sim 2.8c$. A middle weak feature found earlier is not evident from later observations. We note, however, that these observations are ‘snapshots’. More frequent observations with improved resolution and sensitivity are needed to understand the nature of the possible changes in 0646+600.

References

- Akujor, C.E. & Porcas, R.W., 1992, in ‘Extragalactic Radio Sources—From Beams to Jets’, Roland J., Sol H., Pelletier G. (eds), CUP, p. 134.
- Akujor, C.E. *et al.*, 1994, in ‘Multi-Wavelength Continuum Emission of AGN’, T.J.-L. Courvoisier & A. Blecha (eds), Kluwer, p. 419.
- Burstein, D., Heiles, C., 1982, AJ, 87, 1165.
- Fugmann, W., Meisenheimer, K., 1988, AAS, 76, 145.
- Marcaide, J.M. *et al.*, 1990, in ‘Parsec-Scale Radio Jets’, J.A. Zensus & T.J. Pearson (eds), CUP, p. 59.
- Meisenheimer, K. & Röser, H.-J., 1983 AAS, 51, 41.

- Patnaik, A.R. *et al.*, 1992, MNRAS 254, 655.
Philips, R.B. & Mutel, R.L. 1982, AA, 106, 21.
Shaffer, D.B. *et al.*, 1987, ApJ, 314, L1.
Shaffer, D.B. & Marscher, A.P., 1987, in 'Superluminal Radio Sources', J.A. Zensus & T.J. Pearson (eds), CUP, p. 67.
Stickel, M., Kuhr, H., 1993, AAS, 101, 521.
Stobie, R.S., Sagar, R., Gilmore, G., 1985, AAS, 60, 503.
Young, P. *et al.*, 1981, ApJ, 244, 736.
Zensus, J.A. & Porcas, R.W., 1985, in 'Active Galactic Nuclei', J. Dyson (ed), Manchester Univ. Press, p. 54.

Multifrequency VLBI Monitoring and Jet Physics

A.P. LOBANOV^{1,2} and J.A. ZENSUS¹

¹National Radio Astronomy Observatory, Socorro, NM, USA

²Astro Space Center of P.N.Lebedev Physical Institute, Moscow, Russia

Abstract

We present results from multifrequency VLBI monitoring of 3C345. Spectral and kinematic evolution of the bright features in the jet are discussed, with application to different types of jet models. We show preliminary results from mapping the distribution of the turnover frequency in the jet.

Introduction

The radio emission of the quasar 3C345 has been monitored closely for a few decades using VLBI and single dish observations (cf. Terrasranta 1991; Hughes, Aller, and Aller 1991; Zensus, Cohen, and Unwin 1994, [ZCU94]). The VLBI monitoring has been performed at 1.4, 2.3, 5, 8.4, 10.7, 22.3, 43, and 89 GHz; the single dish observations have been made at 5, 8, 15, 22, and 37 GHz. The morphology and kinematics of the jet have been determined and studied (cf. Biretta, Moore, and Cohen 1986, [BMC86]; Krichbaum 1991, Matveenko *et al.* 1992; Unwin and Wehrle 1992), altogether with obtaining information about spectral properties of the jet emission (Lobanov, Zensus, and Leppänen 1993). Several physical models have been used for explaining the observed flux and kinematic evolutions, including the *relativistic shock* model (Rabaça and Zensus 1994), *helical jet* model (Steffen *et al.* 1994) *two-fluid* scenario (Lobanov and Zensus 1994, [LZ94]), and a composition of the Königl *inhomogeneous-jet* model with homogeneous spheres for superluminal components (ZCU94).

In this contribution, we present results of a combined study of spectral and kinematic evolution in the compact structures of 3C345. We discuss them in the framework of possible shocked and non-shocked emission schemes. In the last section, we show the first result from mapping the turnover frequency distribution in the jet of 3C345.

Jet kinematics

The kinematic parameters of the compact jet in 3C345 are discussed in ZCU94. The trajectories of jet patterns were fitted by polynomials; the evolution of apparent speed and the 3-dimensional trajectories were calculated. The strong curvature of the component trajectories near the core is reflected by the significant changes of their apparent relative acceleration $d\mu/\mu$ (Figure 1). At larger distances, the changes become less pronounced (see the trajectories of C2 and C3 in Figure 1). Apparent speed of the components continuously increases with distance from the core, from about 3 to $10 h^{-1}c$.

We use the results from ZCU94 in our discussion about applicability of the shocks to the description of the observed spectral changes in the jet.

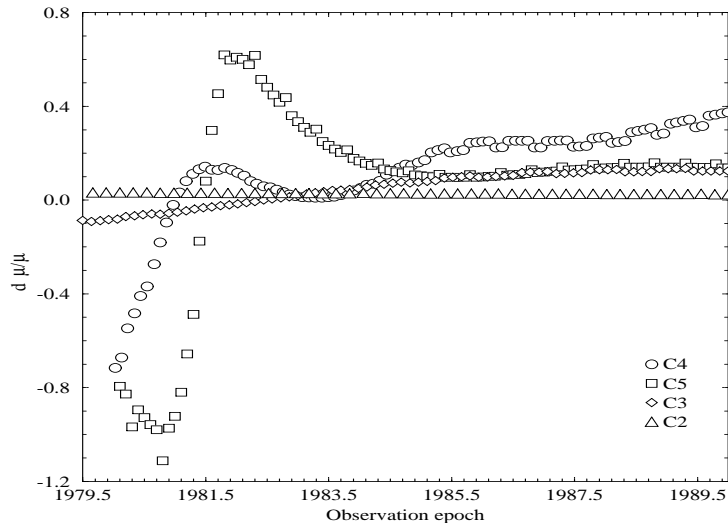


Figure 1: Apparent relative accelerations $d\mu/\mu$ of the jet components in 3C345. The variations in C4 and C5 are due to the jet curvature on the small distances from the core. At larger distances, the jet seems to become less curved, resulting in smooth changes of acceleration (see the curves for C2 and C3).

Synchrotron spectra of the jet components

We have used 43 VLBI observations of 3C345 at 2.3, 5, 8.4, 10.7, 22, 43, and 89 GHz (BMC86, ZCU94, Zensus *et al.* 1995). The VLBI images have been model fitted by optically thin spherical components, so that every model fit component corresponds to a unique bright feature observed in the source (traditionally for 3C345, the components have been denoted as D – the VLBI core, and C2–C7 – superluminal features in the jet).

We have extracted the component fluxes from the model fits, and formed the *multifrequency datasets* [MD] by combining the data for each component observed at close epochs at different frequencies. We limit the time separation between individual observations combined into a MD to 6 months, profiting from the fact that the amplitude of the flux variations on these timescales do not exceed the amplitude of the flux errors from model fitting. The total number of 10 MD has been produced, each assigned to a median *spectral epoch*. In order to calculate the shape of synchrotron spectra, we have developed the *loose-cutoff* algorithm (Lobanov and Zensus 1995) which uses Monte Carlo simulations and a χ^2 -minimization procedure for improving the spectral fitting. The fitting has been done in assumption of self-absorbed emission from a plasma with the power-law energy distribution (Pacholczyk 1970).

From the fitted spectra, we have calculated the integrated flux between 4 and 25 GHz, peak flux density, and turnover frequency, for every component at every spectral epoch.

The correlations between the integrated flux and turnover frequency found in LZ94 suggest that there might be different emission mechanisms involved in the core and in the jet components. The turnover frequency of the core experiences a sharp rise at the epochs of emerging a new component. LZ94 found that the evolution of the turnover frequency in C4 and C5 did not follow the shocked emission scenario suggested in Marscher and Gear 1985; Marscher, Gear, and Travis 1991. In C4 and C5, the turnover frequency is lower in the beginning of their evolutions, and reaches their maxima a few years later ($t_m \approx 3.9$ years and ≈ 8.3 years for C4 and C5, respectively).

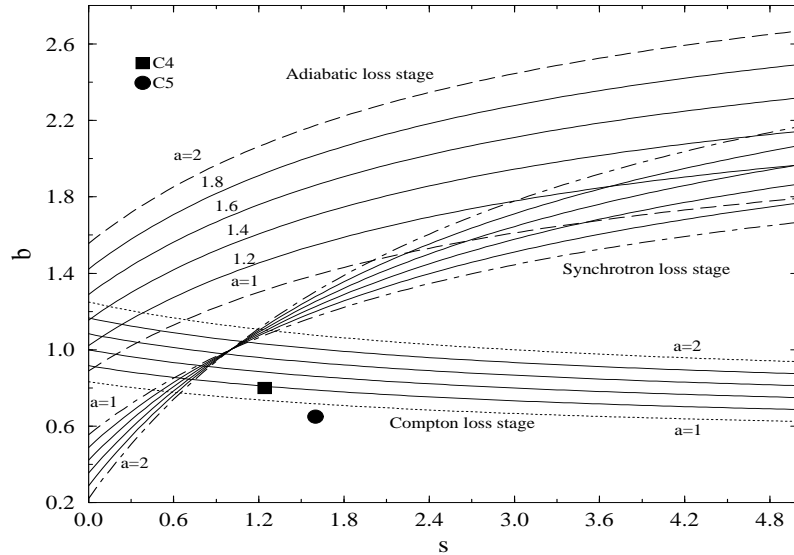


Figure 2: Conditions of existence of a maximum in evolution of the turnover frequency ν_m expressed through the energy spectral index s , and constants a and b describing the magnetic field and Doppler factor, respectively. Black circle and black square denote the upper limits of b determined from the observations.

Jet physics

In this section we would like to provide some arguments for choosing between the shock and the two-fluid approaches to the jet physics.

Shock-in-jet model

We investigate the possibility of the variable Doppler boosting factor to produce the observed spectral evolution, in the frame of the shock models. We use the formalism from Marscher and Gear 1985, and constrain the model parameters by the condition of peaked evolution of the turnover frequency

$$\epsilon R^{\epsilon-1} \frac{dR}{dt} = 0, \quad (1)$$

where R – distance from the injection point of relativistic electrons; $\epsilon = \epsilon(a, b, s)$ – a function of model parameters describing: a – magnetic field $B \propto R^{-a}$, b – Doppler factor $\delta \propto R^b$, and electron energy spectral index s .

We plot the solution $\epsilon = 0$ of Equation 1 in Figure 2, for each of the three stages of shock development considered by Marscher and Gear. Then, we calculate the observed values of b , and s for C4 and C5 at the epochs of the maximum turnover frequency. We use the small angle solution for the component trajectories (see ZCU94). Redshift, time dilation, and relativistic aberration have been corrected for, assuming the standard cosmological model (Weinberg 1972) with $H_0 = 100 \text{ km/s}\cdot\text{Mpc}$, and $q_0 = 0.5$. The energy spectral index is determined from the spectral index data, using the relation $s = 1 - 2\alpha$. Using the minimum kinematically allowed values of the Lorentz factor for C4 and C5 (from ZCU94), we estimate the upper limits on b , and these estimates are presented in Figure 2 by the black circle (C4) and black square (C5).

In Figure 2, C4 satisfied the maximum condition for the Compton-loss stage, and C5 lies beneath. It is difficult to explain why the shock constituting C4 is still at the

Compton-loss stage, after more than 40 years of intrinsic evolution. The maximum in C5 occurred after about 50 years of evolution in the jet frame; and one would expect the maxima in both components to occur rather during the adiabatic-loss stage.

Two-fluid model

The two-fluid model (Henri and Pelletier 1991, Roland *et al.* 1992, 1994) assumes existence of a thermal ($\beta \approx 0.3c - 0.4c$) $e^\pm - p$ plasma in jets, alongside with relativistic ($\gamma \sim 10$) e^\pm plasma. The model explains the observed kinematic properties of the jet, including (1) curved trajectories and variations of apparent acceleration of components near the core; (2) increasing acceleration of C4 at the latest epochs (see ZCU94, LZ94). The observed spectral evolution can be explained by reacceleration of the relativistic plasma due to the interaction with the thermal outflow. The observed high-frequency spectral maximum of the core (ZL94) can be explained by the e^\pm escaping the relativistic channel in the vicinity of the central engine.

One of the apparent difficulties of this scheme is the existence of the jet components which had appeared very close in time (the epochs of origin for C4 and C5 are within 1 year from each other (ZCU94); the first detection of C6 and C7 was made simultaneously (Krichbaum 1991)); while in the shocked scenarios this can be viewed as an evidence for some sort of relation between the preceding and succeeding component (such as *forward* and *reverse* shocks (LZ95), or the opposite edges of an elliptical distortion in the jet (Hardee, personal communications)).

New observations

With the new facilities and techniques available, the goals of this monitoring program will be extended to providing continuous information about physical conditions in the jet. With increasing number of antennas and improving uv -coverage, spectral index mapping has become more reliable for VLBI images (LZL93). The absolute astrometry programs and phase referencing are expected to provide better position information essential for spectral index mapping. Simultaneous multifrequency observations with the VLBA may enable a continuous spectral fitting. The preliminary result from this approach is presented in Figure 3 showing the *turnover frequency distribution* along the jet of 3C345. With the multifrequency VLBA data available, we expect to distinguish between shocked (reaccelerated) areas of the jet, as well as to verify the presence of a relativistic channel suggested by the two-fluid scenario.

We also plan to extend this monitoring to polarization measurements, attempting to provide a more complete picture of the parsec-scale structures in AGN.

Conclusion

The multifrequency VLBI monitoring of 3C345 has revealed a significant information about the very compact structures in the source, and enabled us to study their long-term kinematical and spectral evolution. Continuation of the monitoring and expanding its goals are very likely to bring a better understanding of the central regions in AGN.

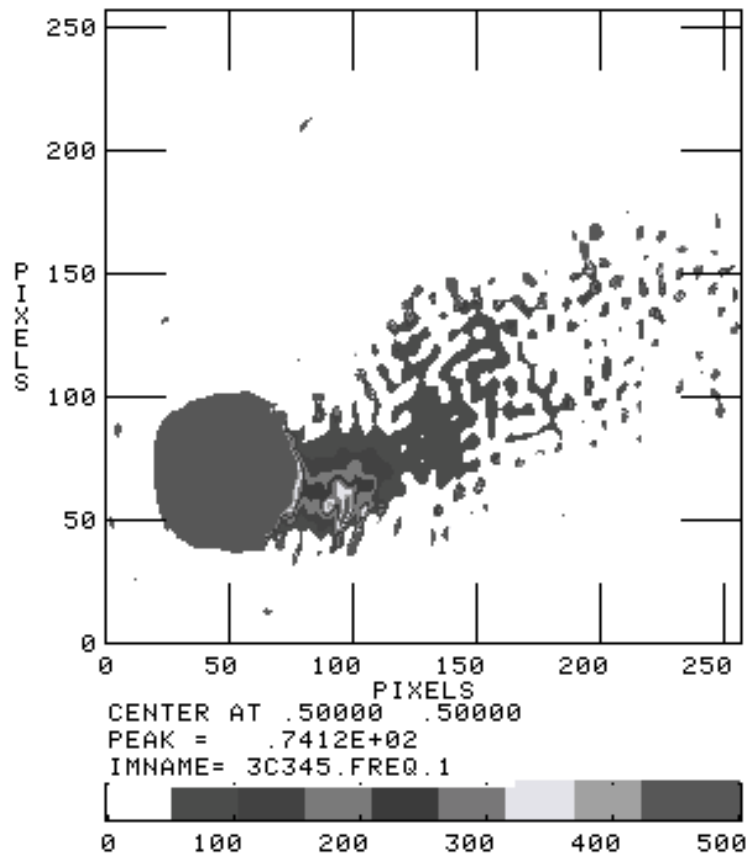


Figure 3: Preliminary map of the turnover frequency distribution in the jet of 3C345. The map has been produced from three Global VLBI observations at 1.3cm (Jun'92), 3.6cm (Sep'92), and 6cm (Jun'92). The high turnover frequency region in the jet corresponds to the location of C5 and may reflect the actual location of the shock, or the cite of reacceleration of the e^{\pm} plasma. The channel of higher turnover frequency going through the jet may correspond to the relativistic channel in the two-fluid model.

Acknowledgement:

The National Radio Astronomy Observatory is operated by Associated Universities Inc., under cooperative agreement with the National Science Foundation.

References

- Aller, H.D., Aller, M.F., Latimer, G.E., and Hodge, P.E. 1985, *Astrophys. J. Suppl.*, **59**, 513.
- Biretta, J.A., Moore, R.L., Cohen, M.H. 1986, *Astrophys. J.*, **308**, 93.
- Henri, G., and Pelletier, G. 1991, *Astrophys. J. (Letters)* 383, L3.
- Hughes, P.A., Aller, H.D., Aller, M.F. 1991, *Astrophys. J.*, **341**, 54.
- Hughes, P.A., Aller, H.D., Aller, M.F. 1991, in *Variability of Blazars*, E. Valtaoja, M. Valtonen eds., Cambridge University Press.
- Krichbaum, T. 1991 *Astrophys. J.*, **303**, 21.
- Lobanov, A.P., Zensus J.A., Leppänen, K.J. 1993 *Bull. Am. Astron. Soc.*, **25**, 1382.
- Lobanov, A.P., and Zensus, J.A. 1994, in *Compact Extragalactic Radio Sources*, NRAO Green Bank, USA.
- Lobanov, A.P., and Zensus, J.A. 1995 *Astrophys. J.* (submitted).

- Marscher, A.P., and Gear, W.K. 1985, *Astrophys. J.*, **298**, 114.
- Marscher, A.P., Gear, W.K., and Travis, J. 1991, in *Variability of Blazars*, E. Valtaoja, M. Valtonen eds., Cambridge University Press.
- Matveenko, L.I. *et al.* 1992 *Soviet Astron. Lett.*, **18**, 379.
- Pacholczyk, A.G. 1970, *Radio Astrophysics* (W.H. Freeman and Co.: San Francisco).
- Rabaça, C.R., and Zensus, J.A. 1994, in *Compact Extragalactic Radio Sources*, NRAO Green Bank, USA.
- Roland J., Lehoucq, R., and Pelletier, G. 1992, in *Extragalactic Radio Sources: From Beams to Jets*, eds. J. Roland, H. Sol & G. Pelletier, Cambridge University Press, Cambridge.
- Roland J. *et al.* 1994 *Astron. Astrophys.* (submitted).
- Steffen, W. *et al.* 1994, (in preparation).
- Teräsraanta, H. *et al.* 1991, in *Variability of Blazars*, E. Valtaoja, M. Valtonen eds., Cambridge University Press.
- Unwin, S.C., and Wehrle, A.E. 1992, *Astrophys. J.*, **398**, 74.
- Wardle, J.F.C., Roberts, D.H., Potash, R.I., and Rogers, A.E.E. 1986, *Astrophys. J. (Letters)*, **304**, L1.
- Weinberg, S. 1972, *Gravitation and Cosmology*, (New York: John Wiley & Sons).
- Zensus, J.A., Cohen, M.H., Unwin, S.C. 1994, *Astrophys. J.* (submitted).
- Zensus, J.A., Lobanov, A.P., Unwin, S.C., and Leppänen, K.J. 1995, (in preparation).

DISCUSSION

H. van Langevelde (Q): What is the resolution in your “turnover-frequency-map”? Can we believe that the “shock” seen in that map is real?

A. Lobanov (A): Technically, the feature in the map I have shown is overresolved. However, we can expect spectral fitting to be very sensitive to variations of the turnover frequency. And in this case, we are dealing with the same kind of overresolution as that of the model fitting.

L. Matveenko (Q): Is the visible size of the core real (in your 3C345 map) or is it determined by saturation?

A. Lobanov (A): This is the saturation level chosen, in order for the jet features to be better displayed in the map.

Aberration of Light and Time Delay Effects in Parsec-scale Relativistic Jets

A. ALBERDI^{1,2}, J.L. GÓMEZ^{2,3}, J.C. GUIRADO^{2,4}, L. LARA²
and J.M. MARCAIDE⁵

¹L.A.E.F.F., Madrid, Spain

²I.A.A., Granada, Spain

³Boston University, Boston, MA, USA

⁴JPL, Pasadena, CA, USA

⁵University of València, Valencia, Spain

We have developed a numerical code which solves the transfer equation for the synchrotron radiation in extragalactic relativistic jets with bends and shock waves (Gómez, Alberdi, Marcaide 1993, 1994a, 1994b; Alberdi, Gómez, Marcaide 1993). Our computer code studies the spatial, frequency, and temporal behaviour of bent shocked relativistic jets, using the transfer equation of synchrotron radiation, the jump conditions for shocks with relativistic flow speed and equation of state, and the change in the Doppler boosting factor produced by bends in the jet axis. In our computer code, we consider the integration columns parallel to the line of sight, thereby calculating the emergent flux density produced by the inhomogeneities present in the integration columns when the jet is not seen side on. We have also considered the differential Doppler boosting effect across the jet flow, since the jet convects diverging flow. Here, we summarize our main results:

1.— We have studied the effects which produce on the VLBI maps the presence of bends in the jet (Gómez, Alberdi, Marcaide 1993). When there is a bend in the direction towards the observer, these bends may produce enhanced emission in the total and polarized flux density maps, although a bend towards the observer can also decrease the polarized flux (depending on the opacity at the jet position where the bend is located) producing a relative minimum. In a similar way, bends away from the observer can lead to the appearance of new components through relative minima in the total and polarized flux densities. These components resulting from bends can explain the stationary components in non-ballistic models.

2.— We have studied the effects of shock waves in the relativistic jets radio structure (Gómez, Alberdi, Marcaide 1994a; Alberdi, Gómez, Marcaide 1993). The evolution of the shock wave along the jet is characterized at the early epochs by a quick increase in the total flux density of the source accompanied by a decrease in the polarized flux density associated to the high opacity of the shocked flow. Thus, by comparing the total and polarized flux maps we observe an anticorrelation in the region associated with the shocked flow at these earlier epochs. At later epochs, this anticorrelation turns into a correlation, and both the total and polarized flux maps show the existence of a component at the position of the shocked flow.

3.— We have studied the combined effects of both bends and shock waves in the emission of relativistic jets. With this intention, we have computed the emission from a reverse shock wave travelling along a helical jet (Gómez, Alberdi, Marcaide 1994a, 1994b). When the shock wave reaches the position of a bend towards the observer, the differential increase of the Doppler boosting, the lengthening of the integration column, and shock effects are simultaneously present and add together, producing relative maxima in the total and polarized flux densities. The shock wave reorders the magnetic field within the shocked region, resulting in a magnetic field perpendicular to the jet ridge line (if the jet is optically thin) in contrast to the rest of the jet where the magnetic field is parallel to the jet ridge line. This rotation of the magnetic field vector in the shocked region can alter the measured value of the polarization angle of the source as a whole if the shock is strong enough to influence the emission of the whole jet.

In this contribution, we consider the influence on the emission of bent jets of two relativistic effects: aberration of light and time delays. These effects can alter significantly the observed synchrotron emission from extragalactic relativistic bent shocked jets (Gómez, Alberdi, Marcaide 1994c).

- The influence of relativistic aberration on the emission of relativistic jets depends on the degree of randomly oriented magnetic field within the jet. For fractions of $\sim 70\%$ of randomly oriented magnetic field we have demonstrated that aberration does not alter significantly the total flux density of relativistic jets, with the corrections being smaller than about the 10% on it. On the other hand, for this same fraction of randomly oriented magnetic field ($\sim 70\%$), the polarized flux density is strongly influenced by aberration, with changes as important as the 50% in the polarized emission. It is clear that, for a totally randomly oriented magnetic field aberration, there is not any change in the emission of relativistic jets due to this effect.

- The importance of the time delay effect depends basically on the viewing angle and on the opening angle of the jet. Since the jet convects diverging flow, the time delay is different for different fluid lines, and causes rotations and deformations of the shock fronts as viewed in the observer's frame. This results in variations in the length of the shocked region and in the apparent velocity between different fluid lines. Hence, both the total flux density and specially the polarized flux density, from a certain shocked region is strongly altered.

Influence of the aberration of light

When we solve the transfer equations for the synchrotron radiation, the orientation of the plasma fluid lines with respect to the line of sight is influencing mainly two physical parameters: i) in the emission and absorption coefficients, which are proportional to $B \sin \theta$, where B is the magnetic field and θ is the angle between the magnetic field and the line of sight; ii) in the polarized emission, mainly through the angle between the projected magnetic field on the sky plane and the axis with respect to which we are measuring the polarization angle.

Let's consider a rectilinear jet with a Lorentz factor ($\gamma=6$), and a viewing angle of 10° for the fluid elements in the ridge line of the jet. In this particular case, when we observe this jet with an angle of 10 degrees, we are observing the emission that was emitted in a direction perpendicular to the velocity of the fluid in the fluid reference frame. This suggests that these corrections can be very important depending on the degree of randomness of the magnetic field within the jet. Continuing with the same example,

in case the randomly oriented magnetic field fraction is small, the factor $B \sin \theta$ in the absorption and emission coefficients acquires a value of $B \sin 90$ if aberration is included, and $B \sin 10$ if it is not. Thus, when the aberration is not included, the situation is similar to the case of a smaller magnetic field (and then, smaller opacity), and the maximum intensity position shifts to a position closer to the core of the jet.

It should be noted that the percentage of randomly oriented magnetic field can be significantly smaller in regions excited by shock waves than in the rest of the jet, and therefore greater corrections due to aberration in these regions are to be expected. However, we must be cautious in the sense that the presence of a shock wave does not necessarily imply a reordering of the magnetic field: this is strongly dependent on the strength of the shock wave and on the initial percentage of randomly oriented magnetic field. As an example, if the basic magnetic field is oriented parallel to the jet ridge line and the degree of randomness is reduced, the presence of the shock wave will only introduce a higher degree of randomization.

Influence of the time delay

The time delay effect is relevant when we consider relativistic jets which are not stationary with time, when any class of inhomogeneity travels along the jet. In such situations, the difference in time of arrival at the observer of emission from different positions in the jet will produce changes in the shape and width of shocked regions, as viewed in the observer's frame, as function of the viewing angle.

Due to time delay, as the shock travels along the bent jet, the two shock fronts rotate and the length of the shocked region is modified when viewed in the observer's frame. This effect is strongly dependent on the orientation of the jet with respect to the observer. The rotation produced by time delay causes both shock fronts to be almost aligned with the line of sight, and produces a lengthening of the edge of the shocked region closer to the line of sight. All these facts translate into an enhancement of the emission of the shocked region.

A particular model

Let's consider the particular case of a helical shocked jet model which was presented in Gómez, Alberdi & Marcaide (1994). We refer the reader to that work for details about the helical geometry and the physical parameters of the model. Basically, we can describe the geometry of the bent jet through the presence of two kinks: the first one very close to the core region, and the second one far away from the core position. We are also considering the presence of a planar shock wave travelling along the structure of the relativistic jet.

We present in Figure 1, the total flux maps and polarized flux maps corresponding to different positions of the shock wavetravelling along the jet. In these models we have not taken into account the aberration of light and the time delay effects. The shock wave can be seen as a moving component travelling from the core of the jet to the position of the stationary component, the latter being associated with the most favorably oriented portion of the twisted jet, where the Doppler factor is maximized. When the shock wave reaches the position of the stationary component, the flux increases markedly to a higher value than that of the core, resulting in a new merged component and in a maximum in the light curve.

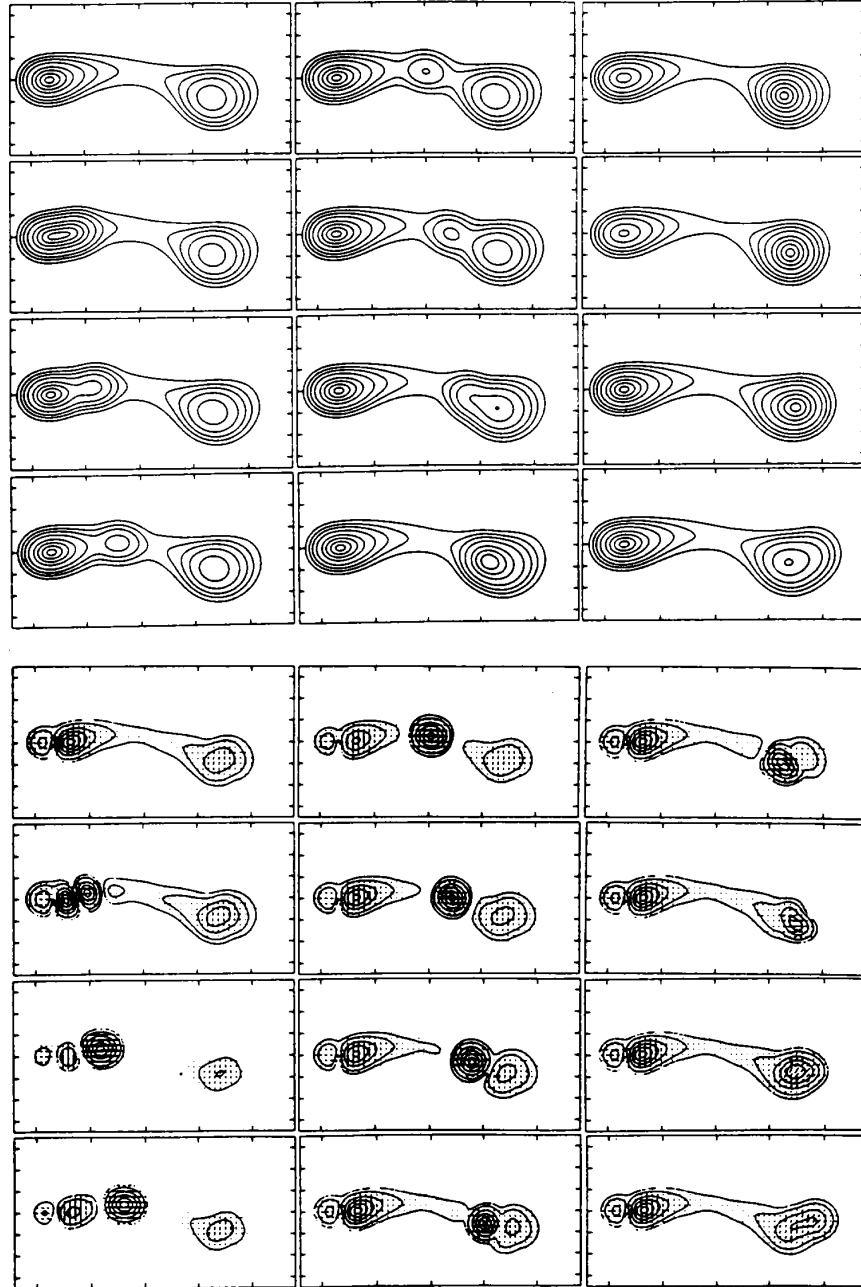


Figure 1: a) Evolution of the total intensity maps for the shocked helical jet models at 22 GHz, without taking into account aberration and time delay effects. The contours shown correspond to 2, 5, 10, 35, 65 and 95% of the peak brightness. Tick marks on the horizontal axis represent 0.5 mas, whereas those on the vertical axis represent 0.2 mas. b) Evolution of the polarized intensity maps for the shocked helical jet models at 22 GHz, without taking into account aberration and time delay effects. The contours shown correspond to 2, 5, 10, 35, 65 and 95% of the peak brightness. The bars shown correspond to the orientation of the electric vector. Tick marks on the horizontal axis represent 0.5 mas, whereas those on the vertical axis represent 0.2 mas.

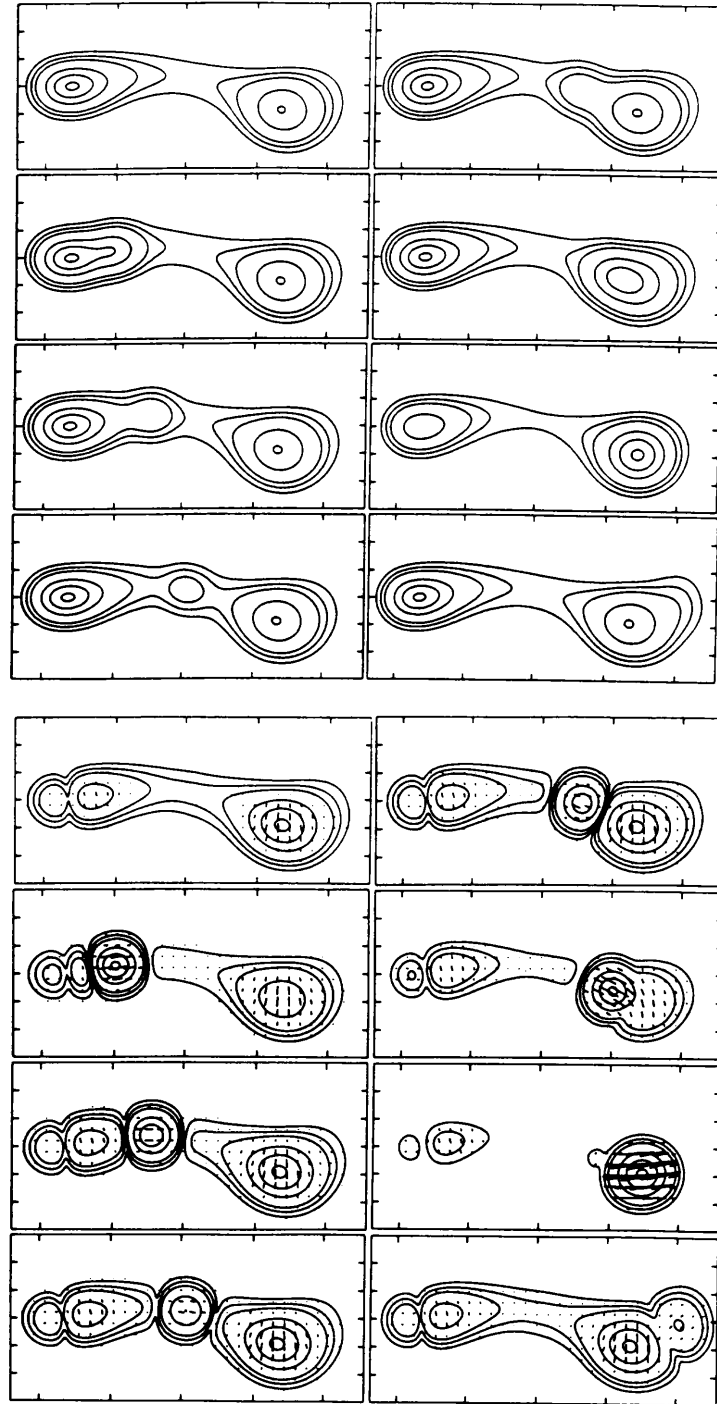


Figure 2: a) Evolution of the total intensity maps for the shocked helical jet models at 22 GHz, incorporating aberration and time delay effects. The contours shown correspond to 2, 5, 10, 35, 65 and 95% of the peak brightness. Tick marks on the horizontal axis represent 0.5 mas, whereas those on the vertical axis represent 0.2 mas. b) Evolution of the polarized intensity maps for the shocked helical jet models at 22 GHz, incorporating aberration and time delay effects. The contours shown correspond to 2, 5, 10, 35, 65 and 95% of the peak brightness. The bars shown correspond to the orientation of the electric vector. Tick marks on the horizontal axis represent 0.5 mas, whereas those on the vertical axis represent 0.2 mas.

We also show in Figure 1 the polarized intensity maps which correspond to the total intensity maps. The first map corresponds to the quiescent situation, and consists of three components. The first two components correspond to the core of the jet and to the beginning of the optically thin portion of the jet. The third component corresponds to the region of the helical jet which is most favourably oriented with respect to the observer, and is stationary in flux and position.

In Figure 2, we show the total and polarized intensity maps corresponding to the previous jet, with the same geometry and the same physical parameters, but incorporating the time delay and aberration of light effects. We can observe the differences between the two sets of maps, and we can immediately conclude that differences are specially significant in the polarized flux density, degree of polarization, and polarization angle of the jet.

As a global result, we can conclude that the improved model shows a higher degree of polarization (the region in which the magnetic field is ordered has increased its size due to time-delay effects) and the polarization angle of the source as a whole is significantly different. When the shock wave gets closer to the position of the stationary component, the polarized emission of the jet is dominated by the shocked region producing a complete rotation of 180 degrees in the polarization angle.

References

- Alberdi, A., Gómez J.L., Marcaide, J.M. 1993, in *Sub-Arcsecond Radio Astronomy*, ed. R.J. Davis and R.S. Booth, Cambridge University Press, p. 355.
 Gómez, J.L., Alberdi, A., Marcaide, J.M. 1993, *Astronomy & Astrophysics*, 274, 55–68.
 Gómez, J.L., Alberdi, A., Marcaide, J.M. 1994a, *Astronomy & Astrophysics*, 284, 51–64.
 Gómez, J.L., Alberdi, A., Marcaide, J.M. 1994b, in *Compact Extragalactic Radio Sources*, ed. J.A. Zensus and K.I.K. Kellermann, NRAO, p. 239.
 Gómez, J.L., Alberdi, A., Marcaide, J.M. 1994c, *Astronomy & Astrophysics*, (in press).

DISCUSSION

D. Dallacasa (Q): What is the linear scale of the tangling of the magnetic field?

A. Alberdi (A): Scale of milliarcseconds, in the case of our simulations.

Current Observational Status of the Object 1308+328

JERZY MACHALSKI

Astronomical Observatory, Jagiellonian University, Kraków, Poland

Another newly detected example of interesting *GHz-peaked-spectrum* (GPS) highly variable radio sources is the object 1308+328 (Machalski & Engels 1994). Its radio spectrum peaks at about 20–40 GHz, and is strongly self-absorbed at lower frequencies. Small angular size ($\leq 0.03 - 0.04$ arcsec) of the source, its stellar counterpart, and the low-resolution optical spectrum with emission lines suggest a compact quasar with redshift of 1.65. The source is monitored now in the optical R-band, and radio 22 and 37 GHz (H. Teräsranta, priv. comm.). Fig. 1 shows high optical (3–3.5 mag) and radio (about 50%) variabilities over timescales of a few years.

Its *X-ray* emission has been detected in the *ROSAT* 0.15–2.2 keV band with $S/N > 13\sigma$ (N. Brandt, priv. comm.) enabling him to extract the spectrum (Fig. 2, upper panel), and fit a power-law model with a photon index $\gamma = 2.0 \pm 0.6$ and column density

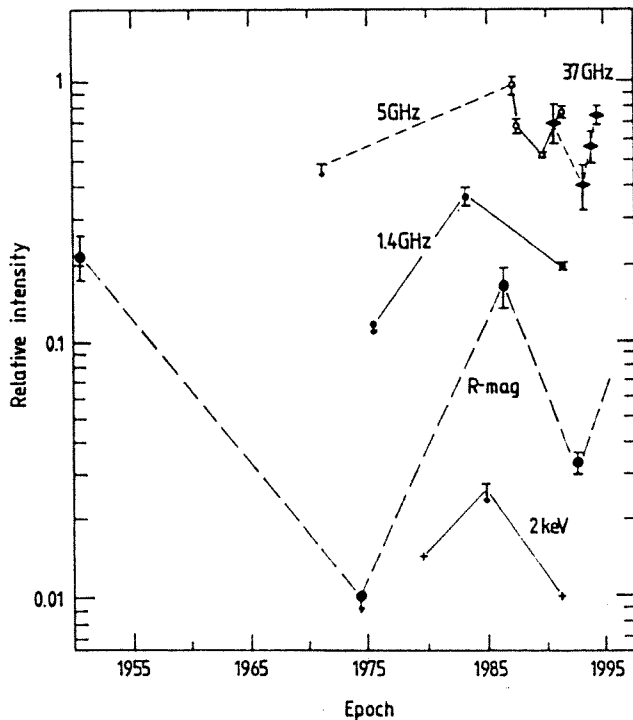


Figure 1: Radio, optical, and X-ray brightness variations

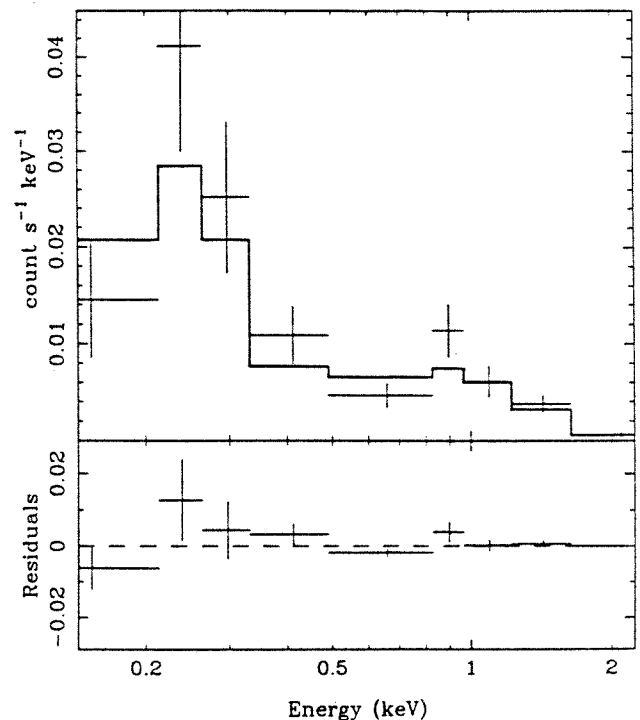


Figure 2: ROSAT PSPC spectrum with its best-fit power-law model overlaid

$N_H \approx 1.6 \times 10^{20} \text{ cm}^{-2}$. This N_H value is consistent with the Galactic N_H value of $1.1 \times 10^{20} \text{ cm}^{-2}$ at the position of the source. The lower panel of Fig. 2 shows residuals of the fit, where $\chi^2 = 8.4$ for 9 bins. Also the archival 1979 and 1980 *EISTEIN* data contain *X-ray* detection of the source, and an upper limit to its *X-ray* flux in 1984 is determined from the *EXOSAT* data. The *X-ray* flux-densities calculated for 2 keV band are also shown in Fig. 2. The corresponding *X-ray* luminosities in the 0.2–2.0 keV band are about 1.7, < 5.9 , and $2.2 \times 10^{45} \text{ erg s}^{-1}$ in 1979.95, 1984.47, and 1991.48, respectively [for $H_0 = 50$; $q_0 = 0.5$].

A broad-band *SED* for the object 1308+328 is shown in Fig. 3, and compared with those for two highly-polarized QSOs and one BL Lac object (*Mrk 421*). The *radio-to-Xray* spectral index of the source, $\alpha_{rx} \approx 1.0$ (hereafter $F_\nu \propto \nu^{-\alpha}$), is very steep suggesting rather a weak *X-ray* emitter, but its *X-ray* spectral index is close to the mean for radio-loud BL Lac objects (cf. Worrall & Wilkes 1990), and is flatter a little than the mean of about 1.2 found in the *ROSAT All-Sky Survey of AGN* (Brinkmann 1991). Therefore, its *X-ray* characteristics are similar to those of *X-ray* selected objects.

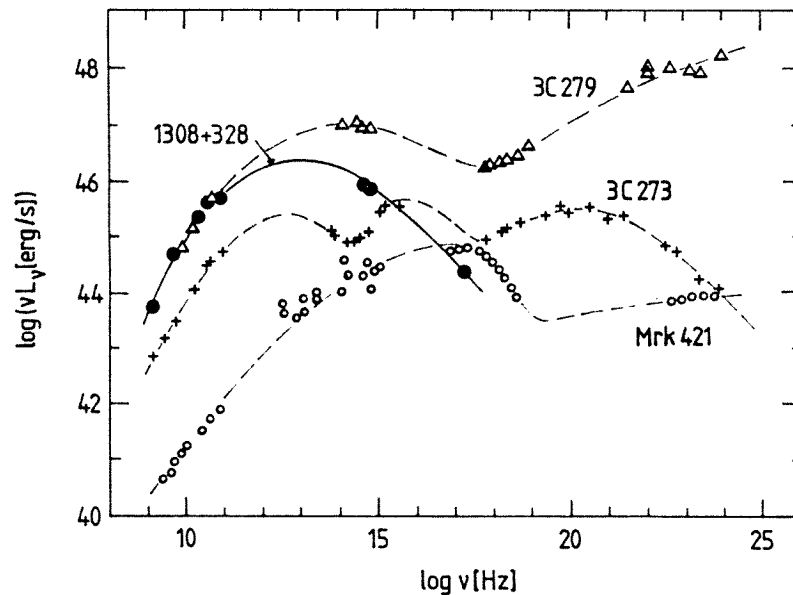


Figure 3: Broad band SED compared with those for other very well studied AGNs

The source is only 14.4 arcmin apart from the BL Lac source 1308+326 which can be used as an external reference frame for very precise (≤ 50 micro-arcsec) astrometric studies with the *VLBI* techniques. High-resolution maps and astrometric measurements can put further constraints on the *synchrotron self-Compton* (SSC) mechanism proposed for *AGNs*, and provide an independent estimate of the Doppler factor().

References

- Brinkmann, W., 1991, in *X-ray Emission from Active Galactic Nuclei and the Cosmic X-ray Background*, ed.: W. Brinkmann and J. Trümper, p. 143.
 Machalski, J., Engels, D., 1994, *MNRAS*, 266, L69.
 Worrall, D.M., Wilkes, B.J., 1990, *ApJ*, 360, 396.

The Recent Status of the TIGO Project

HAYO HASE

Institut für Angewandte Geodäsie, Fundamentalstation Wettzell, Germany

Abstract

The Institute for Applied Geodesy (IfAG) carries out the TIGO project. TIGO will be a transportable fundamental station for geodesy, which will contain all important geodetic space techniques like VLBI, Satellite Laser Ranging (SLR), and Global Positioning System (GPS). Fundamental stations are necessary to derive and improve the ITRF. TIGO will allow to fill the gaps in the ITRF, especially on the southern hemisphere. For VLBI operation a new designed 6 m offset-antenna will be used. TIGO will be checked out in Wettzell during 1995–1996 and used abroad afterwards.

Introduction

Among the stations which contribute to the IERS Terrestrial Reference Frame (ITRF) there are only a few fundamental stations, which permanently operate using the geodetic space techniques like VLBI, SLR and GPS. Furthermore, the global distribution of the existing ITRF sites is insufficient for a representative coverage of the Earth surface.

The three major advantages of fundamental stations are (1) permanency, which means observations on long term basis; (2) complementarity, which means to gain the synergies of different techniques for improvements in accuracy; (3) redundancy, which means a control of results with independent techniques.

The situation of ITRF and the advantageous characteristics of a fundamental station lead to the basic concept for a “Transportable Integrated Geodetic Observatory” (TIGO) with an observation period of about one year in selected sites, preferably in the southern hemisphere. The design goals for the geodetic observatory were state-of-the-art technology adapted for easy transportating in five standard 12 m containers (see Fig. 1).

The implementation period for TIGO is 1992–1997.

TIGO modules

The TIGO modules will offer the space techniques, such as VLBI, SLR, GPS (GLONASS) and also PRARE, and the additional necessary equipment for meteorology, time and frequency standard, gravity, seismic, supplementary terrestrial measurements. For internal and external data distribution a LAN and WAN interface will be included. To enable the use of TIGO at remote sites an independent energy supply by generators is intended.

VLBI module

The VLBI module consists of two standard 12 m containers; one for transportation of the 6 m offset radio telescope and another one for the VLBI-operation and transportation of the two side-panels of the reflector (see Fig. 2).

The antenna was designed for S/X-band geodetic wideband observations. The helium cooled low noise amplifier and the Mk IV Data Acquisition Rack and tape recorder shall correspond to the NASA standards. The setup time in a field on the special platform for the radio telescope will be less than 2 days.

Specifications of the Antenna with S/X Feedhorn (MAN)

Diameter	6.0 m
f/D	0.3629
Surface accuracy	0.4 mm
Azimuth slewing rate	6.0 °/s
Elevation slewing rate	3.0 °/s
S-band frequencies	2.216 – 2.350 GHz
X-band frequencies	8.108 – 9.036 GHz
Efficiency at S-band	> 64 %
Efficiency at X-band	> 68 %
Total noise temperature	< 53 K

SLR module

The SLR module consists of one 12 m standard container. The SLR instrument is designed as a two colour system of a subcentimeter accuracy ($\lambda_1 = 423.5$ nm, $\lambda_2 = 847$ nm) with day and night capability based on a Titan-Sapphire laser. The specified ranging distance is 500 to 40 000 km. A 50 cm telescope is used for transmission and reception of the pulses. The telescope will be mounted on a cart, while the laser transmission and reception units are located inside the SLR container. The optical beam will be introduced in the telescope through a tube.

Specifications of the Titan Sapphire Laser

Length of pulses	10 ... 50 ps
Energy for 423.5 nm wavelength	10 ... 50 mJ
Energy for 847 nm wavelength	30 ... 100 mJ
Pulse repetition rate	up to 100 Hz

Basic module

The basic module contains the time and frequency standards like Cesium clocks, GPS-time receiver and Hydrogen masers as well as the central computer for TIGO. The central computer will serve with the auxiliary data e.g. meteorology, absolute time, whenever there is a request from one of the main techniques. In addition the central computer will be an interface to a wide area network in order to distribute data e.g. of the permanent GPS receiver to international archiving facilities.

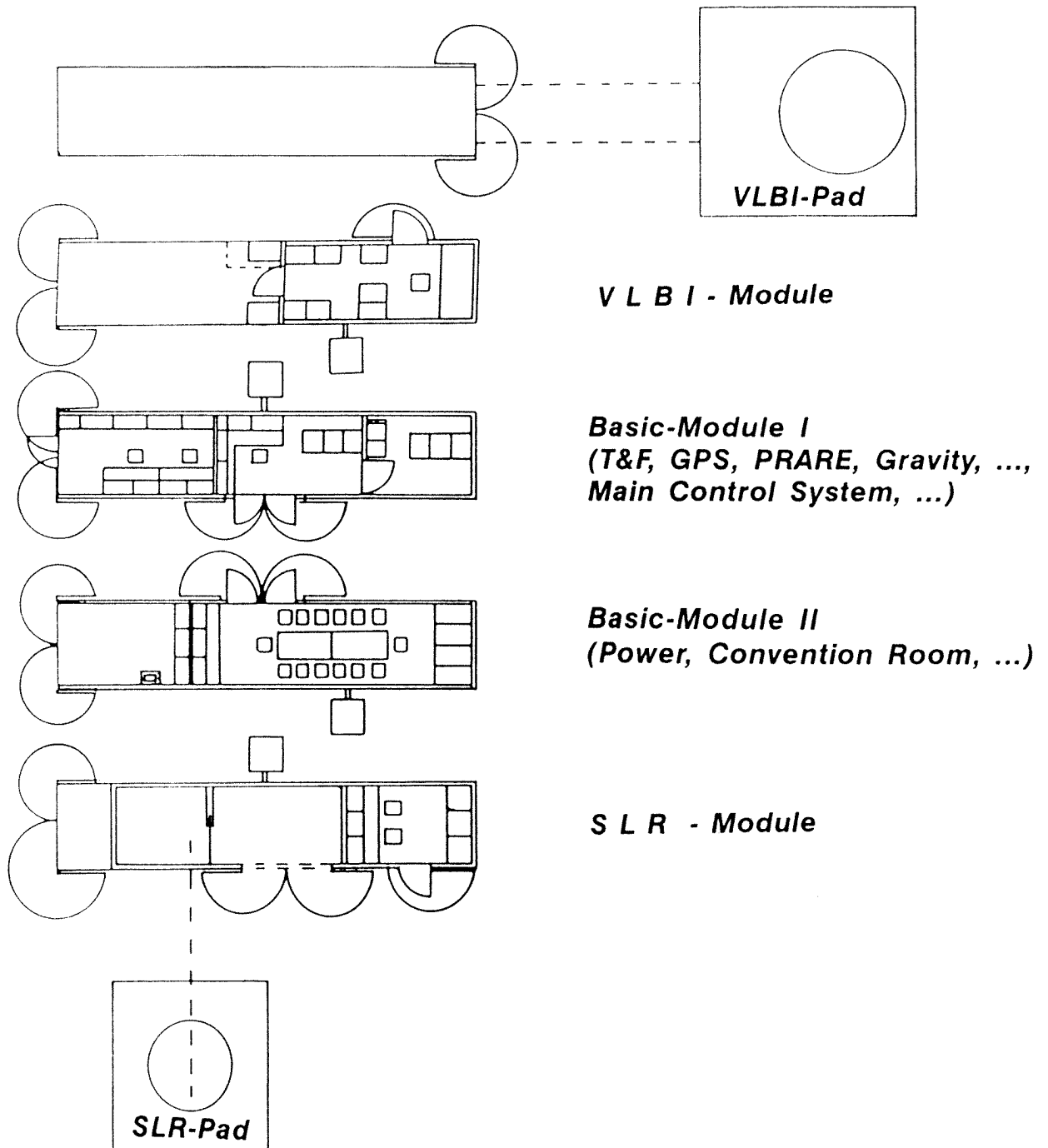


Figure 1: Overview of TIGO. The requested area will be about $30 \times 30 \text{ m}^2$. The VLBI antenna needs a special platform which allows to fix and to center the antenna.

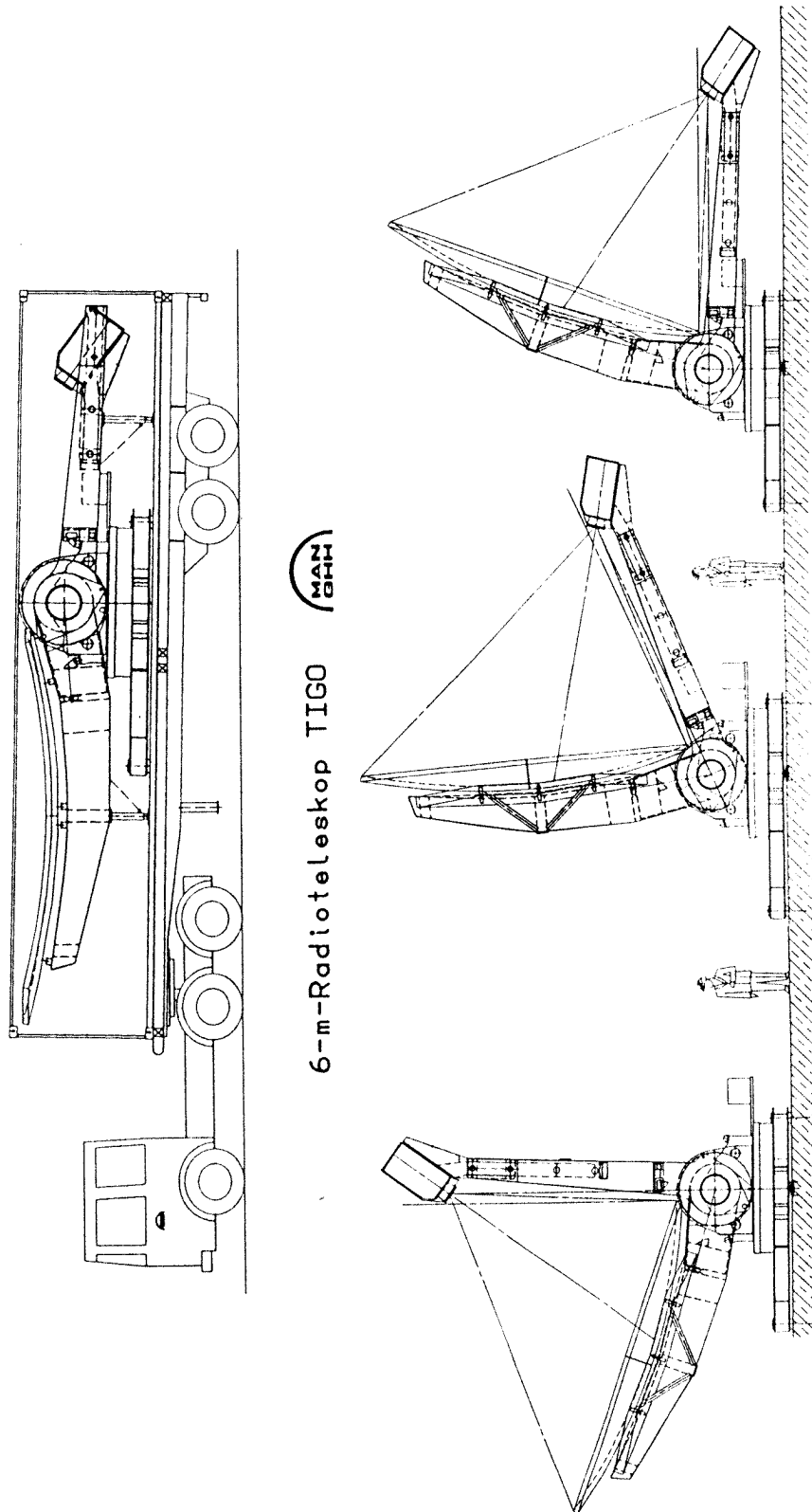


Figure 2: The VLBI antenna during transportation in a standard container and in different elevation positions. The feed holder is drawn out for operation.

TIGO schedule

The implementation schedule for TIGO covers the period of six years. In 1994 the First parts have been manufactured in 1994 and are not just drawings anymore. During the next two years the containers will be completed and the first test operations will be possible at Wettzell.

1992	General Design and Request for Offers First contracts: <ul style="list-style-type: none"> • VLBI antenna • SLR module • Smallsize Maser
1993	Design and begin of manufacturing <ul style="list-style-type: none"> • VLBI module • SLR module
1994	Request for Offers and Contracts for <ul style="list-style-type: none"> • VLBI Receiver, DAR • Titan Saphir Laser • Containers
1995	Setup a platform at Wettzell Delivery of SLR, VLBI modules and Implementation Request for Offers and Contracts for <ul style="list-style-type: none"> • Time & Frequency • Meterological System • Central Computer, LAN/WAN
1996	Request for Offers and Contracts for <ul style="list-style-type: none"> • Gravimeter • Power Generators Integration of the Components
1997	Final Integration and Testperiod at Wettzell Implementation of <ul style="list-style-type: none"> • GPS • PRARE • Seismometer
1998	Expected to be ready for first campaign abroad

DISCUSSION

K. Nurutdinov (Q): Is there any contradiction in the words “transportable” and “fundamental” with regard to stations? In my mind, “fundamental” means permanent and “transportable” — non-permanent.

H. Hase (A): The term “fundamental station” in geodesy and geophysics means that a station is equipped with the space geodesy instrumentation, such as VLBI, SLR, GPS and with the dynamic techniques, such as gravity and seismo-graphs for geophysics. Therefore, there is no contradiction between fundamental and transportable. TIGO will function as a permanent observatory for about 1 year at one site. Later it will come back to that site after 2 – 4 years for another period of 1 year.

A New S/X-band Receiver for the Simeiz VLBI Station

A. IPATOV, I. IPATOVA, D. IVANOV, A. KUTUZOV, V. MARDYSHKIN
and A. MIKHAILOV

Institute for Applied Astronomy, Russia Academy of Sciences, St. Petersburg, Russia

Abstract

The RT-22 radio telescope in Simeiz is a multi-purpose facility which is available for VLBI experiments as a member of the VLBI network. This multi-purpose character introduces special requirements for an S/X-band receiver, which operates from the primary focus of the telescope and is mounted in a special box. This box, according to operational requirements, has to be replaced with other equipment within a rather short time. The experience at Simeiz station in frame of the scientific programs Crimea-1, Crimea-2 etc. showed that radiotelescope RT-22 can be used for VLBI observations only episodically. So it is necessary to construct S/X band receiver that can be operated on this telescope from prime focus and will be installed into special box. This box has to be interchanged fast enough as required.

The paper describes the structure of cryoreceiver and its functional arrangement, gives the results of the measurements of its main parameters.

It is intended to use in this receiver model cooled amplifiers with a noise temperature not higher than 20 K for S-band and not higher than 25 K for X-band .

An International geodetic VLBI station has been created in Crimea on the basis of the radio telescope RT-22. Participants from the USA, Ukraine, and Russia take part in this project.

The US side has provided a Mk 3 data acquisition terminal, feeds, a phase calibration device; the Ukrainian side has provided the required upgrade of RT-22, a part of the cooling system, and an operational support; the Russian side has contributed a Hydrogen maser frequency standard and receivers.

During the first observations, the system temperature of 90 K and 50 K has been achieved in S- and X-band correspondingly. The receivers have been constructed at the Institute for Applied Astronomy of the Russia Academy of Sciences as a part of the receiver complex for the "QUASAR" network [1, 2].

The S- and X-band receiver system with FET amplifiers has been installed in the primary focus of RT-22 and connected to the Mk 3 signal path. The frontend directional coupler and FET amplifiers are cooled in order to obtain low system noise temperatures. The functional diagram of receivers is shown on Fig. 1.

The cryoreceiver consists of two frequency channels. Both channels have the same scheme – a superheterodyne receiver with a gain modulation of the second stage amplifier and a reference signal injection. It gives a possibility to construct a low-noise input line and the first stage amplifiers. A control over the gain fluctuations is also provided. The modulator is excluded from the receiver input and gives a possibility for observations with a high sensitivity both in VLBI and single antenna modes.

Every channel of the cryoreceiver consists of the following blocks:

Low noise amplifier (LNA): The cooled receiving block is situated inside a vacuum dewar. The block contains the cooled low noise transistor amplifier, ferrite isolators and a part of the input line. There is also a cold load inside the dewar for matching the unused port of the feed.

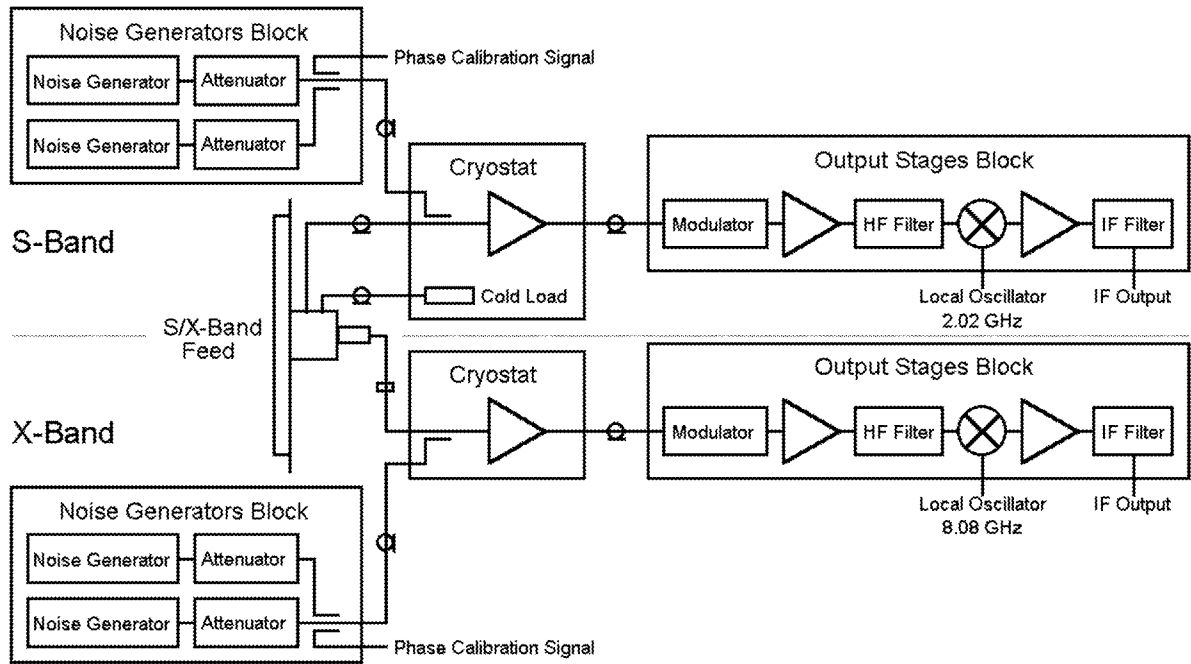


Figure 1: The receiver functional diagram

Output stages block comprises an amplification modulator, some ferrite components and an amplification-conversion device, which allows to unite the microwave amplifier and traditional output cascades of a radiometer (mixer, intermediate frequency (IF) amplifier, and IF filter) in a single unit. There are also power supply circuits and a thermostabilization circuit inside this block.

The noise generator block forms either a modulated signal or a continuous signal of noise balancing and a modulated or continuous calibration noise signal. The level of the signals above can be set in several steps. There are semiconductor noise generators for compensation and calibration, power supply circuits, controlled and fixed attenuators, a thermostabilization circuit, ferrite components, directional couplers for injection in the receiver input noise calibration signals and picosecond pulses (for phase calibration) inside this block.

Besides of the three main blocks above, there are also the local oscillator (developed in the IAA laboratory under S.G. Smolentsev supervision), the connection unit, the power supply equipment, a control and diagnostic block.

Monitoring and control of the receiver and its parameters can be done by a computer.

One circular polarization was observed in each frequency band using the primary focus feed (provided by T.A. Clark of the NASA/GSFC).

Fig. 2 and 3 show the scheme of the receiver's cryoblock and noise temperature of receiver at S and X band. Contributions of various units into the receiver noise temperature are shown.

Losses of the signal in the line between cryoblock and the output stages block are an approximation because the actual cables' length will be verified in future.

Main parameters of the receivers are presented in the Table 1.

The results of receiver noise temperature measurements correspond to the input flange.

By this time the Crimea station had already taken part in several geodetic and testing astrophysical experiments, that gave satisfactory results. At the same time an excessive

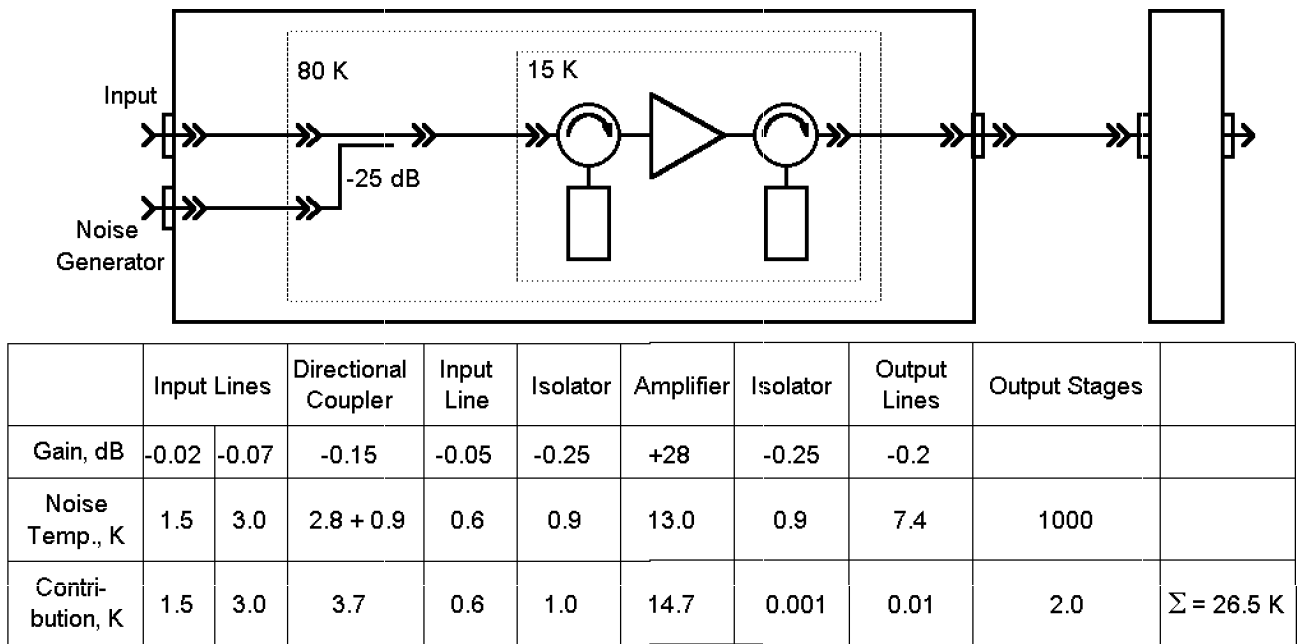


Figure 2: Contributions of various units in the receiver noise temperature at S-band

noise temperature in the S-band has been detected in these experiments. This might be attributed to the poor matching of the feed with the input cryoblock. In the last session we used a cold load with lower physical temperature. This measure decreased the system noise temperature from 90 K to 70 K.

At present, an installation of the receiver in the primary focus requires too much time for assembling and dismantling the equipment prior or after observations. This is why a

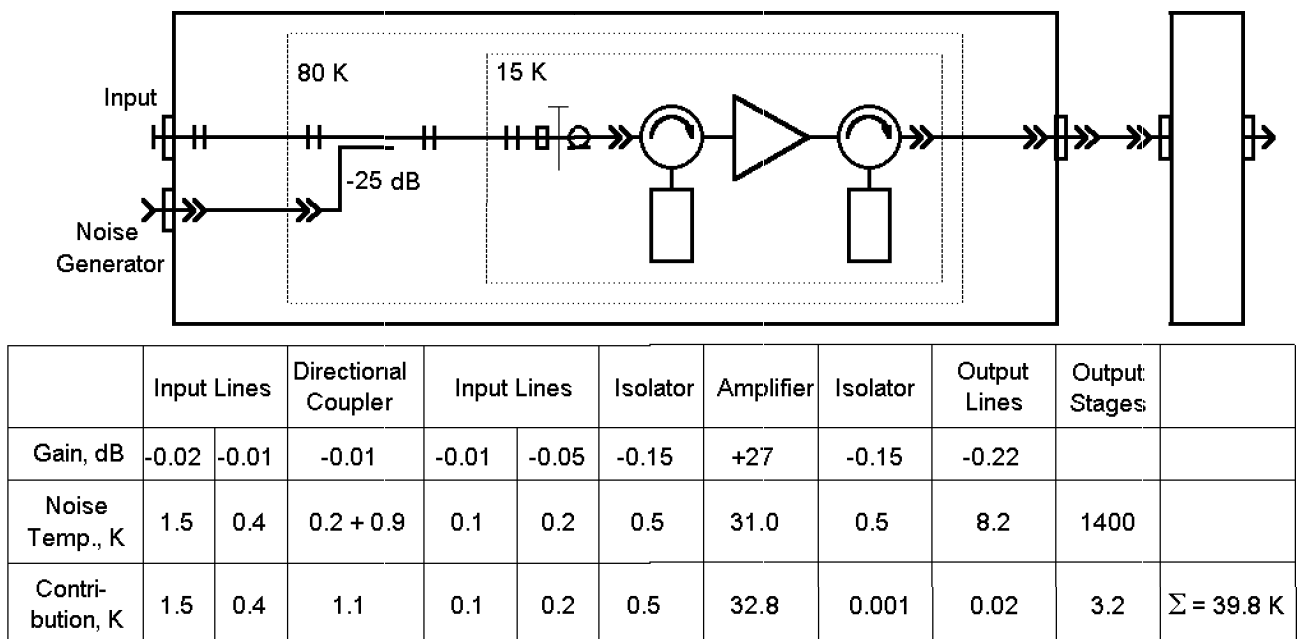


Figure 3: Contributions of various units in the receiver noise temperature at X-band

Table 1: The S/X-band receiver parameters.

Wavelength cm	Band	Frequency GHz	Receiver noise temp., K	System noise temp., K	SEFD Jy
13	S	2.15–2.5	27	70	1300
3.5	X	8.18–8.68	40	50	800

participation in short observational sessions is currently unreasonable. In order to simplify mounting/dismounting workload and to achieve higher time efficiency, it is necessary to construct an S/X-band receiver built-in into a special box. The latter has to be easily installed and dismantled when required.

In conclusion we would like to point out that further improvements and elaborations of the receiver are necessary in order to provide a high quality of observations and to achieve higher sensitivity. Using a HEMT as the first stage, it is possible to reduce the noise temperature by a factor of 1.5–2 at the X-band.

References

- [1] Ipatov A.V., Ipatova I.A., and Mardyshkin V.V., 1994, “Cryogenic Cooled Receivers for the QUASAR Network”, in *VLBI Technology: Progress and Future Observational Possibilities*, eds. T. Sasao, S. Manabe, O. Kameya and M. Inoue, Terra Sci. Publ., p. 200.
- [2] Finkelstein A.M., Golubchin G.S., Gorodetsky V.M. *et al.*, 1990, “Dedicated Soviet VLBI-network QUASAR”, in *Proceedings of the IAU Symposium No. 141: Internal coordinate system on the sky*, eds. J.H. Lieske and V.K. Abalakin, Kluwer Acad. Publ., Dordrecht, p. 293.

DISCUSSION

R. Wielebinski (Q): In the picture your receivers are open. Do you have no temperature stabilization.

A. Ipatov (A): We have no temperature stabilization in joint box, but we provide the good temperature stability inside of each unit.

VLBI Station “Simeiz”

A.V. STEPANOV¹, L.I. MATVEENKO² and A.V. IPATOV³

¹Crimea Astrophysical Observatory, Crimea

²Space Research Institute, Moscow

³Institute of Applied Astronomy, St. Petersburg

The first VLBI observations at 22 m parabolic antenna of Crimea Astrophysical Observatory had been in 1969 (Broderick *et al.*, 1970). Then the radio telescope was equipped with a hydrogen frequency standard, receivers at 1.3 – 92 cm wavelengths, terminal MK-2 and observations continued with compliance with the international programmes (Matveenko *et al.*, 1992).

Now the radio telescope equipment has been supplemented with the S/X band feed, Mk3A terminal, GPS receivers (GSFC) and S/X-band receivers (IPA). First VLBI observations were carried out in June 1994. Accurate position of the antenna was determined to be:

$$\begin{aligned}x &= 3785230826.8 \pm 6 \text{ mm} \\y &= 2551207490.5 \pm 6 \text{ mm} \\z &= 4439796120.0 \pm 6 \text{ mm}\end{aligned}$$

The discrepancy with the earlier results is around 12 m, which corresponds to an error of the early measurements (Matveenko *et al.*, 1992).

λ , cm	3.6	13	6
A_{eff} , m ²	150	150	200
T_{sys} , K	45	80	200
T_{sys} , Jy	800	1500	2700

In September 1994 we had VLBI observations of radio sources at 3.6 and 6 cm.

References

Broderick *et al.*, 1970, *Sov. Astron. J.*, **47**, 784.

Clark *et al.*, 1995, *Sov. Astron. Letters*, No 2.

Matveenko *et al.*, 1992, *Sov. Astron. Letters*, No 10, 891.

Pulsar Processing Facility of the EVN MK-IV Correlator[†]

S. POGREBENKO¹ and G. TUCCARI²

¹JIVE and NFRA, Dwingeloo, The Netherlands

²IRA/CNR, Stazione Radioastronomica di Noto, Italia

Introduction

Pulsar VLBI observations provide us with the accurate position information on pulsars including their proper motion with the accuracy of few microarcsec per year. The importance of the pulsar astrometric VLBI observations in a frame of the EVN Upgrade Project was outlined by J.-F. Lestrade (1994, private communication). Pulsar VLBI processing is an important feature of the EVN MK-IV Correlator being currently under construction at JIVE, Dwingeloo.

The way to increase the sensitivity of VLBI pulsar observations is to enable the correlator to accumulate a correlation function only during a pulse. This way the increase of sensitivity may be equal to

$$K_{S/N} = (P/W)^{1/2},$$

where P is the pulsar period and W is the pulse width. For typical pulsars the P/W ratio is about 30 – 100, so a sensitivity increase of the order of 5 – 10 is achievable.

To enable the correlator to accumulate data only during selected periodic intervals the technique of “pulsar gating” is used. Periodic gate function should be generated and mixed into “validity” stream of interferometric data.

To normalize “gated” correlator output correctly one needs to count statistics of the gated input signals before correlating them.

To apply pulsar gating correctly one must take into account such effects like dispersion caused by the propagation of the pulsar radiation through the interstellar media and the change of the apparent pulsar period with a time caused by different kind of motion not compensated by usual VLBI processing algorithms: Earth-Moon barycentre motion, annual Earth motion, binary pulsar orbital motion. Effect of the Earth rotation on the apparent phase of the pulse arriving time is automatically compensated when interferometric delay is compensated in the VLBI processor.

As the millisecond pulsars became the very interesting objects for radio astronomy, a requirement of the effective VLBI processing of them arose at the design stage of the EVN MK-IV Correlator project.

Other possible targets of the VLBI pulsar observations may be an investigation of inter-pulse emission, both pulsed and continuous. For this purpose one will need to apply different (in each case specific) gate patterns.

[†]Presented at the EVN Users Meeting, Toruń, October 21, 1994

Application characteristics

To fulfil the modern pulsar astronomy requirements the following characteristics of the pulsar processing subsystem were specified at the design stage (Anderson and Pogrebenko, 1993; Pogrebenko and Anderson, 1993; Pogrebenko, 1994):

1. Gate timing accuracy:

1/1024 of a period processed or 0.36 degree of phase.

This seems to be enough to make effective gating in all cases.

2. Gate patterns:

Arbitrary programmed pattern of 1024 independent phase points.

3. Pulsar periods processed:

16 s – 0.25 ms.

Periods longer than 16 s are processed without the use of gating, but using the re-arrangement of the correlator output data which are basically accumulated with 16 ms intervals, so 1000 points per period of 16 s are automatically available.

The shortest period is specified in accordance with the theoretical limit of the 0.3 – 0.6 milliseconds of the rotational rate of a neutron or strange matter star (Kondratyuk *et al.*, 1990; Madsen, 1992; Glendenning, 1992). Nevertheless, the possibility to process even twice shorter than 0.25 ms periods is kept, but with 1/512 of a period timing accuracy.

4. Period change rate:

A correct performance of the Pulsar Gate Generator (PGG) with the gate timing accuracy of 1/1024 of the period is specified (Pogrebenko, 1994) for the theoretically extreme case of the binary pulsar with orbital period of 0.5 h (Verbunt *et al.*, 1990) and rotational period of 0.25 ms. A correction of the period variation caused by Earth/Moon barycentre motion and annual Earth motion may be done as well.

5. Multi-pulsar correlation mode::

Either 2 or 4 pulsars can be processed simultaneously. This is based on two assumptions.

First is the possibility of EVN MK-IV Correlator to be sub- divided into several independent “sub-array correlators”. This way we could expect that more than one sub-array at a time will process pulsar observations.

Second is the possibility to observe more than one pulsar per the telescope primary beam like in the case of globular clusters (Biggs *et al.*, 1993). In this case more than one pulsar can be processed simultaneously.

Currently there are technical problems implementing four independent generators. If the problem is not solved shortly, only two independent generators will be available.

All generators may be programmed to the same period.

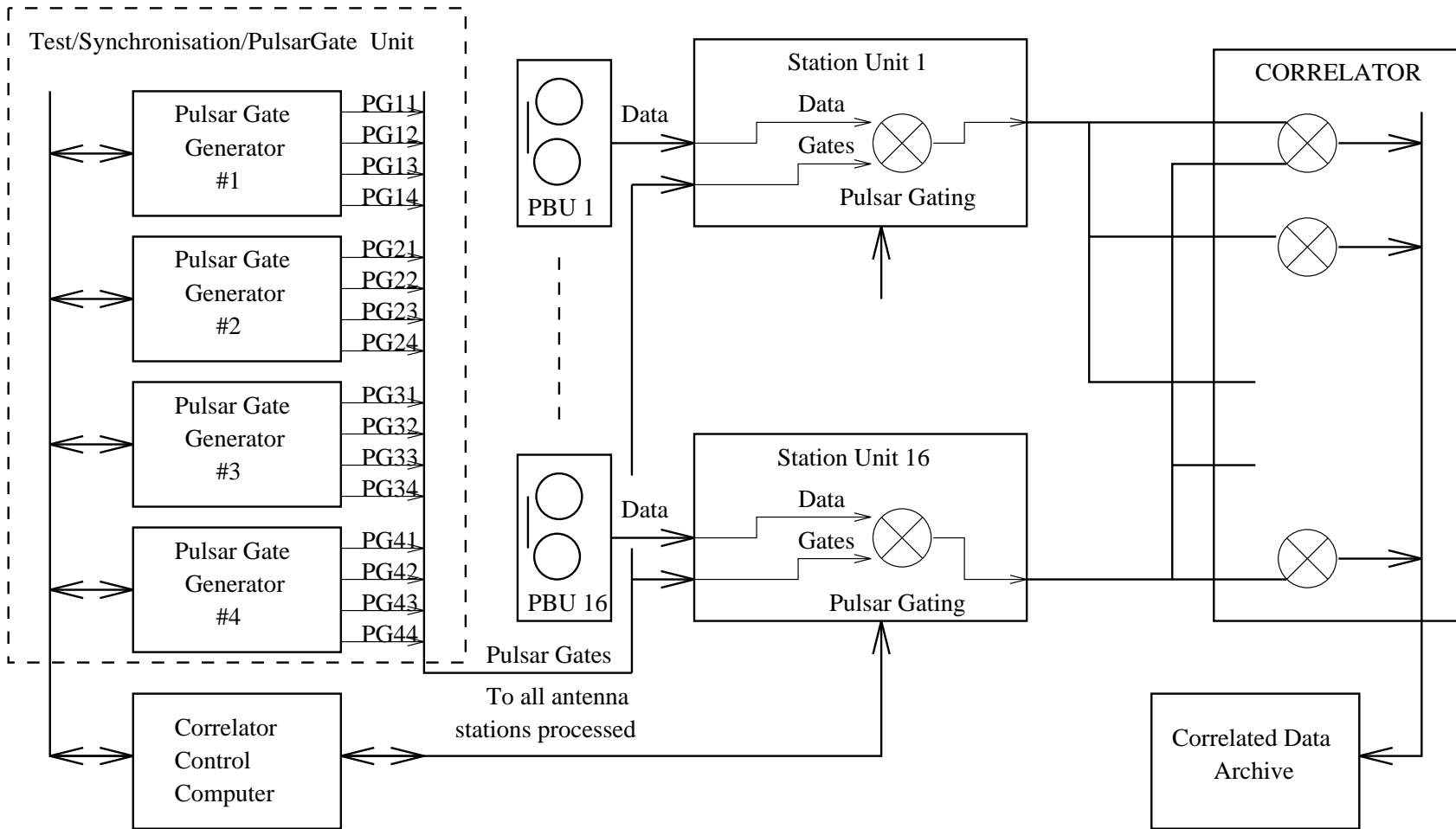


Fig.1. Pulsar Processing Architecture of the EVN MK-IV Correlator

6. Maximum number of independent gates:

Maximum number of gates generated is 16, the same as the maximum number of frequency channel processed by correlator. Gates are grouped in 4 or 2 groups of 4 or 8 (it depends on the number of PGGs to be implemented).

Each group may be programmed to its independent period and period change rate. Within the group of the same period all the gates may be programmed independently for different phase, duty cycle or even different inter-pulse structure.

All the groups may be programmed to the same period and period change rate, so all the 16 gates may be used as “dispersed” with different phases.

7. Routing flexibility:

Each frequency channel of each baseline processed may be gated with any selected gate pattern of 16 available.

In addition direct or inverted gate pattern may be used to correlate separately “on-gate” and “off-gate” data.

8. Dispersion compensation:

The dispersion compensation algorithm implemented in the correlator is basically post-detector compensation scheme, but implemented differently to get advantage of flexibility. This way the dispersion compensation capability is limited by the bandwidth of a single frequency channel observed.

To compensate the interstellar dispersion one may use up to 16 differently phased gate patterns. In the case of a smaller number of frequency channels processed (say, for low frequency observations) the smaller number of gates may be used.

Pulsar processing subsystem architecture

A functional block-diagram of the pulsar gating facilities of the EVN MK-IV Correlator is presented in Fig. 1.

Pulsar gates are generated by the four (or two) independently programmed PGGs. Pulsar gates are delivered to all Station Units, where the gating is performed and statistics is counted. After that the gated signals are correlated and archived.

References

- Anderson and Pogrebenko, 1993, EVN Doc #9, Dwingeloo.
 Biggs *et al.*, 1993, Jodrell Bank Preprint #1094.
 Glendenning, 1992, Phys. Rev. (D), 46 (10), 4161.
 Kondratyuk *et al.*, 1990, Sov. Astr. L., 16, 954.
 Madsen, 1992, Phys. Rev. (D), 46 (8), 3290.
 Pogrebenko, 1994, EVN Doc #41, Dwingeloo.
 Pogrebenko and Anderson, 1993, EVN Doc #26, Dwingeloo.
 Verbunt *et al.*, 1990, A&A 234, 195.

Author Index

- | | |
|--|--|
| <p>AKUJOR, C.E. 87
 ALBERDI, A. 99
 ANTERRIEU, E. 19</p> <p>BÅÅTH, L.B. 47
 BOLOTIN, S.L. 13
 BOOTH, R.S. 47
 BORISOV, N. 33
 BREMER, MALCOLM 71
 BRITZEN, S. 9
 BROWNE, I.W.A. 79
 BRUYN, GER DE 71</p> <p>COLOMER, FRANCISCO 55</p> <p>DESPRINGRE, V. 19
 DEWEY, R. 61
 DOELEMAN, S. 39</p> <p>FRAIX-BURNET, D. 19
 FUJISAWA, K. 61</p> <p>GARRETT, M.A. 73
 GONTIER, A.-M. 9
 GÓMEZ, J.L. 99
 GRAVE, A. 47
 GREWING, M. 47
 GUIRADO, J.C. 99
 GURVITS, L.I. 61</p> <p>HASE, HAYO 107
 HENSTOCK, D.R. 79
 HIRABAYASHI, H. 61</p> <p>INOUE, M. 61
 IPATOV, A.V. 113, 117
 IPATOVA, I. 113
 IVANOV, D. 113</p> <p>JAUNCEY, D. 61
 JONES, D.L. 1</p> <p>KRICHBaum, T.P. 47
 KUTUZOV, A. 113</p> <p>LANNES, A. 19
 LARA, L. 99
 LEPPÄNEN, KARI 65
 LESTRADE, J.-F. 1
 LOBANOV, A.P. 93</p> | <p>MACHALSKI, JERZY 105
 MARCAIDE, J.M. 99
 MARDYSHKIN, V. 113
 MATVEENKO, L.I. 117
 MIGENES, V. 61
 MIKHAILOV, A. 113
 MILEY, GEORGE 71
 MINGALIEV, M. 33
 MOELLENBROCK, G. 61
 MONTEBUGNOLI, S. 33
 MORAN, J.M. 39</p> <p>NEIZVESTNY, S. 33
 NOSZTICZIUS, I. 25</p> <p>PATNAIK, A.R. 73
 PEARSON, T.J. 79
 PHILLIPS, R.B. 1
 POGREBENKO, S. 33, 119
 PORCAS, R.W. 73, 87
 PRESTON, R.A. 1, 61</p> <p>READHEAD, A.C.S. 79
 ROBERTS, D. 61
 ROGERS, A.E.E. 39, 47</p> <p>SCHALINSKI, C.J. 47
 SCHILIZZI, R. 61, 71
 SJOUWERMAN, LORÁNT 57
 SMOKER, J.V. 87
 SNELLEN, IGNAS 71
 STANDKE, K.J. 47
 STEPANOV, A.V. 117
 STOLYAROV, V. 33</p> <p>TAYLOR, G.B. 79
 TINGAY, S. 61
 TUCCARI, G. 119</p> <p>VALTAOJA, ESKO 65
 VERMEULEN, R.C. 79</p> <p>WIIK, KAJ 65
 WILKINSON, P.N. 79
 WITZEL, A. 47</p> <p>XU, W. 79</p> <p>ZENSUS, J.A. 47, 61, 93</p> |
|--|--|

List of Participants

A

ALBERDI Antxon
CSIC
Istituto de Astrofísica de Andalucía
GRANADA
Spain
antxon@iaa.es

BUTCHER Harvey R.
Netherlands Foundation for Research in
Astronomy
P.O. Box 2
7990 AA DWINGELOO
The Netherlands
tel +31 5219-7244
fax +31 5219-7332
hrb@nfra.nl or Butcher@nfra.nl

B

BÅÅTH Lars
Onsala Space Observatory
ONSALA
S-43992 Sweden
tel +46 300 62590
fax +46 300 62621
lbb@oso.chalmers.se

BONDI Marco
University of Manchester
Nuffield Radio Astronomy Laboratories
Macclesfield
Cheshire
SK11 9DL JODRELL BANK
United Kingdom
mb@jb.man.ac.uk

BORKOWSKI Kazimierz
Nicolaus Copernicus University
Toruń Radio Astronomy Observatory
ul. Gagarina 11
87-100 TORUŃ
Poland
tel/fax +48 56 11651, +48 56 783327
kb@astro.uni.torun.pl

C

CASSE Jean
Netherlands Foundation for Research in
Astronomy
P.O. Box 2
7990 AA DWINGELOO
The Netherlands
tel +31 5219 7244
fax +31 5219 7332
JCasse@nfra.nl

CHYŻY Krzysztof
Jagiellonian University
Astronomical Observatory
ul. Orla 171
30-244 KRAKÓW
Poland
tel +48 12 251294
fax +48 12 251318
chris@oa.uj.edu.pl

COLOMER Francisco "Paco"
Observatorio Astronomico Nacional
Alfonso XII-3
28014 MADRID/YEBES
Spain
colomer@cay.es

D

da COSTA Antonio A.
 Centro de Electrodinamica
 Instituto Superior Tecnico
 1069 LISBOA CODEX
 Portugal
 fax +351 1 352 43 72
 dsc25_08@beta.ist.utl.pt

DALLACASA Daniele
 Netherlands Foundation for Research in
 Astronomy
 P.O. Box 2
 7990 AA DWINGELOO
 The Netherlands
 tel +31 5219 7244
 fax +31 5219 7332
 daniele@nfra.nl

DESPRINGRE Vincent
 Observatoire Midi-Pyrenees
 14 Avenue Edouard Belin
 31400 TOULOUSE
 France
 despring@obs-mip.fr

DOELEMEN Sheperd
 MIT Haystack Observatory
 Westford, MA
 U.S.A.
 dole@dopey.haystack.edu

DONGRONG Jiang
 Chinese Academy of Sciences
 Shanghai Observatory
 80 Nandan Road
 200030 SHANGHAI
 P.R.China
 fax +86 21 4384618
 bmasao@ica.beijing.canet.cn
 xytan@fudan.ihep.ac.cn

F

FEILER Roman
 Nicolaus Copernicus University
 Toruń Radio Astronomy Observatory
 ul. Gagarina 11
 87-100 TORUŃ
 Poland
 tel/fax +48 56 11651, +48 56 783327
 rf@astro.uni.torun.pl

FEJES Istvan
 FÖMI Satellite Geodetic Observatory
 PENC
 Hungary
 fejes@rmk530.rmki.kfki.hu

FOMALONT Ed
 National Radio Astronomy Observatory
 PO Box 0
 NM 87801 SOCORRO
 USA
 tel (505)835 7298
 fax (505)835 7027
 efomalon@nrao.edu

FRAIX-BURNET Didier
 Laboratoire d'Astrophysique de Toulouse
 14 Avenue Edouard Belin
 31400 TOULOUSE
 France
 fraix@obs-mip.fr

G

GARRETT Mike
 University of Manchester
 Nuffield Radio Astronomy Laboratories
 Macclesfield, Cheshire
 SK11 9DL JODRELL BANK
 United Kingdom
 tel +44 (0)477-571321 x209
 fax +44 (0)477-571618
 mag@jb.man.ac.uk

GAWROŃSKA Grażyna
 Nicolaus Copernicus University
 Toruń Radio Astronomy Observatory
 ul. Gagarina 11
 87-100 TORUŃ
 Poland
 tel/fax +48 56 11651, +48 56 783327
 gg@astro.uni.torun.pl

GURVITS Leonid I.
 Joint Institute for VLBI in Europe (JIVE)
 P.O. Box 2
 7990 AA DWINGELOO
 The Netherlands
 tel +31 5219 7244
 fax +31 5219 7332
 lgurvits@nfra.nl

GIOVANNINI Gabriele
 Istituto di Radioastronomia, C.N.R.
 Via Gobetti 101
 I-40129 Bologna
 Italy
 fax +39 51 6399431
 tel +39 51 6399385
 ggiovannini@astbo1.bo.cnr.it

H

HASE Hayo
 Institute for Applied Geodesy (IfAG)
 Fundamentalstation Wettzell
 D-93444 KOETZTING
 Germany
 fax +49 9941 603 222
 hase@wettzell.ifag.de

GOMEZ-GONZALEZ Jesus
 Observatorio Astronomico Nacional
 Alfonso XII-3
 28014 MADRID
 Spain
 fax +34 492 900 63
 gomez@cay.es

HENSTOCK David
 University of Manchester
 Nuffield Radio Astronomy Laboratories
 Macclesfield, Cheshire
 SK11 9DL JODRELL BANK
 United Kingdom
 tel +44 (0)477-571321
 fax +44 (0)477-571618
 drh@jb.man.ac.uk

GONTIER Anne-Marie
 Max-Planck Institut für Radioastronomie
 Postfach 2024
 53010 BONN
 Germany
 v708amg@mpifr-bonn.mpg.de

I

IPATOV Alexander
 Institute for Applied Astronomy
 SANKT PETERSBURG
 Russia
 fax +7 812 230 7413
 iparan@sovam.com

GORGOLEWSKI Stanisław
 Nicolaus Copernicus University
 Toruń Radio Astronomy Observatory
 ul. Gagarina 11
 87-100 TORUŃ
 Poland
 tel/fax +48 56 11651, +48 56 783327
 sgo@astro.uni.torun.pl

IWANOWSKA Wilhelmina
 Nicolaus Copernicus University
 Institute of Astronomy
 ul. Chopina 12/18
 87-100 TORUŃ
 Poland
 tel +48 56 26018 ext. 52

K

KREMPEĆ-KRYGIER Janina
 Nicolaus Copernicus Center
 Astrophysical Laboratory
 ul. Rabiniańska 8
 87-100 TORUŃ
 Poland
 jkart@ncac.torun.pl

KRICHBAUM Thomas P.
 Max Planck Institut für Radioastronomie
 Postfach 2024
 53010 BONN
 Germany
 p459kri@sun12.mpifr-bonn.mpg.de

KRYGIER Bernard
 Nicolaus Copernicus University
 Toruń Radio Astronomy Observatory
 ul. Gagarina 11
 87-100 TORUŃ
 Poland
 tel/fax +48 56 11651, +48 56 783327
 bk@astro.uni.torun.pl

KUS Andrzej
 Nicolaus Copernicus University
 Toruń Radio Astronomy Observatory
 ul. Gagarina 11
 87-100 TORUŃ
 Poland
 tel/fax +48 56 11651, +48 56 783327
 ajk@astro.uni.torun.pl

L

van LANGEVELDE Huib Jan
 Joint Institute for VLBI in Europe (JIVE)
 P.O. Box 2
 7990 AA DWINGELOO
 The Netherlands
 tel +31 5219 7244
 fax +31 5219 7332
 hvanlang@aoc.nrao.edu

LESTRADE Jean-Francois
 Observatoire de Meudon
 92195 MEUDON
 France
 fax +33 145077939
 lestrade@mesiob.obspm.circe.fr

LOBANOV Andrew P.
 National Radio Astronomy Observatory
 P.O. Box O
 SOCORRO, NM 87801
 U.S.A.
 tel (505)835 7298
 fax (505)835 7027
 alobanov@aoc.nrao.edu

M

MACHALSKI Jerzy
 Jagiellonian University
 Astronomical Observatory
 ul. Orla 171
 30-244 KRAKÓW
 Poland
 tel +48 12 251294
 fax +48 12 251318
 machalsk@nac.oa.uj.edu.pl

MAGDZIARZ Pawel
 Jagiellonian University
 Astronomical Observatory
 ul. Orla 171
 30-244 KRAKÓW
 Poland
 tel +48 12 251294
 fax +48 12 251318
 Pawel_Magdziarz@camk.edu.pl
 pavel@oa.uj.edu.pl

MARTIN Jean-Michel
 Observatoire de Paris
 PARIS
 France
 fax +33 145077939
 martin%meleze@mesiob.obspm.fr

MASŁOWSKI Józef
 Jagiellonian University
 Astronomical Observatory
 ul. Orla 171
 30-244 KRAKÓW
 tel +48 12 251294
 fax +48 12 251318
 Poland
 maslowsk@oa.uj.edu.pl

MATVEENKO Leonid
 Space Research Institute VLBI Laboratory
 Profsoyuznaja 84/32
 117810 MOSCOW
 Russia
 fax +7 095 310 7023
 lmatveen@esoc1.bitnet

MAZUREK Janusz
 Nicolaus Copernicus University
 Toruń Radio Astronomy Observatory
 ul. Gagarina 11
 87-100 TORUŃ
 Poland
 tel/fax +48 56 11651, +48 56 783327
 jmz@astro.uni.torun.pl

N

NOSZTICZIUS Istvan
 FÖMI Satellite Geodetic Observatory
 PENC
 (H-1373 BUDAPEST, P.O. Box 546)
 Hungary
 fejes@rmk530.rmki.kfki.hu

NURUTDINOV Konstantin Kh.
 Main Astronomical Observatory
 Goloseevo
 KIEV-22
 252650 Ukraine
 tel +7 044 2664759
 tel/fax +7 044 2662147
 maouas@gluk.apc.org
 nurut@astri.uni.torun.pl

O

OWSIANIK Izabela
 Nicolaus Copernicus University
 Toruń Radio Astronomy Observatory
 ul. Gagarina 11
 87-100 TORUŃ
 Poland
 tel/fax +48 56 11651, +48 56 783327
 iza@astro.uni.torun.pl

P

PADRIELLI Lucia
 C.N.R.
 Istituto di Radioastronomia
 Via Gobetti 101
 I-40129 BOLOGNA
 Italy
 tel +39 51 6399407 / 6399385
 fax +39 51 6399431
 padrielli@astbo1.bo.cnr.it

PATNAIK Alok
 Max-Planck Institut für Radioastronomie
 Auf dem Hugel 69
 53121 BONN
 Germany
 tel +49 (0)228 525 408
 fax +49 228 525 229
 apatnaik@mpifr-bonn.mpg.de
 v719pal@mpifr-bonn.mpg.de

PAZDERSKI Eugeniusz
 Nicolaus Copernicus University
 Toruń Radio Astronomy Observatory
 ul. Gagarina 11
 87-100 TORUŃ
 Poland
 tel/fax +48 56 11651, +48 56 783327
 ep@astro.uni.torun.pl

POGREBENKO Sergei V.
 Joint Institute for VLBI in Europe (JIVE)
 P.O. Box 2
 7990 AA DWINGELOO
 The Netherlands
 tel +31 5219 7244
 fax +31 5219 7332
 svp@nfra.nl

PORCAS Richard
 Max-Planck Institut für Radioastronomie
 Postfach 2024
 53010 BONN
 Germany
 p222rwp@sun22.mpifr-bonn.mpg.de

R

RIOJA Maria
 Joint Institute for VLBI in Europe (JIVE)
 P.O. Box 2
 7990 AA DWINGELOO
 The Netherlands
 tel +31 5219 7244
 fax +31 5219 7332
 p573mjr@mpifr-bonn.mpg.de

RUF Klaus
 Max-Planck Institut für Radioastronomie
 Postfach 2024
 53010 BONN
 Germany
 p275ruf@mpifr-bonn.mpg.de

RYŚ Stanisław
 Jagiellonian University
 Astronomical Observatory
 ul. Orła 171
 30-244 KRAKÓW
 Poland
 tel +48 12 251294 ext. 38
 fax +48 12 251318
 StRys@oa.uj.edu.pl

S

SANGHERA Hardip
 Joint Institute for VLBI in Europe (JIVE)
 P.O. Box 2
 7990 AA DWINGELOO
 The Netherlands
 tel +31 5219 7244
 fax +31 5219 7332
 hss@nfra.nl

SCHILIZZI Richard T.
 Netherlands Foundation for Research in
 Astronomy
 P.O. Box 2
 7990 AA DWINGELOO
 The Netherlands
 tel +31 5219 7244
 fax +31 5219 7332
 rts@nfra.nl

SCHWARTZ Rolf
 Max-Planck Institut für Radioastronomie
 Postfach 2024
 53010 BONN
 Germany
 p589evn@mpifr-bonn.mpg.de

SJOUVERMAN Lorant
 Leiden Observatory
 P.O. Box 9513
 NL-2300 RA LEIDEN
 The Netherlands
 tel +31 71275837
 sjouwer@strw.LeidenUniv.nl

SNELLEN Ignas
 Leiden Observatory
 P.O. Box 9513
 NL-2300 RA LEIDEN
 The Netherlands
 tel +31 71275837
 snellen@reusel.strw.LeidenUniv.nl

SOIDA Marian
 Jagiellonian University
 Astronomical Observatory
 ul. Orla 171
 30-244 KRAKÓW
 Poland
 tel +48 12 251294
 fax +48 12 251318
 soida@oa.uj.edu.pl

STEPANOV Alexander V.
 Laboratory of Radioastronomy of the
 Crimean Astrophysical Observatory
 RT-22 Katzively
 334247 CRIMEA
 Ukraine
 stepanov@rt22.crimea.ua
 stepanov@dynamo.aip.de

SZYMCZAK Marian
 Nicolaus Copernicus University
 Toruń Radio Astronomy Observatory
 ul. Gagarina 11
 87-100 TORUŃ
 Poland
 tel/fax +48 56 11651, +48 56 783327
 msz@astro.uni.torun.pl

T

TRIGILIO Corrado
 Istituto di Radioastronomia, C.N.R.
 NOTO
 Italy
 vlbinoto@astbo1.bo.cnr.it

U

UMANA Grazia
 Istituto di Radioastronomia, C.N.R.,
 NOTO
 Italy
 gumana@astrct.ct.astro.it
 vlbinoto@astbo1.bo.cnr.it

URBANIK Marek
 Jagiellonian University
 Astronomical Observatory
 ul. Orla 171
 30-244 KRAKÓW
 Poland
 tel +48 12 251294
 fax +48 12 251318
 urb@oa.uj.edu.pl

URPO Seppo
 H.U.T.
 Otakkaari 5A
 02150 ESPOO
 Finland
 fax +35 80264531
 sur@vipu.hut.fi

USOWICZ Jerzy
 Nicolaus Copernicus University
 Toruń Radio Astronomy Observatory
 ul. Gagarina 11
 87-100 TORUŃ
 Poland
 tel/fax +48 56 11651, +48 56 783327
 ju@astro.uni.torun.pl

V

VALTAOJA Esko
 Tuorla Observatory
 SF-21500 PIIKKI
 Finland
 tel +358 (9)21 2435822
 fax +358 (9)21 2433767
 valtaoja@sara.cc.utu.fi

VENTURI Tiziana
 Istituto di Radioastronomia, C.N.R.
 Via Gobetti 99/9
 I-40129 BOLOGNA
 Italy
 tel +39 51 6399385
 fax +39 51 6399423
 tventuri@astbo1.bo.cnr.it

W

WALENTYNOWICZ Grażyna
 Nicolaus Copernicus University
 Toruń Radio Astronomy Observatory
 ul. Gagarina 11
 87-100 TORUŃ
 Poland
 tel/fax +48 56 11651, +48 56 783327
 greta@astro.uni.torun.pl

WIELEBINSKI Richard
 Max-Planck Institut für Radioastronomie
 Postfach 2024
 53010 BONN
 Germany
 fax +49 (228) 525229
 p647gbr@mpifr-bonn.mpg.de

WIIK Kaj
 Metsahovi Radio Research Station
 Kylmäla
 Finland
 kwi@vipu.hut.fi

WILKINSON Peter N.
 University of Manchester
 Nuffield Radio Astronomy Laboratories
 Macclesfield, Cheshire
 SK11 9DL JODRELL BANK
 United Kingdom
 tel +44 477 571321
 fax +44 477 571618
 pnw@jb.man.ac.uk

WOLSZCZAN Aleksander
 University of Pennsylvania
 Eberly College of Sciences
 525 Davey Laboratory
 UNIVERSITY PARK, PA 16802
 U.S.A.
 tel +1 814 863 6039
 alex@astro.psu.edu

Z

ZIĘBA Stanisław
 Jagiellonian University
 Astronomical Observatory
 ul. Orla 171
 30-244 KRAKÓW
 Poland
 tel +48 12 251294
 fax +48 12 251318
 StanZ@oa.uj.edu.pl

ZINZ Wolfgang
 Max-Planck Institut für Radioastronomie
 Postfach 2024
 53010 BONN
 Germany
 p026wzi@mpifr-bonn.mpg.de

2nd EVN Symposium and Users' Meeting, Toruń, Poland, 21 October 1994 - group photo

